



**National University of Lesotho**



## **Planning, Optimization and Efficiency Improvement of Telecommunications Solar Plants**

*Maama Ronny Seeiso*

A dissertation submitted in partial fulfilment  
of the requirements for the degree of

### ***Master of Science in Sustainable Energy***

Offered by the

**Energy Research Centre**  
Faculty of Science & Technology

June 2023

## Abstract

Mobile network operators (MNOs) in Lesotho have recently experienced an increase in deploying solar PV-powered base stations in off-grid and bad-grid areas to improve their network coverage to the most underprivileged communities. This justifies the need to model and design the optimal solar PV- battery systems to power telecom base stations (BSs) operating in high-speed technologies that meet both the MNO and regulator targets and act as enablers for other economic sectors in rural areas. This research primarily aimed to audit the existing Vodacom Lesotho solar PV-powered BSs through physical inspections, configurations assessment, and load profile analysis using historical data. Based on the audit results, retrofitting and parameter optimizations were implemented to improve major key performance indicators (KPIs), therefore maximizing telecom solar power plants' energy yield and solar PV arrays' performance ratios (PRs) in a cost-effective and environmentally friendly manner. Five solar PV-battery-powered BSs with different power and radio configurations were selected, and their KPIs, such as battery charging current, solar PV generator power, load current, and PR, were assessed, analysed and optimized for possible maximum energy yield.

The Makebe BS improved charging currents by 15% with no improvements in other KPIs. The Malimong BS increased charging current by 23%, current from the solar generator by 12%, power by 11%, and PR by 3.31%. Mmasemouse BS showed an improvement of 34% in charging current, 19% in harvested current, 17% from the generated power after rewiring and optimizations, and 7.31% in PR. After replacing the faulty batteries and conducting a parameter optimization at Ha Tlhorro, the Tlhorro BS solar plant increased charging current by 60%, harvested current from the solar PV generator by 90%, generated power by 46%, and PR by 20%. After integrating two standalone solar arrays into one, rewiring, increasing the charging current limit and replacing faulty batteries for a high-capacity solar-powered BS in Kolo, it improved solar PV generator current by 7%, battery charging current by 19%, solar PV power by 40%, PR by 19% and able to reach 100% state of charge (SoC).

One high-capacity and grid-powered BS in an urban area was assessed and dimensioned for grid-to-solar migration with a 20.8 kWp solar PV array, 27 kW solar PV charge controller, and 1200Ah backup batteries storage for 0.5 days of autonomy using the month of June,

which has the lowest peak sunshine hours (PSH) as the design month for maximum system reliability.

## **Acknowledgments**

My special gratitude goes to my Supervisor, Assoc. Prof. Leboli Zak Thamae, for his dedicated support and guidance to me in undertaking this MSc dissertation under his supervision. I feel special and honoured to be one of your products Prof. The entire Energy Research Centre (ERC) staff; particularly, Mr. Sebota Mokeke, your support and motivation cannot be unrecognized. All the efforts and engagements to make this journey a success is truly appreciated. Secondly, my gratitude goes to my wife, my daughter, my son, close family and friends, for the support and understanding that I could not always spend quality time with them and participate in other family-related activities while travelling this journey. Lastly, I would like to send special thanks to my manager Mr. Tshepo Chaotsane and the Vodacom Lesotho operations team for their support, wish you more blessings.

## Abbreviation

BBU	Baseband Unit
BS	Base Stations
BTS	Base Transceiver Station
DEBM	Daily Energy Balance Method
DG	Diesel Generator
DoD	Depth of Discharge
ETL	Econet Telecom Lesotho
GHG	Greenhouse Gas
GoL	Government of Lesotho
GSM	Global System for Mobile Communication
HOMER	Hybrid Optimization Model for Electric Renewables
HRES	Hybrid Renewable Energy System
ICT	Information and Communications Technology
IEA	International Energy Agency
IEC	International Electro-Technical Commission
IoT	Internet of Things
KPI	Key Performance Indicators
LMICs	Low and Middle-Income Countries
MCDM	Multi Criteria Decision Making
MNO	Mobile Network Operators
MPPT	Maximum Power Point Tracker
PR	Performance Ratio
PSH	Peak Sunshine Hours
PV	Photovoltaic
PVGIS	Photovoltaic Geographic Information System
PWM	Pulse Width Modulation
RRU	Remote Radio Unit
SIM	Subscriber Identity Module
TSM	Time Step Method
ULCS	Ultra Low-Cost Site
UMTS	Universal Mobile Telecommunications Service
USF	Universal Service Fund

# Contents

Abstract.....	i
<b>List of Figures.....</b>	<b>vii</b>
<b>List of Tables.....</b>	<b>viii</b>
<b>1 INTRODUCTION.....</b>	<b>1</b>
1.1 Background.....	1
1.2 Research Problem.....	3
1.3 Purpose of the Study.....	5
1.4 Significance of the Study.....	6
1.5 Report Outline.....	7
<b>2 THEORY AND LITERATURE REVIEW.....</b>	<b>8</b>
2.1 Overview.....	8
2.2 Site Selection.....	10
2.3 Load Profiles and System Sizing.....	11
2.4 Solar Plants Efficiency / Key Performance Indicators.....	16
2.5 Factors Affecting Solar Plants Efficiency and Mitigation Controls.....	18
2.5.1 Solar Radiation.....	20
2.5.2 Temperature.....	20
2.5.3 Soiling and Shading.....	22
2.6 Solar PV Array Tilt angle.....	25
2.7 Research Gap Analysis.....	26
<b>3 RESEARCH METHODOLOGY.....</b>	<b>28</b>
3.1 Methodology Overview .....	28
3.2 Base Station Meteorological Data: Site Selection.....	31
3.3 Base Station Load Assessment.....	31
3.3.1 System Description.....	31
3.3.2 Base Stations Load Demand Determination: Daily Energy Balance Method...33	
3.3.3 Base Stations Load Demand Determination: Time Step Method.....	35
3.4 Base Station Solar-PV Hybrid Sizing.....	35
3.4.1 Optimal Battery Sizing for Telecom Load.....	35
3.4.2 Optimal PV-Array and Regulator Sizing for Telecom BS Load.....	36
3.5 Existing Base Station Audits and Assessment.....	40
3.5.1 Base Station Selection Criteria and Inspections.....	40
3.5.2 Base Station Key Performance Indicators.....	41
3.6 Performance Ratio Calculation.....	42

3.7 The Solar PV-Battery System Reliability.....	42
<b>4 RESULTS AND DISCUSSIONS.....</b>	<b>43</b>
4.1 Overview.....	43
4.2 Base Station Meteorological Data.....	43
4.3 Base Stations Load Determination.....	44
4.3.1 Base Stations Load Determination: Daily Energy Balance Method.....	44
4.3.2 Load Determination: Time Step Method.....	45
4.3.3 Load Profile Coefficients.....	47
4.4 Base Station System Components Sizing.....	49
4.4.1 Base Station Optimal Battery Sizing for Telecom Load.....	49
4.4.2 Optimal PV-Array and Regulator Sizing for Telecom BS Load.....	51
4.5 Base Station Audits Results and Redesign.....	53
4.6 Base Station Solar PV- Battery: Key Performance Indicators Analysis.....	54
4.6.1 Base Station Power Consumption Against Traffic.....	54
4.6.2 Base Station Solar PV Currents, Voltages and State of Charge.....	55
4.6.3 Base Station Solar PV Power.....	60
4.7 Base Stations Performance Ratio.....	61
4.8 The Base Station Solar PV-Battery System Reliability.....	62
<b>5 CONCLUSION AND RECOMMENDATIONS.....</b>	<b>65</b>
<b>REFERENCES.....</b>	<b>68</b>
Appendix A: 2.2 kW and 3.0 kW Solar PV Charger Controllers.....	73
Appendix B: 330W Solar PV Module and 48V/100AH Lithium-ion Battery.....	74
Appendix C: Selected Base Station's Meteorological Data.....	75
Appendix D: Base Stations Audit Assessment Results.....	77
Appendix E: Base Stations Power vs Actual Traffic.....	79
Appendix F: The Base Stations Current Before Rewiring and Parameter Optimizations.	81
Appendix G: The Base Stations Current After Rewiring and Parameter Optimizations...	82
Appendix H: The Base Stations Solar PV Currents Before and After Optimization.....	83
Appendix I: The Base Stations Battery Currents Before and After Optimization.....	84
Appendix J: The Base Stations Systems Voltages Before and After Optimization.....	85
Appendix K: The Base Stations Solar PV Power Before and After Optimization.....	86
Appendix L: The Base Stations Performance Ratios Before and After Optimization.....	87
Appendix M: The Base Stations Annual Performance Assessment Before and After Optimization.....	89
Appendix N: The Base Stations Load Profile Coefficients (Solar and Grid).....	91

## List of Figures

Figure 1: (a) Evolving generations of MNO with an increase in data speeds; (b) Evolving generations of MNO with an increase in power consumption [8,10].....	1
Figure 2: Technology and device penetration trends in the telecommunication industry [12].	3
Figure 3: Vodacom Lesotho (LS) network performance against the Vodafone Group target (VDC_TRGT) for 2021-2022 [20].....	4
Figure 4: Vodacom Lesotho's base station solar plant performance against the load at Senqu - Thaba Tseka.....	7
Figure 5: Solar PV plant at Vodacom Lesotho's tower located in Qopo, Mokhotlong.....	8
Figure 6: Evaluation Criteria for Selecting Areas Eligible for Solar Plant Installation [5].....	9
Figure 7: Sample BTS energy consumption and traffic load [9].....	11
Figure 8: A simple illustration of the telecommunication base station [31].....	12
Figure 9: Solar PV Module P-V and I-V Curves Showing Maximum Power Point [8].....	17
Figure 10: Main contributors that impact the overall performance of the solar PV Plants [8]	18
Figure 11: (a) I-V and (b) P-V characteristics at a constant temperature but varying solar radiations [8].....	19
Figure 12: (a) Solar cell efficiency decrease, (b) Solar cell power decrease with an increase in temperature, and (c) MPP variation with voltage and temperature [35,46].....	20
Figure 13: Types of shadings on the solar PV module [45].....	21
Figure 14: Different types of soiling resulting from (A) mineral dust in a desert area, (B) bird droppings, (C) algae, lichen, mosses, or fungi, and (D) pollen in wet and moderate climates, (E) engine exhaust from an industrial area, and (F) agricultural emissions [55].....	22
Figure 15: Soiling Mitigations Techniques [46].....	23
Figure 16: Summary of popular techniques used to enhance solar PV system efficiency [8].	25
Figure 17: The research methodology flow chart.....	29
Figure 18: Solar PV-battery hybrid system component diagram [58].....	30
Figure 19: Solar PV-DG-battery hybrid system component diagram [58].....	31
Figure 20: (a) Typical radio configuration and (b) transmission units both covering the BS essential DC loads [61, 62].....	32
Figure 21: (a) Delta PV charger output power and input voltage, (b) Output voltage and current curve for optimal system design [68].....	39



Figure 22: Power profile for 6 BSs with different radio configurations.....	45
Figure 23: Current profile for 6 BSs with different radio configurations.....	46
Figure 24: Normalized load profiles for solar-PV and grid-powered BSs.....	47
Figure 25: Normalized load profiles for four selected solar-PV and three grid-powered BSs	48
Figure 26: Power consumption against data traffic for Mmasemouse BS.....	54
Figure 27: Power consumption against voice traffic for Mmasemouse BS.....	54
Figure 28: Mmasemouse BS currents against SOC for before optimization.....	55
Figure 29: Mmasemouse BS currents against SOC for after optimization.....	56
Figure 30: Mmasemouse BS solar PV generator charging currents.....	57
Figure 31: Mmasemouse BS solar PV array currents before and after optimization.....	58
Figure 32: Mmasemouse BS solar PV-battery system voltage before and after optimization.	58
Figure 33: Mmasemouse BS solar PV power before and after optimization.....	59
Figure 34: Mmasemouse BS performance ratio before optimization.....	60
Figure 35: Mmasemouse BS performance ratio after optimization.....	61
Figure 36: 11.34 kW Mmasemouse BS's simulated annual performance before optimization .....	62
Figure 37: 11.02 kW Mmasemouse BS's simulated annual performance after optimization. .	62

## List of Tables

Table 1: Typical solar-powered base station configuration and its daily power demand.....	32
Table 2: Parameters and equations for battery-sizing.....	34
Table 3: Derating percentage loss to determine PV-module EoL parameters [33].....	35
Table 4: Optimal PV sizing procedure.....	36
Table 5: Selected BSs for the case study.....	38
Table 6: Sample Meteorological data for Mmasemouse BS.....	42
Table 7: BS load requirement using DEBM.....	43
Table 8: Battery sizing using DEBM load.....	47
Table 9: Battery sizing using the TSM load.....	48
Table 10: PV array and PV charger sizing using DEBM.....	49
Table 11: PV array and PV charger sizing using TSM.....	50
Table 12: The traditional BS system sizing using DEBM without derating factors and losses .....	51

# 1 INTRODUCTION

## 1.1 Background

In Lesotho, scattered population settlements and mountain ranges, especially in the rural areas, define the huge majority of the country's landscape, resulting in a negative business case to connect and maintain both the national electricity grid and telecommunications services to these rural villages [12]. Access to clean and reliable sources of energy from the national grid is still not universal, MNOs have expanded their coverage through the deployment of solar PV-powered BSs, mostly with diesel generators as the secondary power source. These challenges, together with an exponential increase in the amount of data traffic over the existing wireless communication as described by Figure 1(a), give rise to the requirement for alternative use of clean and reliable sources of energy [13]. Figure 1(b) shows an increase of 43% in power consumption from the third generation (3G) to the fourth generation (4G), as well as a 68% increase from the fourth generation (4G) to the fifth generation (5G) [14]. This high increase in power consumption triggers a need for an optimally and efficiently designed solar PV battery system for off-grid telecommunication BSs in the rural areas of Lesotho. This initiative benefits the MNOs by increasing network coverage and enabling them to provide a more reliable network while reducing business operating costs and greenhouse gas (GHG) emissions induced by backup diesel generators [2,3].

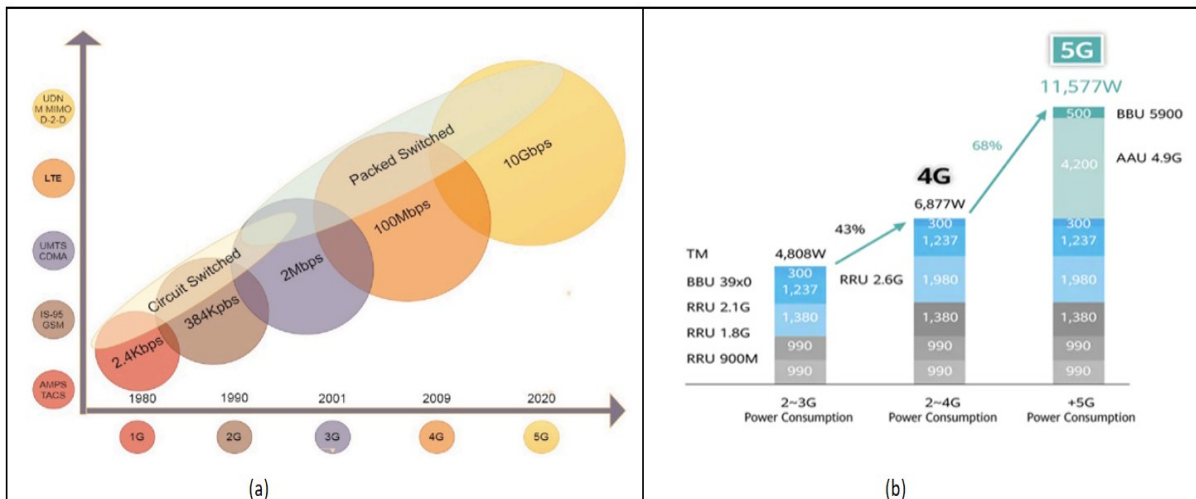


Figure 1: (a) Evolving generations of MNO with an increase in data speeds; (b) Evolving generations of MNO with an increase in power consumption [8,10]

The lack of access to clean, affordable, and reliable energy sources remains a substantial barrier to sustainable socio-economic development such as telecommunication services in many developing African countries [1, 2]. Like other developing Sub-Saharan African countries, Lesotho appreciates the importance of renewable energy solutions to provide clean and cost-effective energy access in remote and rural areas as opposed to grid extension [3, 4]. Solar energy is one of the clean and attractive energy sources, with Lesotho's global horizontal irradiation varying between 4.5 and 6.5 kWh/m<sup>2</sup>/day [5, 6]. Compared to other forms of renewable energy, solar energy is preferred because of its modularity and ubiquity hence it is used to generate electricity to power rural telecommunication base stations, minimize the use of fossil fuels, and manage GHG emissions [5,7]. Solar PV power generation systems are also appraised for their cheap operational cost or low maintenance, although they have a high capital cost, which makes them less attractive in other sectors but mostly used in the telecom sector [8].

Globally, the telecommunication industry has positively altered how people, devices, and animals interact, making it an essential part of people's daily life [7,9]. However, in low and middle-income countries (LMICs), access to mobile connectivity in rural areas has been hindered by the construction of telecom towers with unstable or no access to the national grid, hence powered by unreliable power sources such as diesel generators (DG) [10]. The direct carbon emissions from these diesel generator-powered base stations (BSs) in the information and communications technology (ICT) sector contribute about 4% of worldwide GHG emissions, with more than 10% coming from mobile network operators (MNOs) [11].

The rapid depletion of fossil fuel resources and awareness of climate change motivated the acceleration of renewable energy resources to power telecom towers. The number of telecom towers that are either off-grid or bad-grid is declining in every region [10]. It is estimated that since 2014, the total number of off-grid sites has fallen by 33% from 297,000 to 198,000 in 2020 due to grid expansion, while at the same time, the number of sites that are powered by renewable energy sources has increased by 45% [10]. The decrease in bad-grid-powered sites and the increase in green-powered towers have resulted in an annual reduction of carbon dioxide (CO<sub>2</sub>) emissions estimated at 2.2 million metric tonnes, from 9.2 million in 2014 to 7 million in 2020 [10].

Worldwide, the number of customers subscribed to mobile services has increased exponentially from an estimated 3.6 billion at the end of 2014 to 5 billion in 2018 and to 5.2 billion in 2020 [7,8]. As shown in Error: Reference source not found, mobile subscribers are projected to increase by 1 billion to 6 billion by 2025, with 60% of the new subscribers coming from Sub-Saharan Africa [10, 11]. This massive increase in mobile subscribers, internet users, and smart phones penetrations, as summarised by Figure 2, is not only triggered by population increase but also by advanced technologies, such as the Internet of Things (IoT), which in return calls for additional energy sources to meet the demand [8,9, 11]. The African population is expected to increase by around 2.5 billion people by 2050, of which 80% of that population will be in Sub-Saharan Africa [13]. To meet this demand, electricity generation in different sectors is critical to sustainably meet the energy consumption of these communication technologies while reducing generation costs and negative impacts on the environment [14].

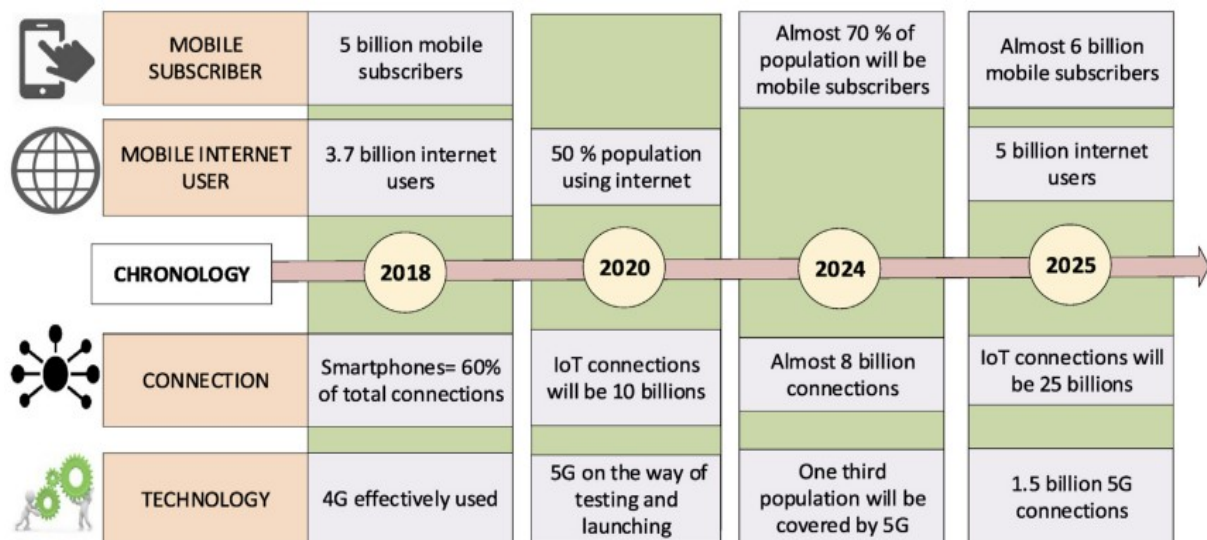


Figure 2: Technology and device penetration trends in the telecommunication industry [12]

## 1.2 Research Problem

Globally, telecommunications BSs have provided services for almost 60% of the population living in urban areas. In comparison, 40% of the population in rural areas lack access to such technologies due to the lack of network transmission, electricity, and low potential returns on investment triggered by low population densities [16]. As a solution, many MNOs, such as Vodacom Lesotho, have already considered deploying the Ultra Low-Cost Site (ULCS) wireless technologies limited to 3G technology single-radio sharing. The ULCSs are designed to provide basic voice and data connectivity to rural communities powered mainly by

unstable solar PV plants [16]. It has also been noted that, like in any other MNOs, the most energy-consuming network elements for Vodacom Lesotho are the BSs, which account for more than 50% of the total power usage [17]. This power usage increases with the annual radio capacity upgrade and new technologies to meet the customer demand or good customer experience. Therefore, efficient use of energy, planning and optimal sizing of the power plants in the access networks positively impact the techno-economical operations of the MNOs.

For some years now, Vodacom Lesotho and other regional MNOs have been struggling to meet the set group and regulator availability/reliability KPIs due to unstable grid and off-grid sources, as illustrated by Figure 3. Vodacom Lesotho BSs' reliability target, as per the regulator, is 99%, while the Vodafone Group's target for Lesotho is 99.5% for the financial year 2021 to 2022. It can be deduced from Figure 3 that Vodacom Lesotho's network reliability performance at times goes as bad as 97.7%. The main contributors to this under-performance were attributed to inadequately-sized solar PV-powered BSs and small-scale unstable grid-connected sites, especially in the isolated and rural regions such as Mokhotlong and Qacha's Nek districts. These two districts entirely depend on ESKOM's grid-connection, which is affected by the planned continuous load shedding. Therefore, to meet the group's availability target and Lesotho's regulatory target, the Vodafone group's net zero emissions target from its operations by 2030 and net-zero targets across its full value chain by 2040, maintaining global carbon emissions level between 7% and 16%, and improving solar plants performance ratio, the optimally designed solar PV plants integrated with battery energy storage systems (BESS) are considered as an efficient way to supply and conserve energy for the rural telecom BSs [20,22].

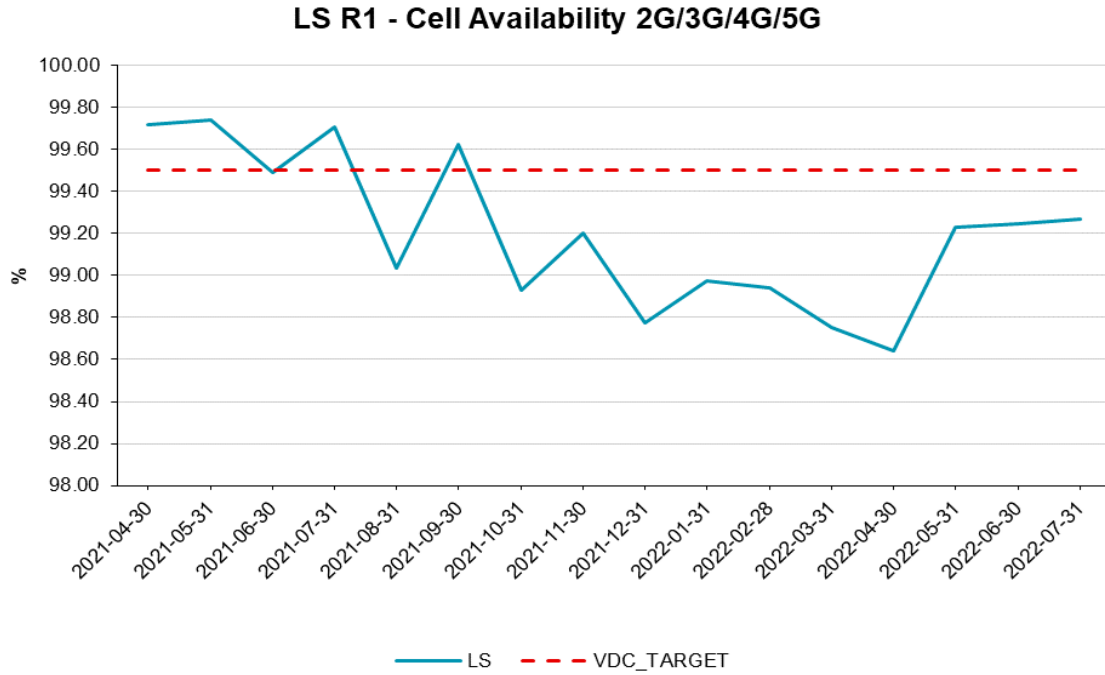


Figure 3: Vodacom Lesotho (LS) network performance against the Vodafone Group target (VDC\_TRGT) for 2021-2022 [20]

### 1.3 Purpose of the Study

The main objective of this project is to evaluate the performance of the existing Vodacom Lesotho solar PV-powered BSs against critical parameters such as the performance ratio (PR) stated in the International Electro-Technical Commission (IEC) Standard 61724 as well as previous studies using Microsoft Excel, Meeonorm software and photovoltaic geographic information system (PVGIS) [21]. Based on the audit results from the existing load profiles, configurations, and physical inspections or audits, the second main intention is to design an optimized solar PV battery system that satisfies the energy demand for the different BS configurations in a less costly and environmentally friendly approach. To derive this optimum design, the following objectives are prioritized:

- ❑ Modeling of the PV-DG hybrid with backup batteries for different BS power requirements and load profiles operating on different technologies (UMTS-GU900-ULCS – very low traffic, UMTS-GU900 – low traffic, GU2100 – moderate traffic and GUL1800 – high capacity).
- ❑ Auditing of the existing Vodacom Lesotho BSs (location/meteorology data; power consumptions/load profiling; system sizing/dimensioning and physical inspections) to assess their reliability/availability and performance ratio.

- ❑ Redesigning (retrofitting) and optimal sizing of the existing and new hybrid power systems (PV panels, batteries, regulators, etc.).
- ❑ Optimization to improve the system efficiency and performance ratio, the solar PV array availability/reliability, and minimizing the dumped PV energy from the oversized plants.

## 1.4 Significance of the Study

As already mentioned, the main challenge faced by Vodacom Lesotho is network instability on solar-powered BSs in rural areas as well as in unstable grids. The second major challenge is its incapability to meet capacity demands offered by the latest technologies such as the Long-Term Evolution (LTE)/4G in rural areas due to grid coverage gaps. As a result of the off-grid or bad-grid power challenges faced by Vodacom Lesotho, the business is only able to provide low data speeds (maximum 14 Mbps) in rural areas as it can only be able to provide basic 3G in 900 MHz spectrum, using single-radio sharing as opposed to acceptable speeds (42 Mbps) in 2100 MHz spectrum still using 3G technology but on grid-powered BS. With a proper BS site selection, monitored solar-powered BS, properly dimensioned and optimally sized hybrid solar PV plant, a BS with data rates of at least 150 Mbps in 4G technology can be designed for Vodacom Lesotho's rural BSs. The research is mostly concentrating on solar sites in rural areas, from the planning up to the commissioning of new solar PV-powered BS, and retrofitting of existing solar-powered BSs.

The primary beneficiary of this research is Vodacom Lesotho which stands to meet its network availability targets while also meeting capacity demand thereby achieving maximum potential revenue collections. The secondary potential beneficiaries are local competitors, Econet Telecom Lesotho (ETL), and other regional telecommunications companies with similar rural telecom sites as the optimized design can be replicated. The Government of Lesotho (GoL), through the Universal Service Fund (USF) sponsored projects, is also financing rural mobile network connectivity in 3G and 4G technologies. Therefore, the GoL also benefit in its USF projects and the implementation of digitization initiatives enhancing e-services to rural communities through telecommunication network services for high-speed internet technologies.

## 1.5 Report Outline

This research project is structured into five chapters. Chapter 1 details the introduction to the research problem, focusing on the importance of telecommunications networks and challenges faced by the MNOs, especially Vodacom Lesotho, in rural areas as a result of poor grid coverage, grid instability and its impact on climate change due to backup DGs. Chapter 2 delves into the theory and literature review concerning the factors affecting solar PV-powered BS performance, procedures and key equations used to improve the solar PV-battery systems efficiency, performance ratio, and reliability. Chapter 3 presents the methodology to be followed in this study for auditing, planning, optimizing and improving the efficiency of the solar-powered telecom BSs. Chapter 4 discusses the results obtained from the audited and optimized solar-powered BSs based on the recommendations and procedures from the literature review. In the last chapter, the results obtained from the optimization are summarized, and a conclusion and recommendations deduced from this research are provided.



## 2 THEORY AND LITERATURE REVIEW

### 2.1 Overview

A telecommunication network is made of a mobile node (mobile phone + SIM card) connected to a BS through the air interface and a core network through a transmission medium (microwave or fibre). BSs are the cornerstone component of the telecommunication network, consuming 50% to 80% of the total energy consumption and acting as the bridge between mobile phone devices and the core network [12,19]. BSs are composed of passive equipment such as primary power sources being grid, renewable energy (RE) or diesel generators, and secondary sources being backup batteries for storage. The tower structure and air-conditioners also form part of the passive and active equipment such as radio and transport devices acting as primary load with the purpose to provide both data and voice services for almost 24 hours a day in 365 days [18].

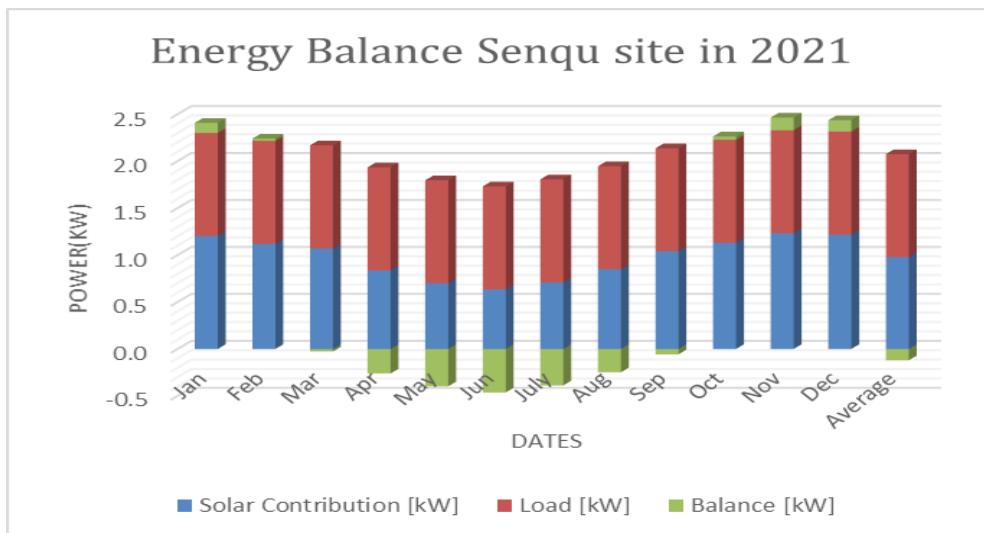


Figure 4: Vodacom Lesotho's base station solar plant performance against the load at Senqu - Thaba Tseka

Experience has revealed that rural network instability is mainly caused by poorly planned solar PV power plants and an increase in load demand due to radio capacity upgrades that do not match the supply, as shown in Error: Reference source not found. Error: Reference source not found shows the solar contribution from the 5.6 kWp solar array capacity powering a 1.2 kW load base station located at Senqu in the Thaba-Tseka district. The solar plant fails to meet the load demand, especially in the winter months of April to August, thus resulting in network instability. The current solution to this is the deployment of diesel generators to

supply the deficit, which contributes to carbon emissions and increases operation costs due to diesel generator (DG) refuelling and maintenance. Inadequately planned solar PV battery systems, lack of proper solar PV plant maintenance, poor solar array monitoring, and vandalism are identified as major challenges affecting Vodacom Lesotho solar PV battery powered rural BSs.

One of the findings anticipated to affect the rural network instability is shading caused by the tower structure itself as well as dust and bird droppings as illustrated in Figure 5. This instability does not only affect the quality of service to customers but also results in business revenue losses and carbon emissions as standby diesel generators have to be deployed. A couple of solutions and suggestions have been proposed to address this issue.



*Figure 5: Solar PV plant at Vodacom Lesotho's tower located in Qopo, Mokhotlong*

Various researchers have recently looked into the use of RE technologies for powering telecommunication towers, especially in rural areas and head offices, either integrated with the grid, energy storage, diesel generators, or any hybrid system to compensate for the RE intermittency [23]. Some of those studies were focusing on the techno-economic impacts of RE-powered telecom base stations but not the efficiency performance of solar plants powering the BSs which is the core task of the current research. The following sections details the theoretical and mathematical models used to improve the solar PV power plant system efficiencies as well as the key factors affecting the overall solar-PV battery systems in the telecom sector and their mitigation controls. The following section provides a summary of

the research gap analysis that needs to be bridged to improve the MNO's solar PV-powered BSs' efficiency, performance ratio and system reliability. The last section covers the procedures and criteria that need to be followed to select the optimum location to deploy a well-performing solar power plant.

## 2.2 Site Selection

In general, determining the location for solar PV power plant installation is essential since it not only impacts the solar plant's technical performance but also directly impacts the plant's economic, environmental, and social factors [5]. Figure 6 summarizes the multi-criteria decision-making (MCDM) technique or evaluation criteria mostly used to rate location sites that are considered feasible for solar PV power plants installation [22–24].

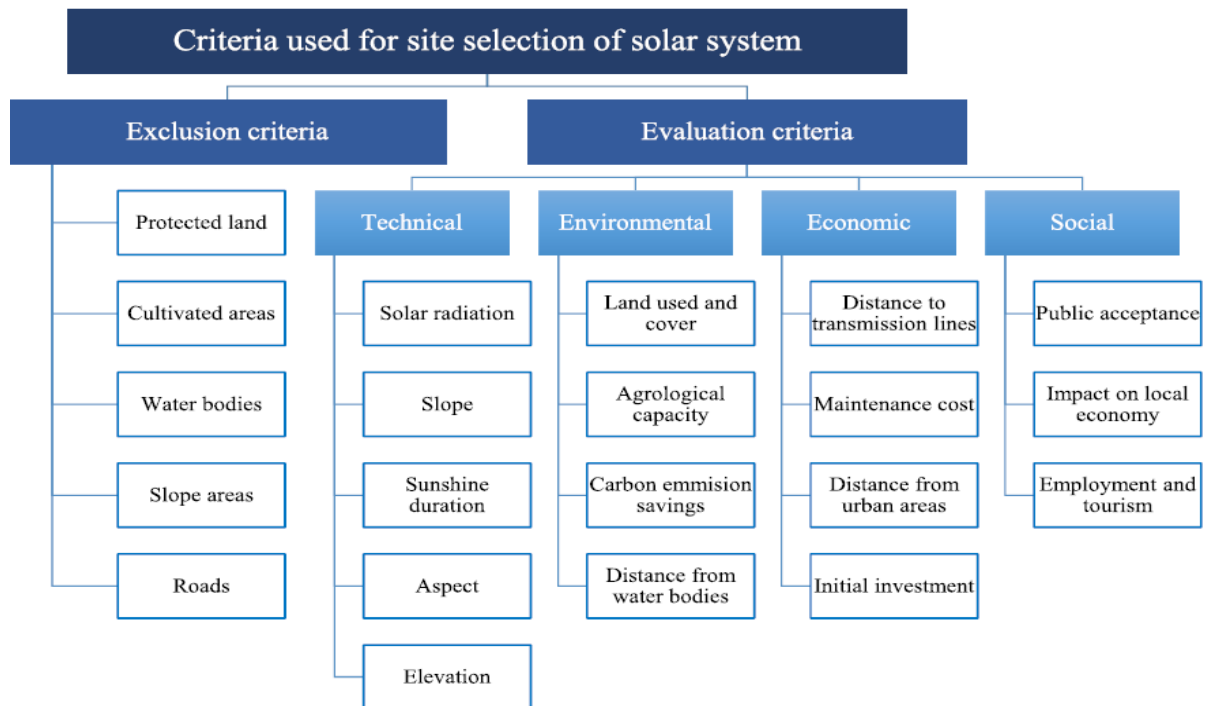


Figure 6: Evaluation Criteria for Selecting Areas Eligible for Solar Plant Installation [5]

An optimal site selection for efficiently performing solar PV power plants is a complicated process for energy planners and policymakers due to many conflicting criteria, hence the need for additional tools for a more informed decision-making [24]. To perform a proper site evaluation and selection for solar PV projects, the geographical information systems (GIS) tools and MCDM technique were found to be very useful [25]. The GIS has proved its primary role in exploiting geographical information for developing a spatial decision support

system for locating solar plants. Project designers use it worldwide to determine solar irradiance and temperatures in a particular area [23, 24]. While the MCDM technique offers a special benefit over single-criterion techniques, it also considers many criteria or qualities to achieve integrated decision-making results. Hence, it does not only assist in best location selection but also resource assessment, sustainability, project performance, and technological performance [21, 22]. Consequently, integrating both fields of GIS and MCDM yield common benefits and result in more reliable decisions for optimal solar site selection [25]. The following section details the best methods from the literature recommended in determining the load requirement and system sizing for the selected location.

### 2.3 Load Profiles and System Sizing

By the year 2022, the mobile internet user population was expected to have increased from 45.3% to 59.7%, while energy consumption in the telecommunication sector would have grown to 1700 TWh, and subscribers are estimated to be 8 billion by the year 2030 [33, 34]. To meet this demand, ascertaining the load profile is the most crucial task for the current type of research since an inaccurately determined load profile results in under-sizing or over-sizing the solar PV power plant, thus affecting both the system's reliability and overall capital cost [28].

The mobile network energy demand is dimensioned for maximum traffic load and assumed to be constant, especially on the outdoor Base Transceiver Station (BTS) without the air conditioner. However, the actual traffic load is unevenly spread, as described in Figure 7 [9]. Figure 7 shows a relatively constant load profile for a telecom BS with some spikes during peak time [9]. The telecom load, a BTS in this regard, is considered the primary load, and its radios configurations and specifications must be intensely analysed to determine the maximum power requirement [27]. The average power of a telecom tower is determined by the number of radios as well as the technology (2G/3G/4G and 5G), consuming 1 kW in rural areas to 8.5 kW in urban areas where more than 80% of the base stations are consuming 3.5 kW on average [30]. It is worth mentioning that over 60% of the DC power is consumed by the BTS power amplifiers (PA). Therefore, optimized use of the PAs and implementing energy-saving features improve energy efficiency [22]. The motivation for optimized green cellular networks is not only due to the rising energy cost and lack of access to the grid in rural areas but also the need for carbon emissions reduction from backup DG [9].

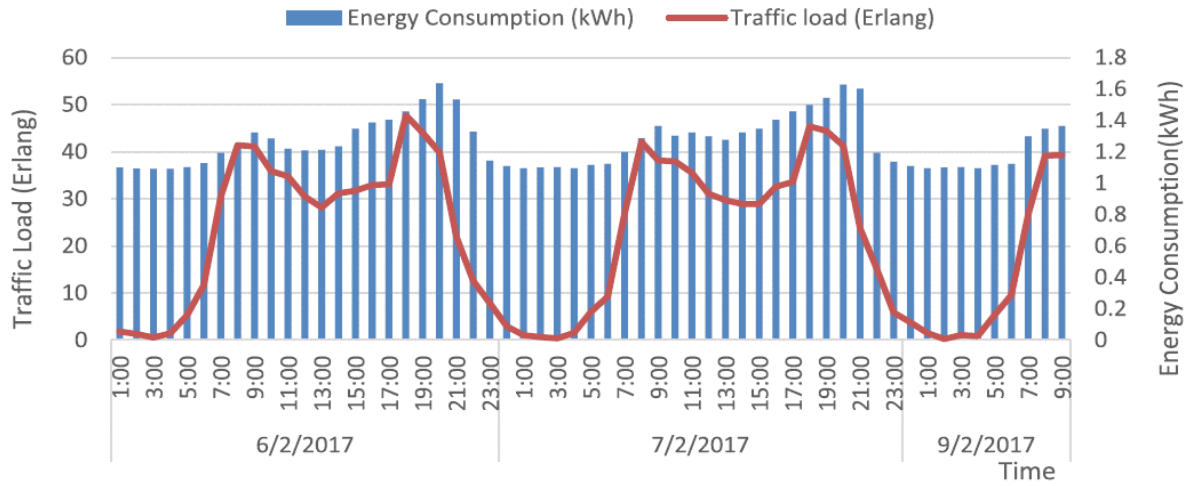


Figure 7: Sample BTS energy consumption and traffic load [9]

After the telecom load profiles' analysis, the second crucial step is the solar PV-battery system sizing, which completely depends on the base station components' power consumption. The optimal design of solar/battery/diesel generator hybrid power generators calls for adequate sizing of components as well as a viable energy management strategy [28]. It should also be emphasized that using proper optimization sizing techniques can assist in ensuring maximum power reliability at a minimal system cost that is also scalable for future demands [30].

As shown in Figure 8, a typical hybrid system is composed of four fundamental components: Primary sources depending on available resources such as solar PV and wind, secondary sources of energy such as batteries for storage or diesel generator, a solar PV charge controller or system regulator, and lastly, an inverter/converter where there is alternating current (AC) load [8, 36]. Due to the intermittent nature of many RES, especially solar PV arrays, since it can only be harvested during the day, it is crucial to integrate it with more than one source for a reliable system forming a hybrid renewable energy system (HRES) [32]. To model a solar PV array and battery capacity (series/parallel combination) that matches the daily energy requirement even on cloudy days, an Excel spreadsheet is usually used. Additional optimization software such as Hybrid Optimization Model for Electric Renewables (HOMER) is mostly used [33]. HOMER is the most commonly used tool for hybrid system optimization and sensitivity analysis with the maximum combination of renewable energy systems among the 19 preferred tools. HOMER can also reduce the complication of accessing the meteorological database and industrial components [34].

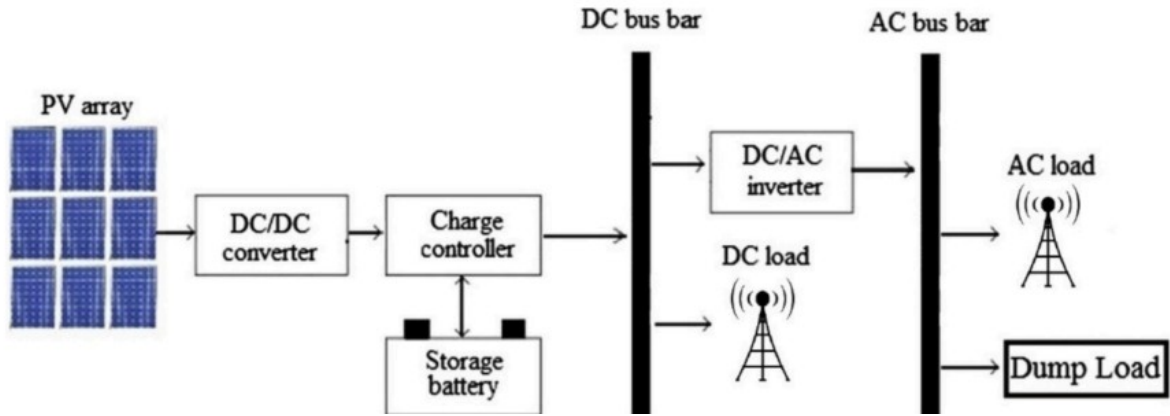


Figure 8: A simple illustration of the telecommunication base station [31]

The solar PV power harnessed during PSHs (kWh/m<sup>2</sup>/day) has to meet the daily load demand with an excess to be stored and used during the intermittence from the backup batteries. Solar PV power can be calculated by the below mathematical expressions [6, 17]:

$$P_{pv} = \dots\dots\dots (1)$$

$$P_{pv} = \left( \frac{\eta_{pv}}{\eta_{cell}} \right) \times \left( \frac{G_T}{G_{T,STC}} \right) \times P_{pvSTC} \dots\dots\dots (2)$$

$$P_{pv} = H_T A \eta_{cell} \dots\dots\dots (3)$$

whereby  $P_{pv}$  is the solar PV power in kW;  $P_{pvstc}$  is the solar module rated capacity under the standard test conditions also in (kW);  $f_{pv}$  is the derating factor of solar PV (%);  $G_T$  is the incident solar irradiation on a horizontal plane (kW/m<sup>2</sup>);  $G_{T,NOCT}$  is the solar irradiation under the standard conditions (800 W/m<sup>2</sup>);  $\alpha_p$  is the temperature coefficient of power (%/°C);  $T_c$  is the temperature of the solar PV cell in °C in the current time step; and  $T_{c,NOCT}$  is the nominal operating cell temperature (NOCT) of the solar PV cell under the standard test conditions (25 °C);  $\eta_{pv}$  is the onsite efficiency of the solar PV generator due to temperature changes.

Solar PV cell temperature  $T_c$  can be calculated by ..... (4 [33]:



$$T_c = \frac{(T_c - T_{a,NOCT}) \left( \frac{G_T}{G_{T,NOCT}} \right) \left[ 1 - \frac{\eta_{mp,STC} (1 - \alpha_p T_{c,STC})}{\alpha \tau} \right]}{1 + (T_c - T_{a,NOCT}) \left( \frac{G_T}{G_{T,NOCT}} \right) \left( \frac{\alpha_p \eta_{mp,STC}}{\alpha \tau} \right)} \dots\dots\dots (4)$$

whereby  $T_{a,NOCT}$  is the ambient temperature at which the NOCT is defined (20 °C);  $\eta_{mp,STC}$  is the maximum solar PV module power efficiency under standard test conditions (%);  $\tau$  is the solar transmittance of any cover over the solar PV array (%); and  $\alpha$  is the solar absorptance of the solar PV array (%) [28].

Once the required solar PV power and system voltages are determined, the number of modules and their connections (series/parallel) can be decided. Solar PV modules are available in different nominal voltages, different cross-sectional areas/sizes, with different technologies, and different wattages [33]. The second crucial component is the solar PV charge controller or solar regulator specifically for threshold settings and monitoring. A solar PV charge controller is not only used to charge the backup batteries by regulating and controlling the output from the solar PV array, but it also protects the batteries from being over-charged or over-discharged [33]. The solar PV charge controller voltage must be compatible with both the input voltage from the solar PV array and the nominal system voltage. It must also be capable of handling the maximum current produced by the solar PV array. Globally, there are two different topologies of solar charge controllers available: the maximum power point tracker (MPPT) and the pulse width modulation (PWM) [36, 37].

The MPPT has proved to have better performance compared to the PWM controller. One of the main characteristics of the MPPT is its ability to harvest maximum power by maintaining the solar PV array to operate at its maximum power point (MPP) while supplying the load and storing the surplus [8]. Previous studies proved that the number of solar modules connected in series results in voltage mismatch between the solar PV array and the MPPT/PV Chargers during low radiation phases thus negatively affecting the solar PV power plant PR. Therefore, it was observed that by optimizing the number of solar PV modules within the string with two additional solar PV modules, the output voltage increased to match the MPPT range of the inverter under low radiation levels and the solar PV plant's PR increased by 4.55% [35].

MNO base stations are mostly designed for 100% system reliability, hence the need for energy storage to provide backup power during RE intermittence, night traffic and grid instabilities [38]. As a result, the integration of energy storage technologies such as backup batteries is very critical as it does not only minimize the use of DGs but it also improves RE utilization, stabilizes operating system voltage and current, and maintains the system's reliability by providing the required power in the event of a production deficit [6, 36, 37]. A battery cell is defined as an electrochemical energy conversion device that converts chemical energy stored in the constituent components directly into electrical energy and it is expressed in units of ampere-hours (Ah) [33]. The solar PV generator needs to be oversized so that the surplus DC can be captured for storage. At real-time conditions, the solar PV output current can be determined using..... (5:

$$I_{pv}(t) = \dots\dots\dots (5)$$

where  $I_{pv}(t)$  is the current output of solar PV power plant at time  $t$ ,  $n_{pv}$  is the number of solar PV modules or solar PV arrays in parallel for constant voltage output, and  $I_r$  is the rated current output of a solar PV panel at STC [41].

Both the peak load and system starting current depend on this solar PV output current, thus making it very crucial to determine the state of charge (SOC) at any given time. SOC is defined as the level of charge of an electric battery relative to its rated capacity. It can be expressed by .....(6[28]:

$$SOC(t) = SOC(0) + \eta_c \sum_{k=0}^k P_c(k) + \eta_d \sum_{k=0}^k P_d(k) \dots\dots\dots (6)$$

where  $SOC(t)$  is the SOC value at time  $t$ ;  $SOC(0)$  is the initial SOC value;  $k$  is the time index;  $P_c$  is the charged energy (kWh);  $P_d$  is the discharge energy (kWh);  $\eta_c$  is charging efficiency (%) ranging between 65% and 85%; and  $\eta_d$  is the discharging efficiency (%) and equal to 100%.

Battery selection during system sizing depends on the cost and other technical parameters such as the amount of energy required per day, depth of discharge (DoD), cycles and calendar life, energy density and specific energy, and the wide operating temperature range [8,37]. To determine the total battery capacity, the following have to be established: the efficiencies of



the inverter charger, nominal system voltage, the recommended DoD of the selected battery, and days of autonomy (that is, the maximum number of days with minimal sun intensity). The required battery storage capacity can be expressed by **Error: Reference source not found** [33]:

$$\text{Battery Capacity} = \frac{Wh / (\text{day}) \times \text{Days of autonomy}}{\eta_{inv} \times \eta_{battery} \times DoD \times V_b} \dots\dots\dots (7)$$

where  $\eta_{inv}$  is the system inverter charger efficiency,  $\eta_{battery}$  is the battery charge and discharge inefficiency, and  $V_b$  the system battery's nominal voltage.

## 2.4 Solar Plants Efficiency / Key Performance Indicators

Having understood the load profile, power requirement, and system components sizing, the next step is to understand the key parameters that affect the overall system performance. This section covers the theories and mathematical equations behind solar PV-battery system key performance indicators. Solar PV cells are semiconductor materials that have the potential of developing electron-hole (negative and positive charges) pairs when solar energy is incident on them thus converting that solar energy into direct current [22,30]. The efficiency of a solar cell or PV cell refers to the fraction of the incident solar energy reaching the solar PV cell that can be converted to usable electrical energy. It can be determined using ... ..(8 [35]:

$$\eta_{cell} = \frac{I_{mp} V_{mp}}{S A} \dots\dots\dots (8)$$

where  $I_{mp}$  and  $V_{mp}$  are the current and the voltage of the maximum power point respectively,  $S$  is the solar radiation falling on the tilted solar PV module surface in  $W/m^2$ , and  $A$  is the total surface area of the solar PV cell in  $m^2$ .

The same efficiency definition still hold for solar PV array efficiency. The solar array is a series and/or parallel connection of the solar modules. Solar PV array efficiency can be calculated by

$$\dots\dots\dots (9 [35]:$$

$$\eta_A = \frac{P_{DC}}{SA} \dots\dots\dots (9)$$

where  $P_{DC}$  is the output power of the solar PV array in W.

The overall efficiency of the solar PV arrays does not only depend on the material used to manufacture solar cells but also on the seasonal and weather conditions [42]. Solar PV modules' efficiency ranges between 17–22% under certain standard conditions with the latest technologies reaching a higher efficiency of 24.7% [42]. However, owing to the intermittent nature of solar energy resources, it is necessary to integrate more than one source for a reliable solar power plant hence forming a hybrid system [32]. Therefore, to determine the overall hybrid system efficiency, each component of the system such as the inverter-converter has to be understood [35]. The inverter-converter efficiency can be described by

$$\eta_{inv} = \frac{P_{inv}}{P_{DC}} \quad \dots\dots\dots (10)$$

where  $P_{inv}$  is the output power from the inverter-converter in W.

Another critical KPI used to evaluate solar plant performance is the performance ratio (PR) [16, 19]. The PR describes the ratio of the total output energy from the system to the theoretical generating system capacity and reflects the total loss of the solar PV system inclusive of the solar PV array and the inverter conversion [35]. It is thus a measurement indicator for how close a solar power plant approaches ideal performance during real operation [21]. Daily solar PV plant PR value is significantly affected by irradiation and ranges between 40% and 70% [35]. For a well-optimized solar power plant, PR can reach 0.89 which is very high compared to the 0.75 recommended by the International Energy Agency (IEA) [35]. Worldwide, the mean annual PR has shown an increasing trend from 0.64 to 0.74, while the previously analyzed Moshoeshoe I Airport solar power plant in Lesotho averaged at 0.70, with monthly ranges of 0.35 to 0.79 [21]. PR can be calculated by

$$PR = \frac{E}{G_T A_{p_{pv}} \eta_{cell}} \quad \dots\dots\dots (11)$$

where  $E$  is the solar power plant output energy or power measured in (kWh or kW),  $G_T$  is the irradiation received by the solar PV array per unit area over some time in kWh/m<sup>2</sup> or W/m<sup>2</sup>.  $A_{p_{pv}}$  is the solar PV array area in m<sup>2</sup>, and  $\eta_{cell}$  is the solar PV module efficiency at NOCT.

As per the Bureau of Indian Standards, the PR shows the overall effect of the rated solar PV array's losses as a result of solar PV cell temperature, incomplete use of incident radiation to

solar PV collectors, and system components such as solar PV module and solar PV chargers inefficiencies or failures [43]. Performance ratio can also be defined as the ratio of actual output power to the expected output power for a given reporting period based on the system rating and can be expressed by

$$PR = \frac{Y_A}{Y_R} \quad (12) \quad [23, 47]$$

where

$$PR = \frac{Y_A}{Y_R} \quad (12)$$

where  $Y_A$  represents kWh/kW PV array energy yield (DC output power) and  $Y_R$  is [kWh/kW] reference yield (rated DC power) as defined in IEC. The reference yield  $Y_R$  can be calculated using the location radiation on the horizontal plane and/or the tilted solar PV array structure using

.....(1 or

..... (2. The next subsection discusses the key factors which affect solar plant performance.

## 2.5 Factors Affecting Solar Plants Efficiency and Mitigation Controls

The solar PV panel technical specifications summarize the electrical characteristics such as the rated maximum power output ( $W_p$ ), solar panel short-circuit current ( $I_{sc}$ ), and open-circuit voltage ( $V_{oc}$ ) as per supplier [45]. These rated parameters are obtained under special test conduction such as the STC or NOCT. Hence any deviation from these standard conditions results in a significant drop in the solar module performance as well as the solar array performance [46]. The maximum solar PV current ( $I_{mpp}$ ) and corresponding maximum voltage ( $V_{mpp}$ ) can also be obtained from the same specifications. They are used to determine the solar PV's maximum power point (MPP) summarized in Figure 9 [8].

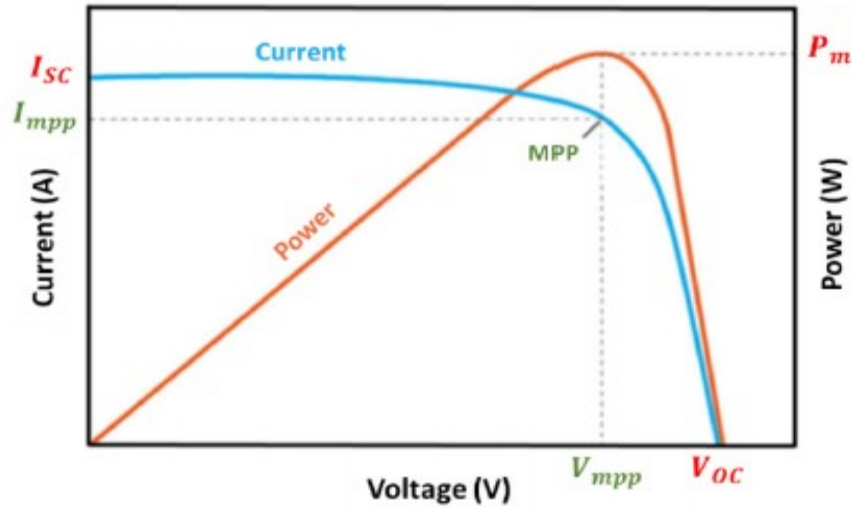


Figure 9: Solar PV Module P–V and I–V Curves Showing Maximum Power Point [8]

Apart from these parameters, other external factors which affect the overall solar power plant performance include partial shadings such as soiling and dust, solar radiation, solar PV module tilt angle, ambient temperature and humidity [35, 36]. The major factors affecting solar array performance are introduced in Figure 10 and is covered in more detail in the next subsections [8].

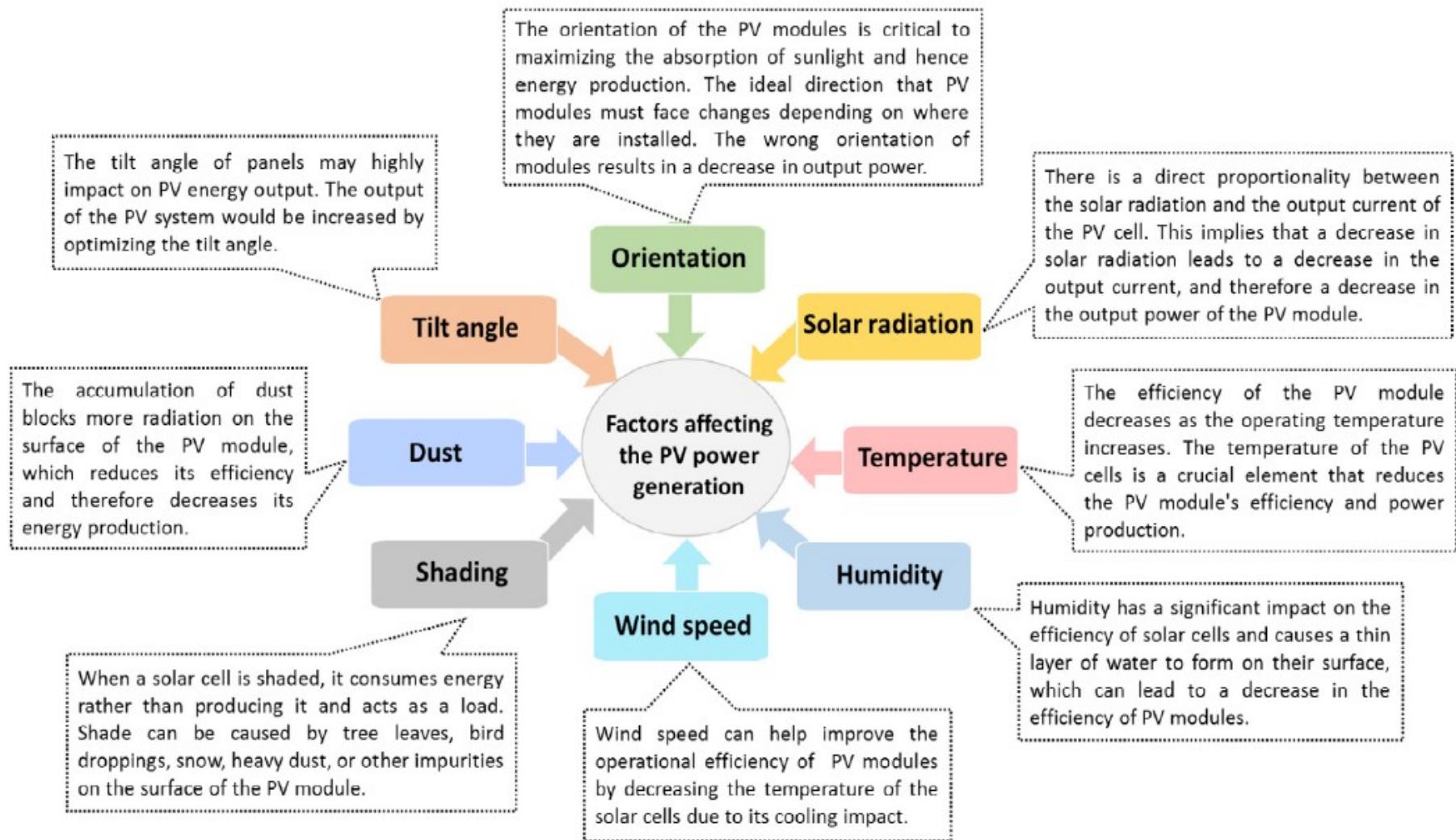


Figure 10: Main contributors that impact the overall performance of the solar PV Plants [8]

### 2.5.1 Solar Radiation

The intensity of solar radiation hitting the solar PV module's cross-sectional area plays a substantial role in deciding the power generated by the solar PV modules [48]. It is worth mentioning that the eminent solar radiation and ambient temperature way above test conditions lead to a high operating solar PV cells temperature  $\dot{\iota}$ ) therefore reducing its power production and lifespan [8]. Figure 11 shows that the solar panel output current is directly shaped by the variation in irradiance as it increases with the solar radiation incident on it. Hence the reduction in power as irradiance decreases, whereas the open-circuit voltage remains approximately unchanged [8]. It can be safely concluded that the solar PV MPP decreases with a decreasing level of irradiance received by the solar module. The solar PV power plant PR also decreases severely in the winter or on cloudy days with low radiations [16, 41].

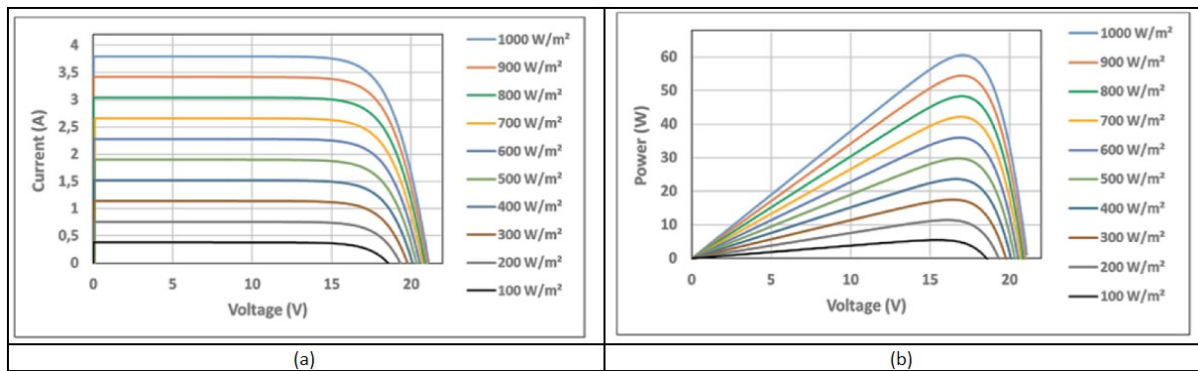


Figure 11: (a) I-V and (b) P-V characteristics at a constant temperature but varying solar radiations [8]

### 2.5.2 Temperature

High solar PV module temperature is caused by the surplus energy as well as the photon energy which is below the solar PV cell band gap energy that is not used during electricity conversion hence converted into heat energy [50]. The second factor which increases the cell temperature is partial shading by causing a hot-spot phenomenon on the shared PV cells [51]. Previous findings reveal that an increase of  $1^{\circ}\text{C}$  in the solar PV cell's temperature reference to the nominal temperature of  $25^{\circ}\text{C}$  results in a 0.2% to 0.5% drop in its electrical power production [4, 46]. Figure 12 shows the temperature effects on a solar module against the corresponding electrical efficiency on a hot summer day and the impact of the increase in the surface temperature on different types of solar PV panels which results in a significant reduction in power production [50]. Moreover, it is important to note that an increase in cell

temperature causes a slight increase in the short-circuit current ( $I_{sc}$ ) while significantly decreasing the open-circuit voltage ( $V_{oc}$ ) which results in an overall decrease in MPP [45].

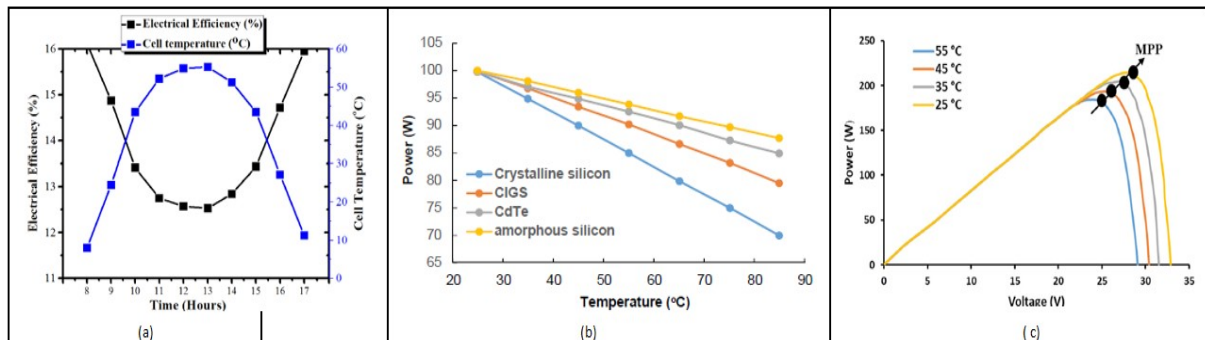


Figure 12: (a) Solar cell efficiency decrease, (b) Solar cell power decrease with an increase in temperature, and (c) MPP variation with voltage and temperature [35,46]

To foreclose catastrophic damage to the solar PV module due to an increase in temperature and improve its efficiency, solar PV cooling systems and other thermal control techniques are used to suppress the high temperature in the solar PV cells and try to maintain it as close to its nominal operating temperature as possible [4, 46]. Apart from installing solar PV systems on floating structures like dam reservoirs, there are two main types of cooling systems, namely, passive and active cooling systems [42, 47]. Passive cooling systems refer to the integration of other technology such as the use of the thermosiphon effect with solar PV technology to reduce the temperature of the solar PV module by absorbing heat from it without consuming additional energy [8]. Active cooling systems refer to the integration of other technologies which are energy-consuming devices such as fans or pumps to draw out the heat from the solar PV panels.

Several investigations in the literature proved that a 12% to 60% increase in solar PV energy efficiency could be obtained by cooling the solar PV cell when experiencing high temperatures by using a possible and affordable cooling system [8]. The use of floating technology alone decreases the solar PV panel's temperature and their efficiency can be enhanced by up to 12% on average and by about 20% during hot summer days [8]. Theoretically, when the solar irradiance reaches the highest value of  $1000 \text{ W/m}^2$  and the lowest PV cell temperature value, the open circuit voltage is the maximum value resulting in maximum power production [35].



### 2.5.3 Soiling and Shading

The accumulation of dust on the solar PV panels commonly known as soiling severely affects the visible light's absorptance and transmittance of the solar panel covering glass; this in turn significantly reduces or completely blocks the incoming sunlight hence impacting the power generation efficiency of the solar PV modules [5, 34, 37]. Dust can be defined as any material or particle obtained in the atmosphere with a diameter less than 500  $\mu\text{m}$  including solid organic and inorganic particles such as smoke, soil particles, volcanic vapor, microfibers, bacteria, fungi, pollen, and limestone erosion [34].

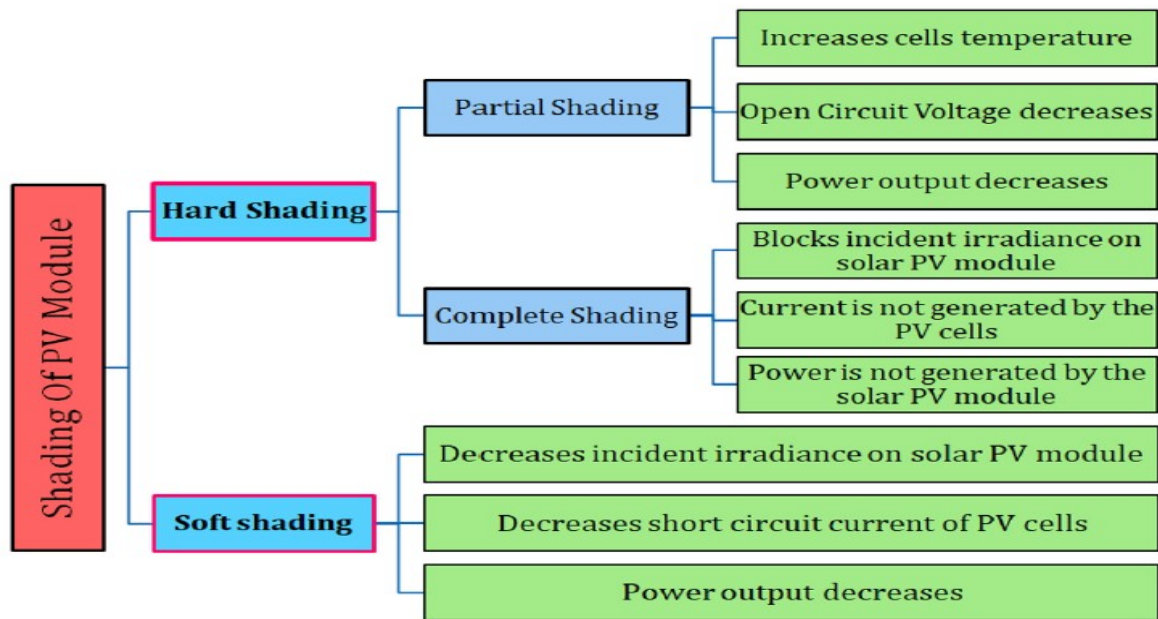


Figure 13: Types of shadings on the solar PV module [45]

There are two types of shading, namely, soft shading and hard shading as summarized in Figure 13 [45]. Soft shading happens when particles are randomly scattered on the surface of the solar PV module through the atmosphere, while hard shading takes place when a solid with a definite shape such as accumulated dust, snow, or bird dropping exists on the front surface of the solar PV module. Hard shading can further be categorized into two, namely, complete and partial shading [45]. Complete shading occurs when all the solar PV cells in a solar PV module are shaded and do not produce any power while in the case of partial shading, the solar PV module decreases the open circuit voltage (Voc) therefore reducing the maximum power output of the solar PV module. Partially shading the solar PV module can also heat the shaded cells introducing hot spots on the surface which damages the solar PV module and decreases its overall efficiency [45]. That is, during partial shading conditions



(PSC), some of the shaded solar PV modules in an array become reverse-biased and act as a load forming the hotspot issues and consuming the current instead of supplying [48, 49].

Soiling can also result from pollution, deposition of particulates and organic contaminants, bird droppings, algae, lichen, mosses, agricultural emissions, and engine exhaust fumes in urban areas [15, 35, 44]. Figure 14 summarizes the different types of soiling due to pollution on the solar glass covering the solar PV modules. Bird droppings cause soiling and to some extent completely block the incident sunlight from reaching the solar PV surface or a few solar cells leading to the emergence of hot spots on a solar PV module hence reducing power generation [48]. A solar PV module with dust has a 10°C higher temperature than that of a clean surface [45]. Some key parameters that were found to accelerate soiling are:

- (i) **Surface properties of solar PV modules:** The properties of the solar PV panel coating material properties significantly impact the soiling processes; it was found that the glass cover is less affected by soiling compared to the Tedlar cover [48].
- (ii) **Tilt angle and orientation:** Solar PV module tilt angle and orientation also regulate the soiling processes. Some experiments showed a 19%–47% decrease in the average dust deposition density for each 30° increase in the tilt angle (0–90°) [48].

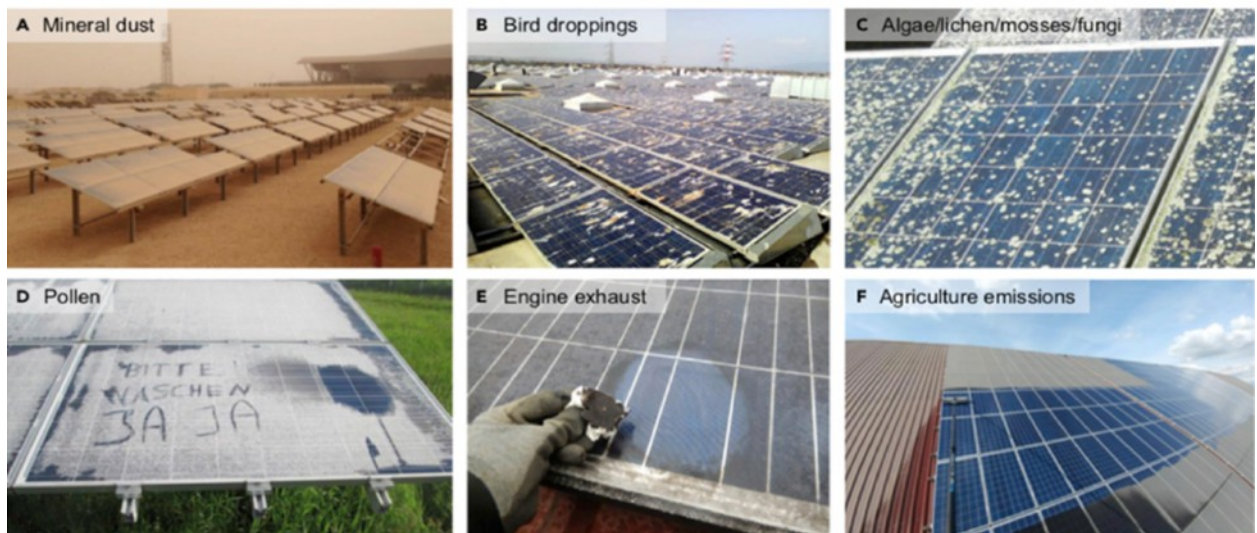


Figure 14: Different types of soiling resulting from (A) mineral dust in a desert area, (B) bird droppings, (C) algae, lichen, mosses, or fungi, and (D) pollen in wet and moderate climates, (E) engine exhaust from an industrial area, and (F) agriculture emissions [55]

For that reason, adopting appropriate shading or soiling mitigation strategies can assist in minimizing the solar PV energy yield loss, maximizing the lifespan of the solar PV modules, and increasing solar PV reliability hence increasing net profits associated with solar PV investment [55]. Soiling mitigation and efficiency improvement techniques can be categorized into restorative and preventive techniques including natural cleaning, manual cleaning, mechanical cleaning, anti-soiling coating, using DC optimizers (DCO), solar PV array reconfigurations, and electrodynamic dust shields. This can be summarized as shown in Figure 15 [42, 44].

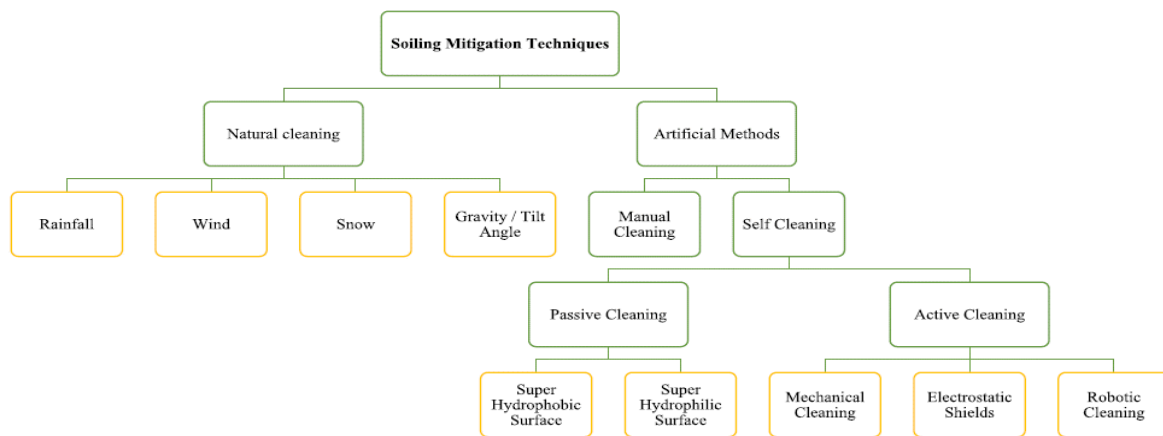


Figure 15: Soiling Mitigations Techniques [46]

Although natural cleaning by rain, wind, and melting snow was believed to be an arguable solution for restoring solar PV efficiency to nearly its rated capacity with zero cost, in recent studies by various research groups, it has been found that mild rain showers, low wind speeds, tilt angle and orientation, and other additional moisture such as heavy morning dew cause soiling [42, 44, 48]. Findings reveal that 2.2 mm of rainfall has a 50% probability of removing dust on the surface of solar PV modules while the wind effectively removes large dust particles greater than  $1\mu\text{m}$  in diameter making both of them unreliable solutions hence the need for other mitigation controls [35, 44]. Manual cleaning: this cleaning technique is similar to normal practices of cleaning building glass where special bristled brushes with water, often coupled with detergents are used to avoid scratching solar PV modules [15, 35]. Manual cleaning of solar PV modules is one of the cheapest cleaning and widely used procedures with close to 100% soiling removal efficiency for low-capacity solar PV plants [48]. However, if solar PV plants are placed in remote areas and are installed in large capacities, manual cleaning is not only difficult, labor-intensive, and time-consuming but

prohibitively expensive hence triggering a need for other alternative mitigation techniques [44, 48].

Lately, soiling mitigation techniques such as self-cleaning with anti-reflective and anti-icing super-hydrophobic and super-hydrophilic have been used to eliminate or reduce the accumulative dust; these can improve solar PV module efficiency by up to 71.8% without any components or water [45]. When rainfall water droplets fall on a hydrophilic solar PV module surface, they penetrate the fouling layer under the surface and with the proper tilt angle slide away from the surface, removing dust particles with them [55]. However, to attain a fully usable self-cleaning technique for coated solar PV modules, the following three criteria must be satisfied [55]:

- (i) Remarkable dust repelling, i.e., self-cleaning/anti-soiling/easy-to-clean.
- (ii) Optical transmission that is greater or the same as the solar glass cover itself.
- (iii) Excellent durability with life expectancy close to the solar device.

## 2.6 Solar PV Array Tilt angle

One factor that proved to increase the amount of harvested solar radiation is the solar PV module tilt angle and its orientation whereby the adjustment of 2° increased annual energy production by 1450kWh compared to the traditional tilt angle method or the rule of thumb that the tilt angle equals the latitude [48, 50]. Some researchers reveal that solar radiation varies not only with latitude but also with elevation changes; therefore, using the location's solar radiation data, the precise optimal tilt angle for a selected area must be assessed [56]. Still, other studies recommend a fixed tilted angle of latitude  $\pm 5$  degrees from the horizontal plane [33]. Other research studies demonstrated that when solar PV arrays are fixed at the optimum tilt angle and azimuth angle an increase of 9% to 11% solar insolation can be obtained per annum [57]. While in South Africa, a country fully surrounding the Kingdom of Lesotho, an additional 10% of solar insolation can be harvested from the optimal tilted solar collector as opposed to the horizontally-fixed solar PV array [57]. The same research measurement concluded that any solar PV module fixed at 30° tilt angle, located in South Africa facing north (magnetic or true north), should be able to harvest 98% of the maximum solar radiation per annum. The obtained tilt angle varies from + 2.6 to 6.9 from the test location latitude. The optimal azimuth ( $\Psi_{opt}$ ) can be expressed as the function of latitude ( $\sigma$ ) as per ..... (13 [57]).

$$\Psi_{opt} = 12 \sin(18\sigma + 105) - 2 \dots \dots \dots (13)$$

The solar irradiation received by the solar PV panel depends on the tilt angle and can be estimated by converting the horizontal irradiation obtained from the NASA database or other weather stations into actual solar radiation received at any tilt angle using the Hay Model described in .....(14 [35]):

$$H_T = H_b R_b + H_d \left[ \frac{R_b H_b}{H_o} + 0.5 \left( 1 - \frac{H_b}{H_o} \right) (1 + \cos \beta) \right] + 0.5 \rho H (1 - \cos \beta) \dots \dots \dots (14)$$

where  $H_b$  is the daily direct irradiation on the horizontal plane measured in kWh;  $H_d$  is the daily horizontal diffuse irradiation in kWh;  $H_o$  is the daily extraterrestrial irradiation on a horizontal surface in kWh;  $\rho$  is the surface reflectance, and generally takes 0.2;  $H$  is the total horizontal irradiation in kWh;  $\beta$  is the tilt angle and  $R_b$  is the ratio of the direct irradiation of the inclined plane to that of the horizontal plane.

**Figure 16** summarizes the most commonly used mitigation techniques that can be used to improve the overall solar PV plant system efficiency [8]. The important factors which affect the PV generator performance as summarised by IEC 61724 are in-plan irradiance incident to the PV array, cell operating temperature and losses due to soiling [44]. Secondary to these major factors as per the same report, there are the MPPT restrictions/limitations and other system component losses.

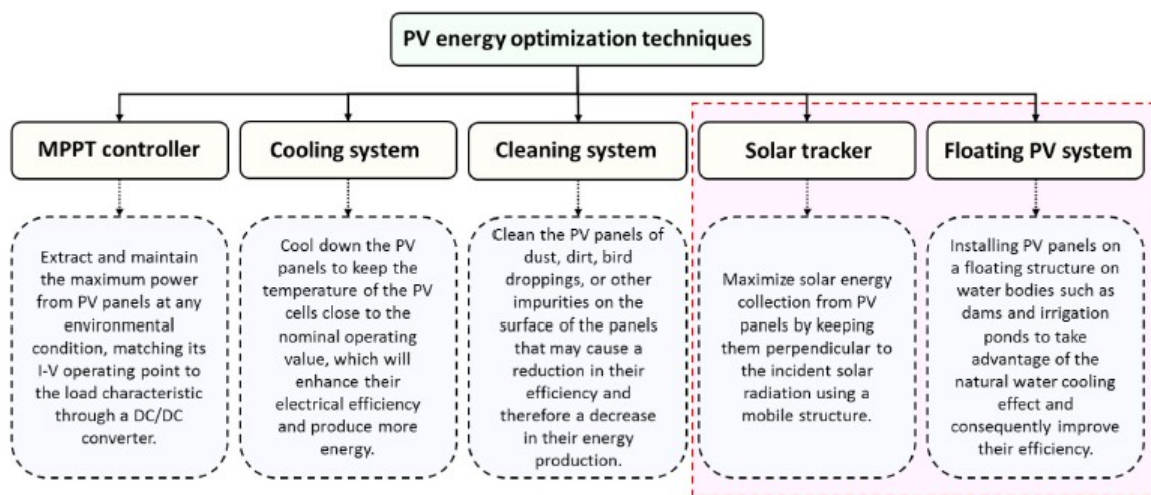


Figure 16: Summary of popular techniques used to enhance solar PV system efficiency [8]

## 2.7 Research Gap Analysis

Based on the comprehensive literature review, it has been found that most researchers have focused on the performance assessment of solar PV-Grid hybrid systems for residential and

other industrial sectors not on the solar PV–battery systems for the standalone telecom base stations. As a result, the identified gap is the lack of specific literature on the key factors affecting the solar PV plants planned for telecom access networks leading to network unreliability and high operational cost. To bridge this gap, the current research undertakes an audit of Vodacom Lesotho solar PV-powered base stations mostly in the rural areas of Lesotho and assess/analyse their physical and electrical installations, load profiles, energy consumption and traffic patterns while identifying key factors with significant contributions to the overall performance ratio. This is followed by applying some of the recommended procedures in optimal system design such as site location, load profiling/determination and component sizing as covered in the methodology chapter.

### 3 RESEARCH METHODOLOGY

#### 3.1 Methodology Overview

This chapter presents the three-step methodology to be followed in this study for planning, optimizing and improving the system efficiency for the off-grid telecom towers or solar PV-powered BSs. It involves undertaking optimal hybrid solar PV system design modelling for new telecom BSs, applying the identified optimal design principles to audit and assess selected existing Vodacom Lesotho solar-powered BSs, making simulations and recommendations for redesigning or retrofitting poorly-performing BSs for the improved solar PV-battery system performance and BS network availability as illustrated in Figure 17.

Each of the main methodological steps is made up of several smaller processes and procedures that have been adapted from recommendations, theories and equations in the preceding literature review. The main objective of the current study is to design an optimal hybrid solar PV battery system that meets both the MNO's and the regulator's KPIs at the minimum cost possible.

Based on the design gap, findings between audit/assessment results, historical load profile data analysis from the existing BSs Solar PV charger controllers' database, obtained PR, optimization and optimal system sizing recommendations; the solar PV-battery system plant redesigning or retrofitting are implemented. The post results after redesigning are expected to give system efficiency improvements or gains. Therefore, the same process and recommendations are used for planning new solar PV-powered base stations as well as grid-to-solar BS migration. Meteonorm software was used to collect annually meteorological data to simulate the solar PV Plant performance. The results obtained is compared with the historical data from existing BSs and determining the PR using Microsoft Excel. PVGIS typical meteorological year (TMY) generator tool is used to determine the monthly radiation to monitor the annual performance, while HOMER was only used to determine the location clearness index.

In summary, the methodology adopted follows this sequence: first, the meteorological resource assessment for selected BSs was analysed, followed by load determination using the daily energy balance method (DEBM) as well as the time step method (TSM); based on the determined load requirement results, the optimal design procedure as per the literature to size the solar array, inverter/PV charger and battery capacity were followed and the results

obtained are compared with the existing BS configuration for the system redesigning to achieve the optimal system that meet the above-mentioned targets as well as the recommended PR [19, 22, 37, 46]; using the generated solar PV power ( $P_{pv}$ ) profiles from the BS historical data logs, the installed rated solar PV array peak capacity and the location radiation data, the PR for each BS are determined using performance ratio equations described in the literature review.



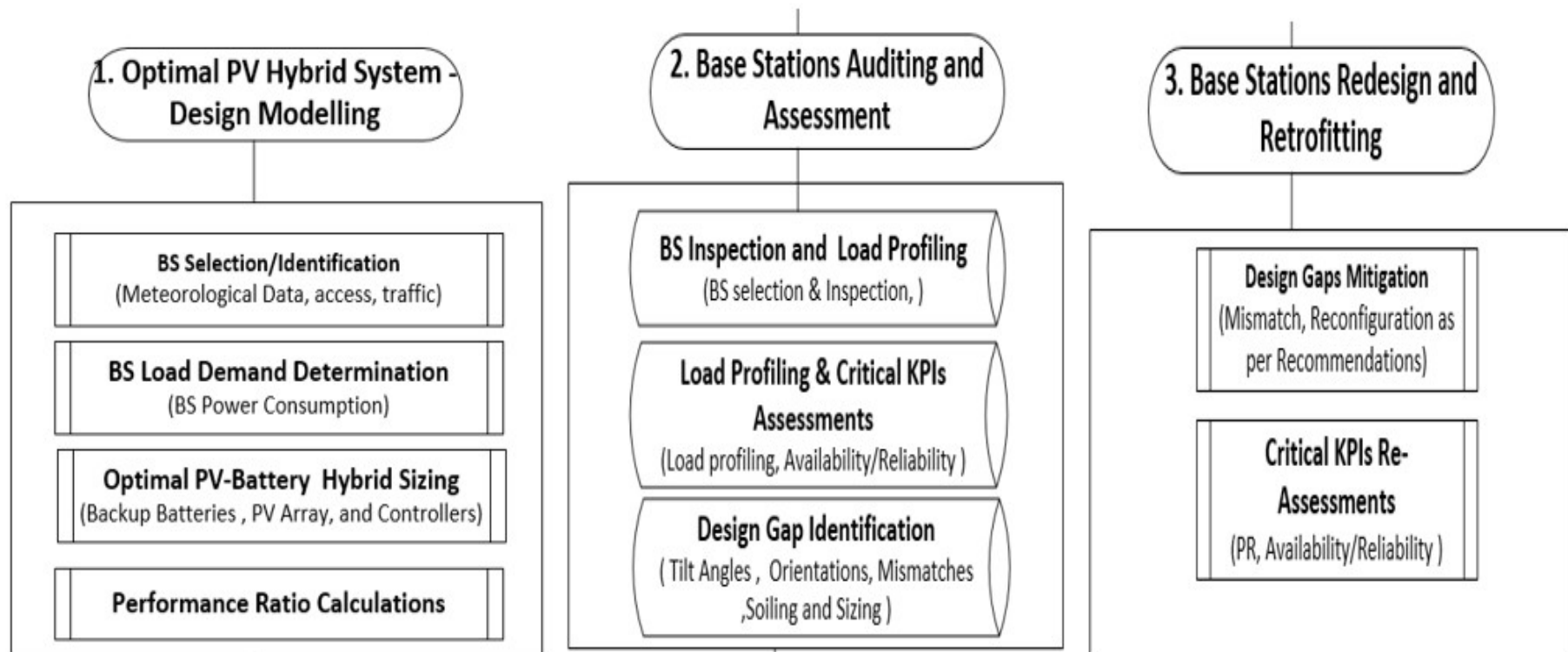


Figure 17: The research methodology flow chart



### 3.2 Base Station Meteorological Data: Site Selection

The meteorological data of the selected BS location were analysed and used to determine the solar PV power variations which the plant can generate on the horizontal and tilted plane under the selected cell temperature as per .....(1 and ..... (2. Both PVGIS typical meteorological year (TMY) generator tool and Meteornorm were used for both hourly radiation and ambient temperatures to determine the expected solar PV power based on the mathematical equations from the literature. HOMER and Meteornorm software were used for the monthly solar PV resource assessment for the selected BS location including monthly radiation data such as global horizontal radiation, clearness index, precipitation and ambient temperatures. The meteorological data was used to compute the expected output PV power and this was compared with the actual PV power for the generator to determine the solar PV generator performance ratio. The PVGIS average daily monthly energy production from the given system in (kWh/d) were used in determining the location of peak sunshine hours (PSH) for optimal design and design month.

### 3.3 Base Station Load Assessment

#### 3.3.1 System Description

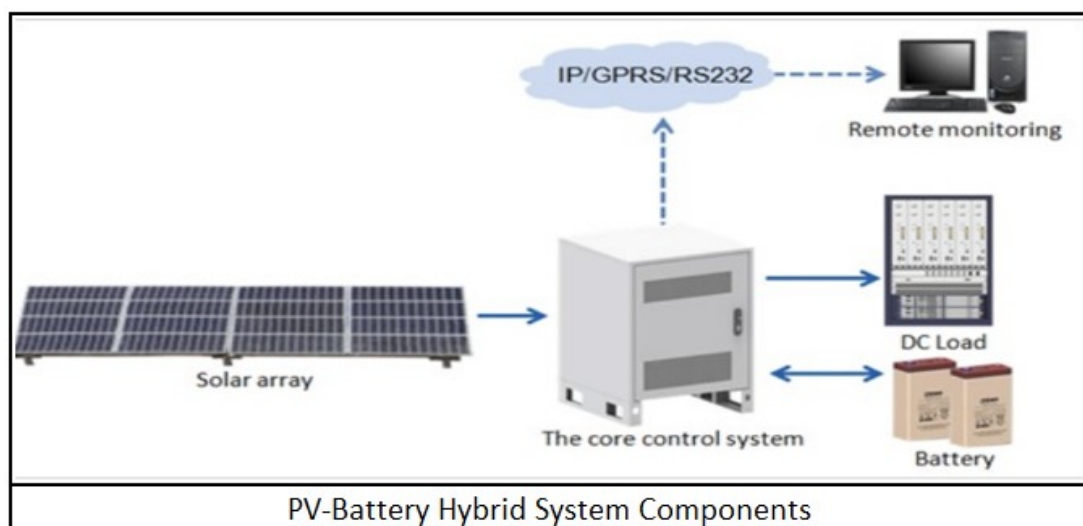
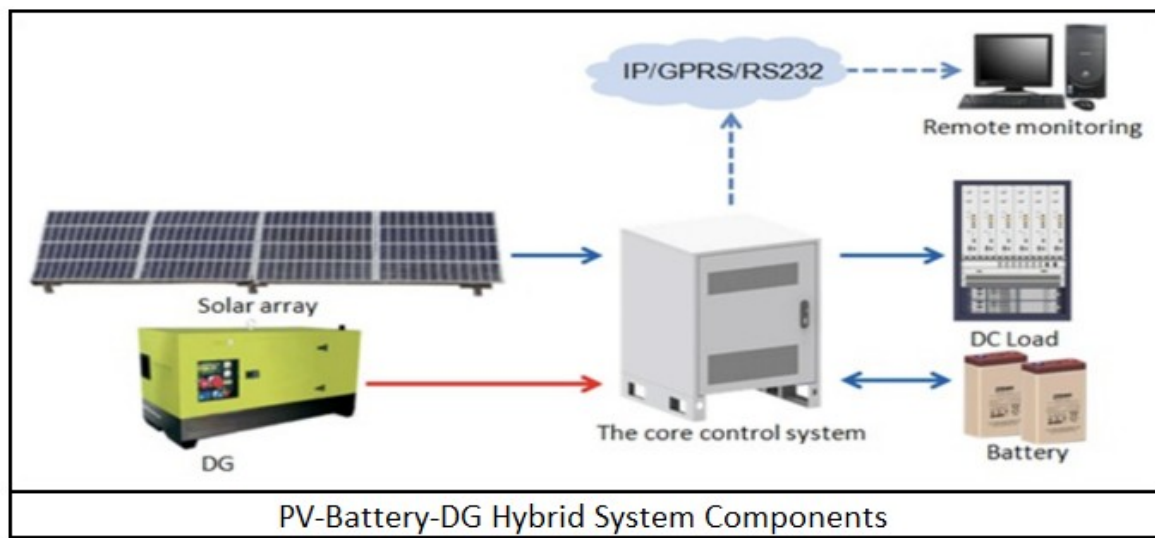


Figure 18: Solar PV-battery hybrid system component diagram [58]

Before the system modelling and redesigning of any standalone off-grid system, it is important to understand the system components and their technical capabilities. Therefore, Figure 18 shows the typical system components diagram for a solar PV-battery standalone

system while Figure 19 shows the solar PV-DG-battery hybrid system for telecom DC load integrated with the remote management system for solar PV plant monitoring [58]. The typical solar PV-powered BS system is mostly composed of solar PV module arrays on tilted or horizontal structures connected to a solar PV charge controller, backup batteries and DC load. The backup DG will only be deployed or planned for deep rural and hub/transmission BSs. For the low-traffic and rural coverage BSs with free outdoor cooling as described in Figure 18, the solar PV-battery standalone systems were assessed/audited and redesigned. While for the low capacity and hub/transmission BS, the solar PV-DG-battery hybrid system was being audited and re-engineered.



*Figure 19: Solar PV-DG-battery hybrid system component diagram [58]*

Once the system components are thoroughly described and the circuit's connection well understood, the next step is determining the load requirement before system components sizing using a spreadsheet illustrated in Error: Reference source not found. For the new sites, employed equipment specifications is used for load determination while for the existing BSs, both equipment specifications as well as load profiles from historical data is used. The next two sub-sections describe the methodology to be used to calculate the typical load requirement of the telecom load and model the solar PV-battery system that will optimally and efficiently perform until its end of life (EOL) using respective daily energy balance from equipment specifications and time step methods from the BS load profiles based on historical data.

### 3.3.2 Base Stations Load Demand Determination: Daily Energy Balance Method

Before designing any solar PV-battery standalone system, it is vital to understand the actual power consumption for the Huawei equipment used in Vodacom Lesotho BSs [56, 57]. Figure 20 shows an overview of Vodacom Lesotho's essential BS load composed of Huawei BTS and Huawei transmission nodes. The consumed power by the BS equipment as per ..... (15 is/was used to determine the overall daily BS energy requirements using the daily energy balance method (DEBM) [33, 56, 57].

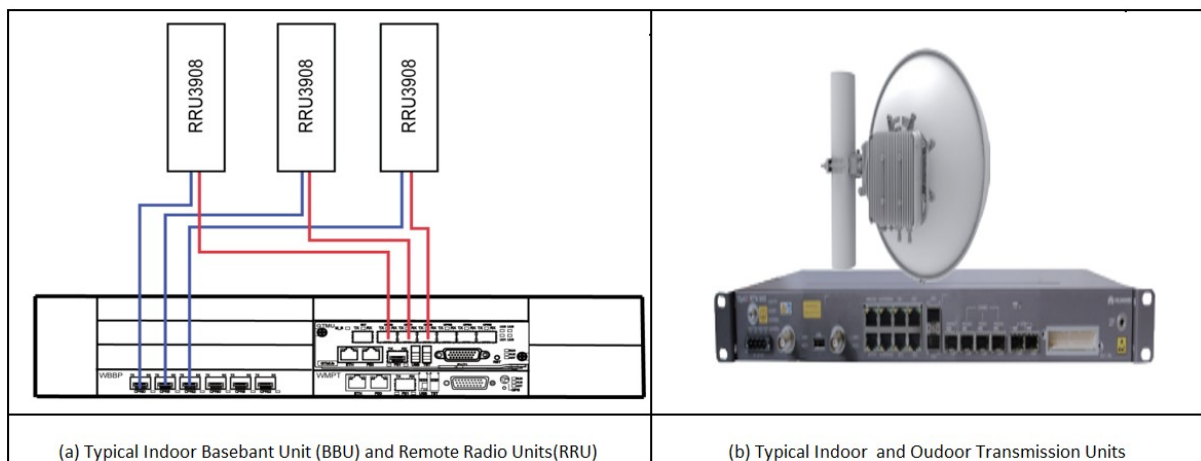


Figure 20: (a) Typical radio configuration and (b) transmission units both covering the BS essential DC loads [61, 62]

The typical and standard rural BS to be modelled is divided into three sectors, each covering  $120^\circ$  of the selected area resulting in a minimum of three radios as described in Figure 20 (a). For a typical solar PV-powered coverage BS in rural areas, each sector has a minimum of two cells, 2G and 3G single radio sharing. Huawei remote radio unit (RRU), baseband unit (BBU) and remote transmission network (OptiX RTN 905 2F) power consumption ratings were used to calculate the load requirements [61, 62]. The typical power consumption used for 2G is obtained when the BS operates with a 30% traffic load, while for 3G, the BS operates at a 40% load. In 4G mode, the BS operates at 50% of urban capacity [59]. For the rural solar PV-powered BS, 30% traffic load was used for system design.

The equipment's typical rated power consumption (wattage) as per the supplier's technical specification and designed system voltage as per the solar PV charge controller specifications were used to calculate the daily load demand in (Ah/day) and (Wh/day) as summarised in Table 1. A1 to A4 show constant parameters for the design system. A5 and A6 in Table 1

show the load requirement for one equipment type (RRU5909) operating on two different technologies and configurations (GSM-3 sectors with four transceivers and UMTS-3 sectors with two carriers) while A7 is only for a transmission note (RTN910) [60, 61]. The product of equipment wattage as per the supplier's specification and the number of sectors results in total wattage per such technology. Dividing the total wattage for each technology (A5 to A7) by system voltage (A1) resulted in hourly load current. The product of load current per technology for 24hrs (A3) results in total daily energy requirement in ampere-hours (Ah). Daily energy (Wh/day) demand as per the DEBM is the product of the typical component's power consumption (wattage) and the number of sectors for 24 hours. The sum of the load demand in Wh/day for each equipment type or radio as per Table 1 from A5 to A7 determines the total power consumption (total wattage in watts-hours) of any BS per Table 1, Column A8. It can be summarized by ..... (15 as [61]):

$$P_{BS} = N_{sector} P_{RF} + N_{TX} P_{TX} + P_{BBU} + P_{EE} + \dots \quad (15)$$

where  $N_{sector}$  is the number of sectors per BS,  $P_{RF}$  is the total power consumption for RRUs,  $N_{TX}$  is the number of transmissions (TX) radios,  $P_{TX}$  is the power consumption per TX radio,  $P_{BBU}$  is the BBU power consumption, and  $P_{EE}$  is the power consumption for other essential nodes.

*Table 1: Typical solar-powered base station configuration and its daily power demand*

Line No	Inputs	Value	Units					
A1	System Voltage	52	V					
A2	Autonomy Hrs	60	Hrs					
A3	Daily	24	Hrs/day					
A4	Autonomy Hrs/day	2.5	Days					
Mmasemouse BS Load Components:The typical power consumption is measured when the base station works at a temperature of 25°C at 30% traffic .								
	Radio Type	Configuration (RRU)	No. of Sectors	Wattage(W)	Total Wattage(W)	Hourly Load Current	Daily Load current AH/d	Total Load demand Wh/day
A5	RRU5909	GSM S4/4/4	3	207	621	12	287	14904
A5	RRU5909	UMTS 3 X 2	3	173	520	10	240	12480
A7	RTN910	1	1	155	155	3	72	3720
A10	Totals		6	328	1296	25	598	31104

It is important to highlight that both the typical power consumption and maximum power consumption are measured when the BS operates at 25°C [59]. The increase in ambient temperature results in a slight increase in power consumption due to the radio equipment's internal self-cooling technology. A 15 W aviation warning light is not considered as it has a minimal impact and does not operate for 24 hrs. The second step to be used for load determination is the load profile assessment using the BS historical data applying the time step method (TSM).

### 3.3.3 Base Stations Load Demand Determination: Time Step Method

To minimize the effect of errors in the load estimation in this study, a non-intrusive energy audit technique using the collected historical data logs was employed on the existing BSs to model the load profile. The averages from the determined load profiles are used as the typical load requirement and as the input for system sizing. The BS power-related historical data logs retrieved from the selected BSs obtained in 5 to 15 min intervals (time steps) for three to six months were converted to hourly, daily and monthly intervals. The main intention for the hourly conversion is to determine the hourly key indicator such as power consumption or load as well as the hourly load coefficients for different telecom loads based on radio configurations.

To determine the hourly load BS coefficients, each hourly power consumption (Hourly\_Load) is divided by the total daily consumption or sum of 24 hrs load (Daily\_Load). The sum of each hourly coefficient should equate to one. As per the literature, the power consumption for the typical solar PV-powered rural telecom BSs was found to be relatively stable while a grid-powered BS shows a low varying load profile due to population [64]. The hourly system power or load averages are used for system sizing and compared with the peak power or load demands. For this study, only the load current, system voltage, and system power are used for system sizing. In contrast, output current ( $I_{pv}$ ) and output power from the ( $P_{pv}$ ) are used to assess and analyse the system performance throughout the day and calculate the PR.

## 3.4 Base Station Solar-PV Hybrid Sizing

### 3.4.1 Optimal Battery Sizing for Telecom Load

Once the BS load demand or power consumption is determined, the subsequent process is to size backup batteries, solar PV-generator, and a solar PV charge controller that meet the power demand while maintaining the MNO and regulator target at the minimal cost possible. This section outlines the methodology used for the optimal battery-sizing of a typical rural telecom BS with a constant 1.3 kW load supporting both 2G and 3G, no single radio sharing per sector as calculated in Table 1 row A8 column 6 using DEBM [33]. It is essential to point out that the procedure for optimal sizing is the same regardless of the method used to determine the load requirements. The methodology adopted for the optimal battery sizing follows the recommended procedures obtained in the literature to compensate for other losses, as shown in B10. [33]. B10. summarizes the step-by-step procedure to be used to size the batteries for the planned autonomy time using both TSM and DEBM to calculate the

optimal energy capacity needed in the ampere-hours [33]. The product of the total daily energy in (Ah) requirement and planned days of autonomy from Table 1 is the total backup battery capacity required before system losses and efficiencies, as shown in B10. B10.

*Table 2: Parameters and equations for battery-sizing*

Line No	Battery Sizing Calculations For Telecom Base Stations	Units
B1	Battery charge discharge	%
B2	Inverter eff (MPPT)	%
B3	PV Charger efficiency	%
B4	Self-discharge of battery	%
B5	Nominal system voltage	V
B6	Minimum battery state of charge (SOC)	%
B7	Excess capacity(5%) per day	%
B8	Excess capacity per days of autonomy $(A4 * B7)$	%
B9	Total Load Wh/day @30% Load (WH)	Wh
B10	Battery capacity @30% Traffic $(A8\_Column\ 6 * A4)$	Ah
B11	<b>Deep Of Discharge</b>	%
B12	Battery capacity @ DoD $(B9 * A4) / (B1 * B3 * A1 * B11)$	Ah
B13	Excess capacity for days of autonomy $(B12 * B8)$	Ah
B14	Total Battery Capacity $(B12 + B13)$	Ah
B15	Selected Battery Capacity	Ah
B16	<b>Number of batteries in parallel</b> $(B15 / B16)$	No

..... (7 calculates the backup battery capacity in (Ah) for the recommended autonomy time using the designed BS system voltage. To minimize capital expenditure while also maintaining system reliability as well as the network availability for the deep rural solar PV-powered BSs with limited access during winter due to snow, sixty hours (2.5 days) of autonomy time and 5% excess capacity per day are used for the optimal solar PV-battery system capacity design and dimensions [33]. Eight hours of autonomy time is used for grid-connected BSs for the current study, as the local grid supplier normally uses as the maximum daily planned outage. The sum of the calculated battery capacity (B12) and the excess capacity for the days of autonomy (B13) results in the optimal backup battery capacity required (B14). The ratio of the optimal backup battery capacity (B14) and the selected single battery capacity (B15) results in the maximum number of batteries that can be connected in parallel (B16). Technical specifications for both delta regulator/PV Charger, solar PV modules and SDA10-48100 Shoto Lithium-ion batteries in Appendices A and B were be used to determine the relevant efficiencies and the depth of discharge (DoD) [66, 67].

### 3.4.2 Optimal PV-Array and Regulator Sizing for Telecom BS Load

Having discussed how the BS load requirements and the backup battery capacity that are used to compensate for the RE intermittency and MNO night traffic are determined, the last step is to size the solar PV array and the solar PV charge regulator/controller to meet the determined load demand. This subsection provides the methodology employed to size the optimal solar PV array using the MNO's recommended delta solar PV charge controller. Before designing the optimal solar PV array system capacity that meets recommended PR as well as other KPIs throughout its life span, the following losses are considered; power losses due to an increase in ambient temperature, solar PV modules disorientation, soiling, solar PV charge controller loss, battery charge/discharge loss and system components inefficiencies as well as degradation factors to determine the designed solar PV-array end of life (EoL) maximum output power. The designed voltage for maximum PV power ( $V_{dmp}$ ) and designed current (in A) for the maximum PV power ( $I_{dmp}$ ) are used to calculate the potential solar PV module derated power ( $W_{pmax}$ ) due to losses and temperature increase. Table 3 represents the derating percentages recommended for the optimal solar PV array system sizing that will satisfy load requirements until the end of its lifespan while meeting MNO KPIs and PR [33].

*Table 3: Derating percentage loss to determine PV-module EoL parameters [33]*

Line No	Derating Factors To Be Considered For Designed $I_{mp}$ and $V_{mp}$	%
C1	Degradation factor in $I_{mp}$ over lifespan considered 8% for 20 years	0.92
C2	Losses due to dust deposit 2%	0.98
C3	Losses due to module/branch mismatch or 2%, whichever is higher	0.98
C4	Losses due to line resistance of cables, losses in field wiring, and array wiring 2%	0.98
C5	Losses due to panel orientation other than specified one as per insolation data 2%	0.98
C6	Total Derating Factor ( $C1 \times C2 \times \dots \times C5$ )	0.85

The derating factors summarized in Table 3 were used to calculate the derated current for the selected solar PV module, namely: the Renosola solar PV module (D1) or the CNBM Sola as summarized by and equipment specifications showing the selected solar PV degradation performance with time [67]. describes the methodology procedure that is adopted for sizing and designing the optimal solar PV array. The product of all the derating factors (C6) in Table 3 and the rated current for maximum power (D2) in is the derated maximum current (D4). The optimally designed current ( $I_{dmp}$ ) (D10) from the solar PV module specification is the sum of the derated current for maximum power (D4) and the  $I_{mpi}$  (D9) which is the increase in current due to an increase in the cell temperature. The difference between the cell operating temperature (D6) and the STC temperature (D7) results in an increase in



temperature (D8). In summary, the optimally designed current ( $I_{dmp}$ ) (D10) is the current that is expected to generate the maximum power after 25 years of operation and can be used to calculate the degradation loss per year. Knowing the degradation percent per year, one can use an accurate reference solar PV array-rated power to determine the performance ratio and the expected solar PV module for the targeted year.

Table 4: Optimal PV sizing procedure

Line NO	PV Sizing to Meet Base Station Load	Units
D1	Rated Module Power of Renesola PV Module Power (Wpmax) module at 25° C	Wpmax
D2	Current for Maximum Power Imp	A
D3	Short Circuit Current Isc	A
D4	Derated Imp due factors in table 3 : (D2 *C6)	A
D5	Temp Coefficcient of Isc(%) 0.04%	A /°C
D6	Selected Maximum Solar Cell Operating temperature	°C
D7	STC temperature	°C
D8	Increase in temperature w.r.t STC : (D6-D7)	°C
D9	Increase in module current due to temperature coefficient : (D5*D8)	A
D10	Imp used for system design (Idmp) :(D4+D9)	A
D11	PV Charger System nominal input voltage for maximum power	V
D12	PV charger module maximum output power	V
D13	Rated Vmp of the selected PV	V
D14	Temp Coefficcient of Voc(%) -0.30%	V
D15	Decrease in module voltage due to temperature coefficient : (D8 * D13)	V
D16	Vmp used for system design (considering temperature Coeff) :(D13+D15)	V
D17	Number of solar modules in series : (D11/D16)	no
D18	Determined BS hourly Load @30% BS Traffic : (A8)	W
D19	Total Daily energy requirement @30% BS Traffic :A8 )	Ah/day
D20	Total Current required to meet BS Load for a Day :(D19/A1)	Ah
D21	Battery charge discharge/ inverter eff	%
D22	PV Charger efficiency %	%
D23	MPPT Efficiency	%
D24	Overall Cable losses	%
D25	Daily energy required in AH to compesate for losses :D20/(D21*D22*D23)	AH/Day
D26	BS location Lowest PSH in June	Hrs
D27	PV Charger output Current Limmitation	A
D28	Total Output from one PV Charger during PSH: (D26*D27)	Ah
D29	The Number of PV charger and solar PV Modules in parallel :(D25/D28)	no
D30	Total Number of Modules required : (D17 * D28)	no
D31	Maximum Solar Module Power after derating factors EoL: (D10 *D16)	Wmp/module
D32	Maximum Power (Vdmp X Idmp) after derating factors : D32*D31)	Wpmax
D33	Rated PV Array Total Capacity Required :(D1*D31)	Wpmax
D34	Inverter capacity /PV Charger Controller :(D29 * D1)	W
D35	Overall System Degradation Loss for 25 yrr : (D34-D33)/D33	%
D36	Derating factor per year for 25 years : (D36/25)	%

The designed maximum current for maximum power  $I_{dmp}$  (D10) is considered as the input current to the solar PV charger module which in return influences the maximum output load and charging current  $I_{omp}$  (D27) as per the solar PV Charger specifications [68]. The ratio of



the load current  $I_{daily}$  (D20) to the product of the inverter, solar PV charger, and cable losses efficiencies resulted in the optimal daily load current  $I_{opdaily}$  (D25) required in ampere-hours [33]. The product of the maximum current from each solar PV charger (D27) during PSH (D26) resulted in the maximum load current ( $I_{daily}$ ) (D28) that the solar PV charger can generate. The product of the maximum output current  $I_{omp}$  (D27) from the solar PV charger and the BS location peak sunshine hours (PSH) (D26) results in the maximum current (D28) that one solar PV module can generate during maximum sun intensity. Therefore, to find the optimal number of solar PV modules as well as the number of solar PV chargers (D29) to be connected in parallel, the optimal daily load current  $I_{opdaily}$  (D25) is divided by the maximum optimal output current  $I_{omp}$  (D28):

$$Daily\ load\ (AH/day) = \frac{Wh/(day)}{\eta_{inv} \times \eta_{battery} \times V_b} \dots\dots\dots (16)$$

Once the number of solar PV chargers and solar PV modules connected in parallel are optimally sized, the next step is to size the number of solar PV modules (D17) to be connected in series, thus determining the final number of solar PV modules in the solar PV array (D30). The optimal solar PV-designed voltage (D16 or  $V_{dmp}$ ) is the sum of the solar PV module-rated voltage for the maximum (D13 or  $V_{mp}$ ) and the voltage decrease ( $-V_{mpd}$ ) due to the increase in the operating cell temperature. To obtain the maximum number of solar PV modules (D17 or  $N_s$ ) in series to gain the maximum input voltage (D11) to the solar PV charger for the maximum output power (D12) as per Figure 21(a), the module input voltage (D11) is divided by the designed voltage for the maximum power (D17) [6, 63].

The product of the number of solar PV modules connected in series (D17) and the number of solar PV chargers in parallel (D28) or solar PV modules in parallel results in the maximum final number ( $N_{pv}$ ) of the solar PV modules (D29) for the optimally designed solar PV array. The product of the number of solar PV chargers (D29) and the maximum solar PV charger output power (D12) as per solar PV charger specifications give the maximum solar PV charge controller capacity (D35) to be used. Figure 21 (a) shows the maximum power curve of the solar PV charger (PVC 2200B RenE) per certain input voltage while Figure 21 (b) shows the solar PV charger's maximum output current (A) per certain output system voltage ( $V_{out}$ ) used for the current study [68]. To emphasize, it is very crucial to understand solar PV charge controller capabilities for any solar PV hybrid system design as this has a direct and huge impact on the overall solar PV plant performance ratio [35].

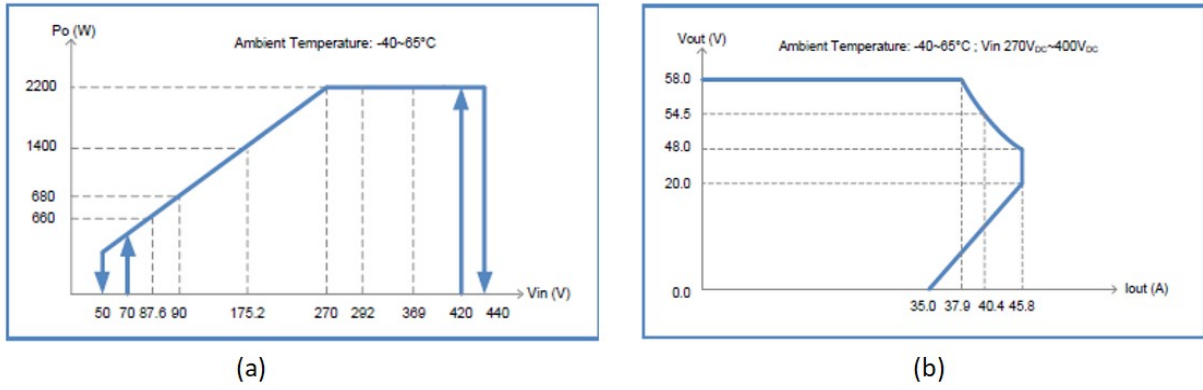


Figure 21: (a) Delta PV charger output power and input voltage, (b) Output voltage and current curve for optimal system design [68]

### 3.5 Existing Base Station Audits and Assessment

#### 3.5.1 Base Station Selection Criteria and Inspections

Once the procedure for optimal hybrid system modelling is tabled and understood, the second step is to audit and assess the existing BS solar PV-battery system setup against the design principles established in the previous section and literature review. The physical BS inspection and a compass to confirm the azimuth are not only used to assess the solar plant orientation, solar PV module mismatch and soiling but also to identify potential shading as well as calculating the actual tilt angle. Although all the MNO solar PV-powered BSs power data logs were collected and analysed, only five solar PV-powered BSs as summarised in Table 5, with different power and radio configurations are used for the current research as case studies and were audited against the optimally designed off-grid BSs [33]. One grid-powered BS is sized for the grid-to-solar migration.

Table 5: Selected BSs for the case study

BS Load Components: The typical power consumption is measured when the base station works at a temperature of $25^\circ\text{C}$ at 30% traffic.								
BS Name	Radio Configuration	No. of Sectors	Wattage(W)	Total Wattage(W)	Current(A)	Daily current AH/day	Total demand Wh/day	Battery Type
Makebe	GU900	1	428	428	8	198	10272	Lead Acid
Malimomg	GU900	3	428	974	19	450	23376	Lead Acid
Mmasemouse	G900+U900	6	328	1295	25	598	31080	Lead Acid
Ha Thloro	G900+U900 x1	4	428	1557	30	719	37368	Lithium-ion
Kolo	G900+U900+U2100	9	677	2182	42	1007	52360	Lead Acid
Scout	G900+U900+U2101	9	803	2100	40	969	50400	Lead Acid

The criteria used for BSs selection is to target one-sectored BS at Makebe with the lowest traffic (ULCS) on a single radio sharing mode configured for 2G and 3G in 900MHz (GU-900). The other preferred BSs is the normal 3-sectored BS located in Malimomg with moderate traffic operating in GU-900 mode single radio sharing. One other selected solar PV-

powered, six-sectored, and high-traffic BS in Mmasemouse configured for 2G and 3G in 900MHz (GU-900), and no single radio sharing. A four-sectored BS located at Ha Tlthoro is also the hub BS in a rural area configured as a solar PV-DG-battery hybrid system. A hop/hub/transmission BS acts as a link via a microwave transmission radio and/or fibre optic system. It, therefore, has a higher power consumption compared to a terminal/standalone BS [69]. The last selected nine-sectored solar PV-powered BS in Kolo is operating in GU-2100 mode and not meeting both MNO and regulator KPIs located in the peri-urban zone with high traffic. Only one high-capacity, nine-sectored and grid-powered BS (Roma – Ha Scout) configured for all technologies which are 2G, 3G, and 4G-1800MHz (GUL-1800) were analysed and sized for possible RE migration.

Once the BSs were selected, the following step was to do physical site visits at the selected BSs for data collection, enabling the solar controller remote access configurations, and most importantly, physical power component inspections. Apart from data logs collections, the main focus during BS physical inspection is auditing the solar structure orientation, tilt angles, solar PV module mismatches, solar PV module cracks, solar PV array soiling, number of solar PV modules, modules specifications, solar PV array series/parallel connections as well as possible external shading. Once the solar PV array is audited, the second step was to inspect the existing backup batteries concentrating on the battery terminal's carbon conditions, circuit connections, and battery cabinet-free cooling status. One last critical circuit component which was inspected is the regulator/solar PV charger/rectifier against dust, the possibility of high temperature, and its remote integration. After the individual components' physical inspection was completed, the circuit connection for the solar power plant was analysed. The main focus during the circuit's connection auditing is on the solar PV modules and their wiring, backup batteries and their wiring, and the solar PV charge controller's physical connections.

### 3.5.2 Base Station Key Performance Indicators

Depending on the availability, two to twelve months' historical data of power stored in 5 to 15 minutes intervals composed of, but not limited to, solar PV power ( $P_{pv}$ ), load power ( $P_{ld}$ ), solar PV current ( $I_{pv}$ ), load current ( $I_{ld}$ ) and battery charging/discharging current ( $I_{battery}$ ) from the BS solar PV power plant controller was retrieved and analysed to model the actual load profiles. Once the load profiles are analysed, the hourly, daily and weekly load coefficients were determined and can be used for other BSs with similar configurations during new BS deployment. The actual power consumption from load profiles is to be compared with the

actual traffic (voice and data) to determine the correlation and to inform the decision regarding the use of energy-saving software parameters for further optimizations. The output current from the solar PV generator was analysed against the load and battery charge and discharge currents. The results obtained from this analysis influenced the conclusion for the solar PV power plant redesigning or optimization.

### 3.6 Performance Ratio Calculation

Once the solar PV-battery hybrid system is fully sized, its performance needs to be monitored and evaluated against certain standard performance indicators such as performance ratio (PR) and system reliability. This section describes how the solar PV array performance ratio was calculated. The obtained BS solar PV power (Ppv) from the data log is used as the actual output power generated by the solar PV power plant. As per the PR definition, the ratio of this Ppv from the base station historical data for the selected month to the solar PV power on the tilted plane from .....(1 or ..... (2 results in the BS performance ratio. As already mentioned, the location Meteoronorm radiation data is used to calculate the reference or expected solar PV power on the tilted surface using the existing tilt angle that equals the Latitude. The actual hourly solar PV power from the base station is compared to the expected hourly solar PV power based on the location efficiency, ambient temperatures, the derating factor as well as the solar PV module temperature coefficient.

### 3.7 The Solar PV-Battery System Reliability

The second approach used to assess solar PV plant performance is to model its annual performance reliability based on the location's monthly radiation or PSH. The product of the lowest PSH for each month and solar PV array capacity results in the total energy produced by the solar plant measured in kWh. Dividing the obtained daily energy by 24-hrs results in the hourly power produced by the solar PV-battery system contribution called a solar contribution summarised by .....( 17. The subtraction of the determined hourly load from the solar PV-battery's solar contribution results in an energy balance value. Zero energy balance means that the solar plant is well-balanced or designed for that particular month since there is no deficit or surplus. Negative energy balance reflects an under-dimensioned solar PV array which needs to be upgraded or integrated with DG as the backup power source.

$$\text{Solar Contribution (kW)} = \frac{\text{PSH (hrs)} \times \text{Solar Array Capacity (kW)}}{24 \text{ (hrs)}} \dots\dots\dots (17)$$



## 4 RESULTS AND DISCUSSIONS

### 4.1 Overview

This chapter presents and discusses the study's results in the form of tables, graphs and figures geared towards the study's objectives. The discussion was based on the main technical findings from physical inspections and system configuration audit assessments as described in the methodology chapter. The obtained meteorological data for the selected BSs is assessed and analysed for optimal solar PV hybrid system sizing. Once the RE resources are analysed and discussed, the next step is to discuss the determined load requirement using the DEBM based on the equipment specifications and the TSM based on BS' historical load profiles data and the determined BS load coefficients for different radio configurations. The results obtained from the optimally sized solar PV hybrid system that meet the dimensioned load requirement for the planned days of autonomy as well as MNO and regulator KPI are discussed and compared with the current sizing.

The solar PV battery system's KPIs from the load profiles are discussed to further understand the system's performance. The findings from these analyses and discrepancies identified between the current and optimally sized systems are further discussed in the BS audit results section and feed into the system redesigning section. The PRs for the selected solar PV battery systems are discussed and compared to the recommended targets as per the literature. The annual performance as per the recommendation from the optimally-sized solar PV array capacity for the selected BS load, is also discussed.

### 4.2 Base Station Meteorological Data

The selected BSs radiation resources were first determined to confirm if the chosen locations are conducive and resourceful for installing solar PV generators. summarizes meteorological data for the solar PV-powered Mmasemouse BS in the country's southern region. The results for five other selected BSs are provided in Appendix C. It should be recalled that Mmasemouse was chosen as the reference since it was found to be a stable and high-traffic solar-powered BS. It was observed that all the BSs have high radiation levels as well as the highest PSHs in summer starting in November to March, but very low clearness indices due to the highest levels of precipitation compared to winter starting in April to July which have high clearness indices but low radiation levels and smallest PSHs.

Table 6: Sample Meteorological data for Mmasemouse BS

<b>1.1 kW Mmasemouse</b>						
BS Latitude	-29.233	BS Longitude:	27.932	Altitude [m a.s.l.]	1606	
Units	H_Gh	H_Dh	Clearance Index	Ta	RR	PSH
Month	[kWh/m <sup>2</sup> ]	[kWh/m <sup>2</sup> ]	[K]	[°C]	[mm]	[kWh/d]
January	244.00	77.00	0.599	21.70	80.00	4.97
February	199.00	58.00	0.581	21.00	84.00	4.64
March	192.00	57.00	0.590	19.10	68.00	4.17
April	153.00	37.00	0.628	15.20	40.00	3.49
May	132.00	24.00	0.678	11.40	18.00	2.93
June	113.00	24.00	0.696	8.00	21.00	2.57
July	124.00	26.00	0.706	7.80	8.00	2.89
August	149.00	32.00	0.699	11.00	9.00	3.44
September	175.00	41.00	0.654	15.00	9.00	4.32
October	221.00	51.00	0.598	18.20	38.00	4.54
November	237.00	57.00	0.595	19.70	61.00	5.11
December	249.00	66.00	0.604	21.30	83.00	5.33
<b>Totals</b>	<b>2188.00</b>	<b>550.00</b>			<b>519.00</b>	<b>48.40</b>
<b>Averages</b>	<b>182.33</b>	<b>45.83</b>	<b>0.64</b>	<b>15.78</b>	<b>43.25</b>	<b>4.03</b>
<b>Maximum</b>	<b>249.00</b>	<b>77.00</b>	<b>0.71</b>	<b>21.70</b>	<b>84.00</b>	<b>5.33</b>
<b>Mininum</b>	<b>113.00</b>	<b>24.00</b>	<b>0.58</b>	<b>7.80</b>	<b>8.00</b>	<b>2.57</b>

Based on these results, the maximum PR is expected between August and October due to favourable radiations, clearness indices, fewer levels of precipitation, and average PSH compared to other months. All the selected BSs have favourable ambient temperatures for the maximum yield similar to the one shown in with a maximum value of 21.7°C, which is conducive for free cooling to facilitate outdoor BS deployment without an air conditioner as most batteries and indoor equipment perform well at 25°C or below [57, 62]. To maintain 100% system reliability throughout the year, the month of June with the lowest PSH of 2.57 hrs, as shown in Table 6, has been chosen as the design month for the Mmasemouse solar PV array and all other BSs modelling.

### 4.3 Base Stations Load Determination

#### 4.3.1 Base Stations Load Determination: Daily Energy Balance Method

This subsection tables the load requirement results using the DEBM and the rated power consumption per the supplier's technical specifications. The obtained results are as per the procedure described in Table 1 (Section 3.3). Error: Reference source not found summarizes the load requirement for the selected BSs used in the study, assuming a constant load throughout the day as per the literature and 52V designed system voltage as per Figure 21. The table describes the one-sectored BS located at Ha Makebe as a 0.428 kW BS with 8.23 A load current, resulting in an energy demand of 10.272 kWh/day. The three-sectored typical rural BS providing both 2G and 3G in single radio sharing mode (GU900) located in

Malimong was found to be a 0.974 kW BS with an average load current of 18.73 A, resulting in 23.376 kWh/day energy demand. The six-sectored and no single-sharing Mmasemouse BS was found to be a 1.295 kW BS with a 24.90 A constant load current for 24 hrs, leading to a 31.080 kWh/day energy requirement. The Tlthoro BS, which is also a typical rural BS but acting as hub BS, was found to be a 1.557 kW BS delivering the same technologies as Mmasemouse and Malimong, but with added transmission radios and additional sector/RRU providing 4G in 900 MHz, resulting in 29.94 A load current and 37.368 kWh daily demand.

*Table 7: BS load requirement using DEBM*

<b>BS Load Components: The typical power consumption is measured when the base station works at a temperature of 25°C at 30% traffic .</b>					
BS Name	Radio Configuration	No. of Sectors	Total Wattage(W)	Load Current(A)	Total Load demand Wh/day
<b>Makebe</b>	1SR_GU900	1	428	8.23	10272
<b>Malimong</b>	3SR_GU900	3	974	18.73	23376
<b>Mmasemouse</b>	3NSR_G900+U900	6	1295	24.90	31080
<b>Ha Tlthoro</b>	3NSR_GU900+L900	4	1557	29.94	37368
<b>Kolo</b>	3NSR_G900+U900+U2100	9	1903	36.60	45680
<b>Scout</b>	3RS_GU900+ 2UL(AAU)_U2100+LTE1800	9	2184	42.00	52416

The Kolo BS was found to be a high-capacity solar-powered BS providing all three technologies (2G, 3G, and 4G on 900 MHz and 2100 MHz) configured on nine RRUs with three per sector. The Kolo BS is defined as a 1.903 kW solar-powered BS with no single radio sharing and having an average load current of 36.60 A, resulting in a 45.680 kWh daily demand. The nine-sectored and grid-powered Scout BS, serving both the Roma community and the National University of Lesotho was also audited for possible grid-to-solar PV migration. It was found to be a 2.184 kW BS with a load current of 42.00 A, resulting in a 50.416 kWh daily demand. It is important to note that although Kolo and Scout have the same number of sectors or radios, they have different load requirements. The Kolo BS is a peri-urban coverage BS, while Scout uses a high capacity RRU since it provides urban coverage with a high capacity resulting in a higher power requirement than Kolo BS. The following subsection discusses and compare the same results obtained from the time step method.

#### 4.3.2 Load Determination: Time Step Method

For optimal solar PV hybrid system components sizing, the actual BS system power ( $P_{sys}$ ) or power consumption and load current ( $I_{Load}$ ) play a very crucial role. Figure 22 indicates the actual hourly power consumption while Figure 23 shows the hourly load current for the different BS radio configurations using the TSM. The Makebe BS is peaking at 0.5 kW and 10.5 A and averaging at 0.44 kW and 8.79 A compared to 0.428 kW and 8.23 A, respectively, as obtained from DEBM. The TSM results in a 10.566 kWh daily energy requirement



compared to 10.372 kWh received from DEBM for Makebe BS. This shows a 3% power requirement deviation from DEBM compared to TSM; it compares well with the recommended 10% deviation between the rated and actual power consumption triggered by the BS actual traffic and the BS operating ambient temperatures.

Malimong BS has a 0.932 kW and 18.06 A average loads and peaks at 1.1 kW, resulting in a 22.4 kWh/day energy demand using TSM compared to 0.974 kW BS with an average load current of 18.73 A, resulting in 23.376 kWh/day as per DEBM. Mmasemouse BS was found to peak at 1.283 kW and 25.72 A due to high traffic, averaging 1.149 kW and 22.25A, with a daily energy requirement resulting in 27.584 kWh, which is 13% less than 31.080 kWh obtained from the DEBM in Error: Reference source not found above. This is due to increased traffic as it is configured as GU900 in no single radio-sharing mode, implying a high-traffic BS.

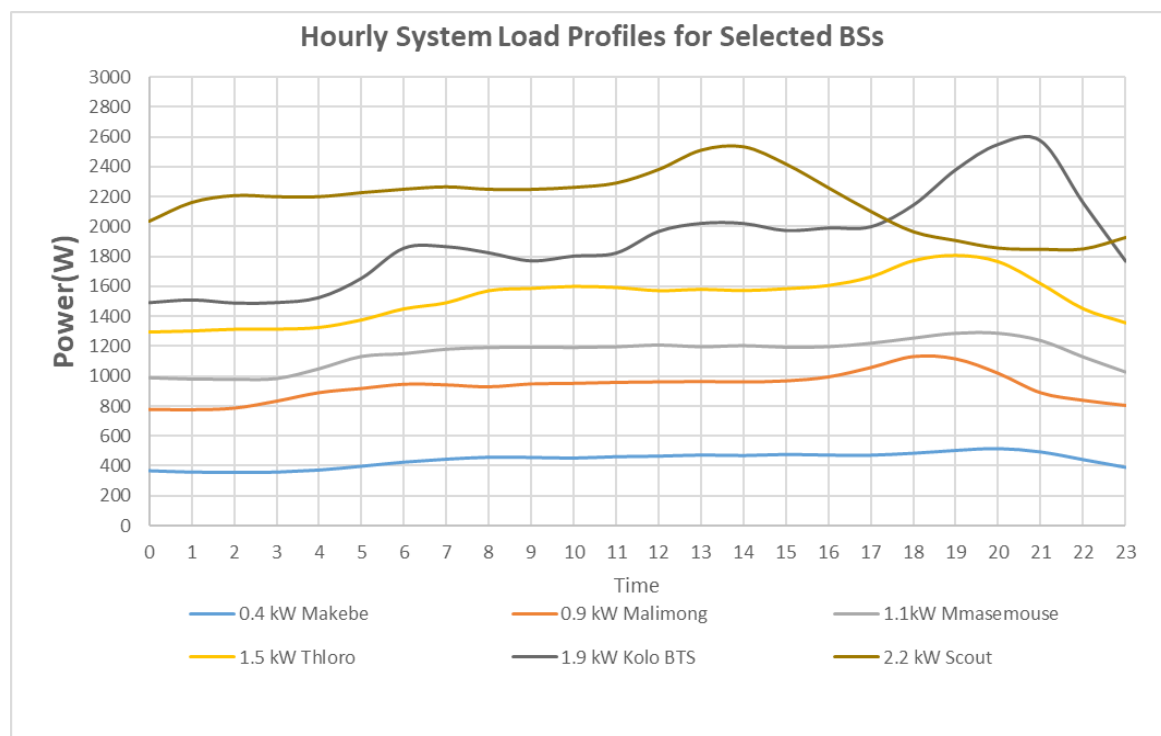


Figure 22: Power profile for 6 BSs with different radio configurations

The Thloro BS, with a DG backup, in the rural area of Quthing district was found to have 1.522 kW and 29.09 A average loads with a 36.538 kWh daily energy requirement compared to 1.557 kWh and 29.94 A average loads, as well as 37.4 kWh (2% variation) daily energy demand from DEBM summarized in Error: Reference source not found. The Kolo BS averages at 1.889 kW and 36.99 A with a 45.596 kWh daily energy demand obtained from

TSM, compared to 1.903 kW and 36.60 A averages with a 45.680 kWh/day energy demand obtained from DEBM, implying almost 0% deviation between the two methods. The Scout BS in an urban area was found to be on 2.174 kW and 40.389 A average loads as well as a 52.170 kWh/day energy demand from TSM compared to 2.184 kW and 42.00 A average loads and a 52.416 kWh/day energy demand obtained through DEBM; this shows close to 0% deviation between the two methods. It should also be highlighted that while these two methods do compare well, they are not 100% the same and that small difference directly affects the overall system components sizing.

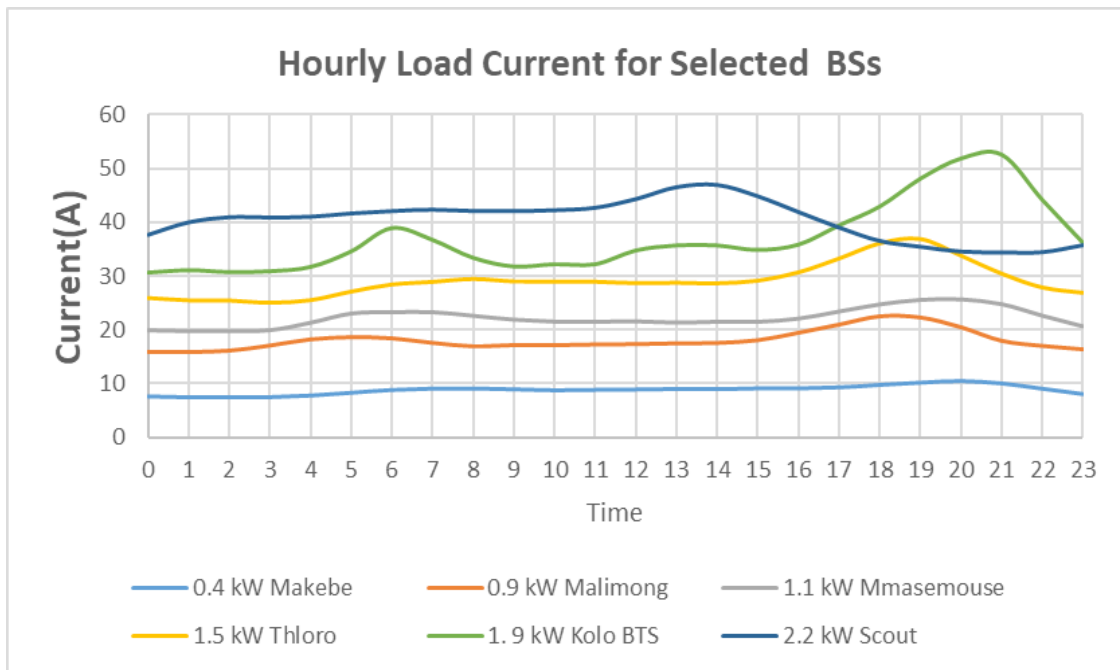


Figure 23: Current profile for 6 BSs with different radio configurations

#### 4.3.3 Load Profile Coefficients

The actual hourly BS power consumption from Figure 22 is used to determine the normalized BS load profile for different power and radio configuration types. The normalized coefficient is the ratio of the actual hourly BS power consumption/load to the total daily consumption/load ( $L_{Hourly}/L_{Daily}$ ). Figure 24 shows the results for normalized load profiles for the selected BSs. It can be noted from the results that although these solar-powered BSs have different capacities as discussed in Figure 24, they have relatively the same coefficients or follow similar load patterns. Solar PV-powered BSs have their lowest consumption between 24H00 midnight and 04H00 in the morning. The load starts to increase at 05H00, remains constant throughout the day, and peaks between 17H00 and 22H00. This follows a typical residential load profile as people are busy with daily activities and some rely on employer

resources for power, voice and data resources. It can be deduced from these load coefficients that indeed the telecom load is relatively constant with a slightly low consumption from midnight to morning around 04H00 due to less traffic and favourable ambient temperatures. The load is constant throughout the day (05H00 -17H00) with a slight increase during the telecom peak hours between 17H00 to 22H00.

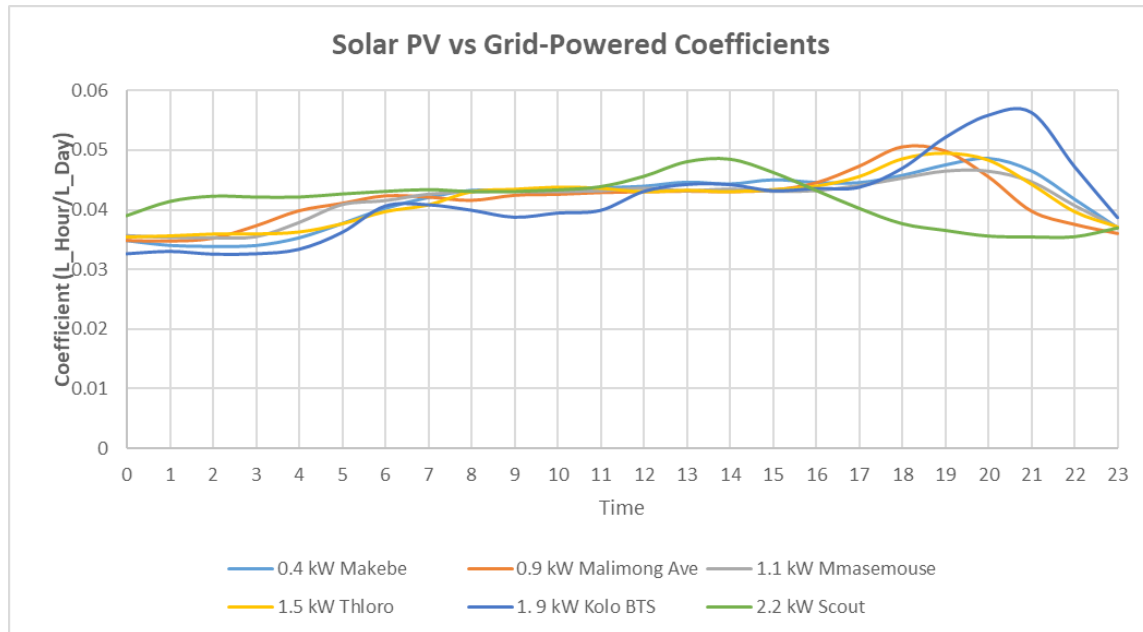


Figure 24: Normalized load profiles for solar-PV and grid-powered BSs

It can be recalled that one of the case study objectives is to model and design an optimal solar PV generator for a high-capacity BS which is currently grid-powered. Figure 24 also shows four-month load profiles for a 12-sectored and urban grid-powered Scout BS in GUL1800 mode located in Roma. The results obtained also show a relatively constant load with a slight peak during lunch hours due to internal cooling and traffic behaviour as the BS serves tertiary students. The normalised results for the Scout BS do not compare well with the normalised load profiles of the solar PV-powered BSs in rural areas with different radio configurations or capacities. It can safely be concluded from the TSM assessment that the telecoms BSs have a relatively constant load with different peak times due to different subscriber behaviours in different regions unlike DEBM assuming a flat and constant load throughout the day. It is also important to note that having determined the load requirement from the TSM, the obtained load profile coefficients can be used to determine the load profiles for any new BS regardless of the radio configurations, capacity, or power type. To further showcase this, the

load coefficients for four selected solar-powered BSs were compared with three other grid-powered BSs, namely, Mabote BS, TY BS and Mapetla BS as shown in . They demonstrated consistency regardless of the radio configuration and power type.

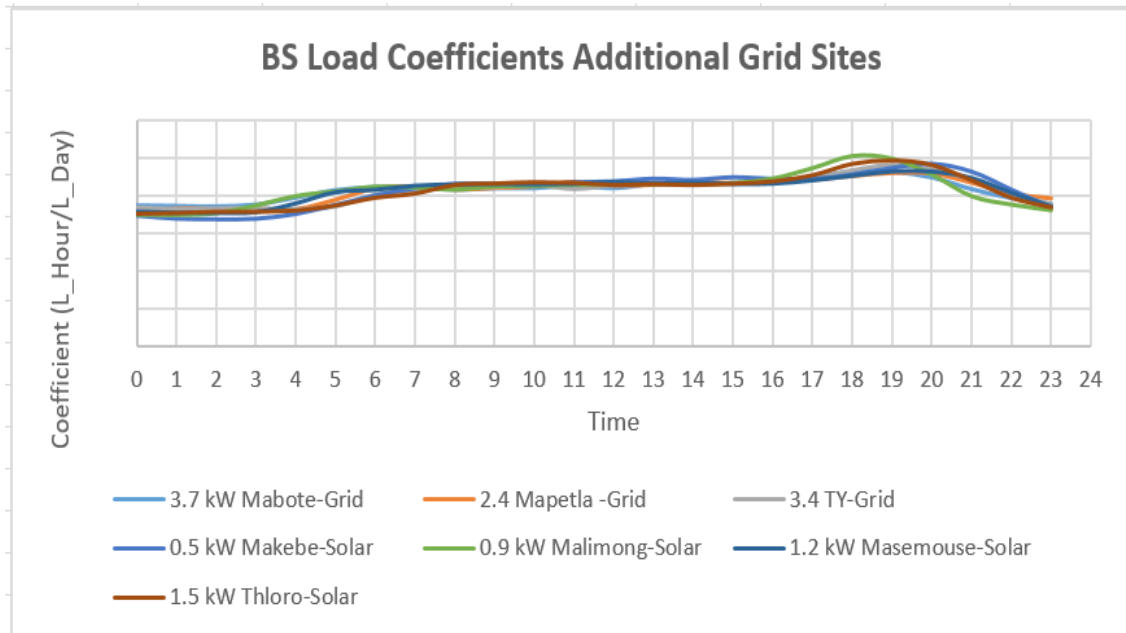


Figure 25: Normalized load profiles for four selected solar-PV and three grid-powered BSs

## 4.4 Base Station System Components Sizing

### 4.4.1 Base Station Optimal Battery Sizing for Telecom Load

summarises the number of batteries and their capacities to meet 2.5 days of autonomy for a 52V system designed voltage for the determined load using DEBM. The sized batteries were obtained using 90% DoD for the selected 48V/100 Ah lithium-ion batteries as per the manufacturer's specification and 5% daily excess storage as per the literature for 100% system reliability.

Table 8: Battery sizing using DEBM load

Line No	Battery Sizing Calculations For Telcom Base Stations	Makebe	Malimong	Mmasemouse	Thloro	Kolo System	Scout	Units
B1	Battery charge discharge(%)	0.98	0.98	0.98	0.98	0.98	0.98	
B2	Inverter eff (MPPT) %	0.995	0.995	0.995	0.995	0.995	0.995	
B3	PV Charger efficiency %	0.98	0.98	0.98	0.98	0.98	0.98	
B4	Self-discharge of battery (%)	0.001	0.001	0.001	0.001	0.001	0.001	
B5	Nominal system voltage	52	52	52	52	52	52	V
B6	Minimum battery state of charge (SOC) %	0.1	0.1	0.1	0.1	0.1	0.1	
B7	Excess capacity(5%) per day	0.05	0.05	0.05	0.05	0.05	0.05	per day
B8	Excess capacity(%) per days of autonomy (A4*B7)	0.125	0.125	0.125	0.125	0.125	0.125	
B9	Total Load Wh/day @30% Load (WH)	10272	23376	31080	37368	45680	52416	Wh
B10	Battery capacity * 30% Traffic (A10_Column 6 *A4)	198	450	1295	719	878	1008	Ah
B11	Deep Of Discharge	0.9	0.9	0.9	0.9	0.9	0.9	
B12	Battery capacity @ DoD (B9*A4)/(B1*B3*A1*B11)	571	1300	1729	2078	2541	2915	Ah
B13	Excess capacity for days of autonomy (B12*B8)	71	163	216	260	318	364	Ah
B14	Total Battery Capacity (B12+B13)	642	1463	1945	2338	2859	3279	Ah
B15	Selected Battery Capacity	100	100	100	100	100	100	Ah
B16	Number of batteries in parallel ( B15/B16)	6	15	19	23	29	33	No

The Makebe BS with a 10.272 kWh daily energy requirement needs 6 batteries connected in parallel for the planned autonomy with 642 Ah storage. For Malimong BS, 15 batteries are required to cater for a 23.376 kWh of daily energy demand. Mmasemouse BS with 31.08 kWh of energy needs 19 batteries, and the Tlhoru BS with 37.368 kWh, requires 23 backup batteries. A high-capacity BS such as Kolo with a 45.68 kWh daily energy requirement needs 29 batteries while Scout with a 52.416 kWh load requirement is sized with 33 backup batteries for same the planned autonomy time, all connected in series.

Table 9 summarises the storage design for the same 60 hrs (2.5 days) autonomy time and 52 V system voltage for the load determined using the TSM. The obtained results require 7 backup batteries for Makebe BS, showing one extra battery compared to DEBM due to a 3% increase in the daily energy requirement from 10.272 kWh to 10.566 kWh in TSM. The results also indicate that Malimong BS with a 0.9 kW average load but 22.387 kWh daily energy demand requires 14 backup batteries connected in parallel, resulting in one battery short compared to DEBM due to a 4% decrease from 23.376 kWh to 22.387 kWh in TSM. The decrease is mainly due to actual load as opposed to rated power in DEBM.

*Table 9: Battery sizing using the TSM load*

Line No	Battery Sizing Calculations For Telcom Base Stations	Makebe	Malimong	Mmasemouse	Tlhoru	Kolo System2	Scout	Units
B1	Battery charge discharge(%)	0.98	0.98	0.98	0.98	0.98	0.98	
B2	Inverter eff (MPPT) %	0.995	0.995	0.995	0.995	0.995	0.995	
B3	PV Charger efficiency %	0.98	0.98	0.98	0.98	0.98	0.98	
B4	Self-discharge of battery (%)	0.001	0.001	0.001	0.001	0.001	0.001	
B5	Nominal system voltage	52	52	52	52	52	52	V
B6	Minimum battery state of charge (SOC) %	0.1	0.1	0.1	0.1	0.1	0.1	
B7	Excess capacity(5%) per day	0.05	0.05	0.05	0.05	0.05	0.05	per day
B8	Excess capacity(%) per days of autonomy (A4*B7)	0.125	0.125	0.125	0.125	0.125	0.125	
B9	Total Load Wh/day @30% Load	10566	22387	27585	36539	45596	52170.78	wh
B10	Battery capacity * 30% Traffic (A10_Column 9 *A4)	211	433	534	698	888	969.32	Ah
B11	Deep Of Discharge	0.9	0.9	0.9	0.9	0.9	0.9	
B12	Battery capacity @ DoD (B9*A4)/(B1*B3*A1*B11) Eqn:6	588	1245	1534	2032	2536	2902	Ah
B13	Excess capacity for days of autonomy (B12*B8)	74	156	192	254	317	363	Ah
B14	Total Battery Capacity (B12+B13)	662	1401	1726	2286	2853	3265	Ah
B15	Selected Battery Capacity	100	100	100	100	100	100	Ah
B16	Number of batteries in parallel (B15/B16)	7	14	17	23	29	33	No
B17	Change in Energy Requirement Between the Two Methods	3%	-4%	-13%	-2%	0%	0%	

The Mmasemouse BS with a 27.585 kWh daily energy load requires 1726 Ah storage capacity (17 batteries), less by 200 Ah (2 batteries) due to a 13% decrease in the daily energy requirement from 31.08 kWh in DEBM to 27.585 kWh from the TSM. Tlhoru BS needs 23 batteries which compares well with DEBM even though there is a 2% decrease in the daily energy requirement. There is no significant change in the daily energy requirement for Kolo and Scout leading to no reduction or addition of batteries. It can therefore be concluded that DEBM is likely to result in system over-sizing or under-sizing since it assumes a constant

energy requirement. The TSM is more accurate and highly recommended for stabilizing and improving the system's reliability for the existing BSs as it relies on the actual power consumption from historical data as well as ambient temperatures. The determined normalized load coefficients from this research project can be used to model new deployments of solar-powered BSs with similar radio configurations, where historical data does not exist.

#### 4.4.2 Optimal PV-Array and Regulator Sizing for Telecom BS Load

This sub-section discusses the optimal sizing of solar PV array generator that meet the above-mentioned load for 24-hour telecom to meet the operator's KPIs. The PV array is sized to load solar during sunshine hours and store the surplus for night traffic or during the RE intermittence. Table 10 shows the results obtained for solar PV sizing based on the load requirement from DEBM and Table 11 shows the same results obtained as the TSM load requirement. The obtained results from these two methods were found to be relatively the same on all parameters except the sized number of solar panels for Mmasemouse BS. The DEBM results in 42 solar PV modules for a 31.08 kWh daily energy requirement compared to 35 solar PV modules for a 27.585 kWh daily load obtained using the TSM highlighted in Table 10. The main reason behind this over-sizing was found during load determination where the DEBM has an average of 25 A load current compared to 22 A obtained from the TSM for the same BS.

Table 10: PV array and PV charger sizing using DEBM

PV Sizing Using Daily Energy Balance Method							
Description	Makebe	Malimong	Mmasemouse	Thloro	Kolo System	Scout	Units
PV Module Power (Wpmax) module at 25° C	330	315	315	330	315	330	Wpmax
Current for Maximum Power Imp Rated	8.74	8.51	8.51	8.74	8.51	8.74	A
Derated Current	7.42	7.22	7.22	7.42	7.22	7.42	A
Voltage for Maximum Power Vmp Rated	37.8	37.1	37.1	37.8	37.1	37.8	V
Imp used for system design (Idmp)	7.42	7.21	7.23	7.42	7.23	7.42	A
Vmp used for system design (Idmp)	37.74	36.54	37.04	37.74	37.04	37.74	V
Total energy required for day@30% Traffic	10272	23376	31080	37368	45680	52416	Ah/day
Daily energy required in AH to compesate for losses	226	514	683	821	1004	1152	AH/Day
BS location Lowest PSH in June	2.87	2.85	2.57	3.03	2.8	2.81	Hrs
Total Output from one PV Charger	135	134	121	142	132	132	Ah
No of solar modules in series	7	7	7	8	7	7	
No of solar modules in Parallel	2	4	5	6	8	9	
Total Number of Modules required	14	28	42	48	56	63	
Maximum Solar Module Power EoL	280	268	268	280	268	280	Wmp/module
Maximum PV Generator Wpmax	4620	8820	13230	15840	17640	20790	Wpmax
Inverter capacity /PV Charger Controller	4400	8800	11000	18000	24000	27000	W
Overall System Degradation Loss for 25 yrr	0.1777	0.1750	0.1764	0.1777	0.1764	0.1777	%
System Degradation Loss per year	0.0071	0.0070	0.0071	0.0071	0.0071	0.0071	%

The total energy demand that is required to meet the determined daily load for Mmasemouse BS was found to be 606 Ah/day using TSM representing a 13% decrease compared to 683 Ah/day for DEBM. The solar PV charge controller power curve in Figure 21 and 52 V system design voltage shows 45.8 A as the designed output current ( $I_{out}$ ) from one solar PV charger, resulting in 121 A for 2.57 peak sunshine hours. Therefore, to generate a 606 Ah daily demand during PSH, five solar PV chargers as well as five solar panels are connected in parallel and seven solar panels resulting in thirty-five solar PV modules for the optimized solar PV generator. In summary, the designed system uses thirty-five solar PV modules, seven in series and five in parallel.

*Table 11: PV array and PV charger sizing using TSM*

PV Sizing Using Daily Time Step Method							
Description	Makebe	Malimong	Mmasemouse	Thloro	Kolo System	Scout	Units
PV Module Power (Wpmax) module at 25° C	330	300	315	330	315	330	W
Current for Maximum Power Imp Rated	8.74	8.2	8.51	8.74	8.51	8.74	A
Derated Current	7.42	6.96	7.22	7.42	7.22	7.42	A
Voltage for Maximum Power Vmp Rated	37.8	36.6	37.1	37.8	37.1	36.6	V
Imp used for system design (Idmp)	7.42	6.97	7.23	7.42	7.23	7.42	A
Vmp used for system design (Idmp)	37.74	36.54	37.04	37.74	37.04	37.74	V
Total energy required for day@30% Traffic	10566	22387	27585	36539	44427	52171	Ah/day
Daily energy required in AH to compesate for losses	220	492	606	803	995	1147	AH/Day
BS location Lowest PSH in June	2.87	2.85	2.57	3.03	2.8	2.81	Hrs
Total Output from one PV Charger	135	134	121	142	132	132	Ah
No of solar modules in series	7	7	7	8	7	7	
No of solar modules in Parallel	2	4	5	6	8	9	
Total Number of Modules required	14	28	35	48	56	63	
Maximum Solar Module Power EoL	280	255	268	280	268	280	Wmp/module
Maximum PV Generator Wpmax	4620	8400	11025	15840	17640	20790	Wpmax
Inverter capacity /PV Charger Controller	4400	8800	11000	18000	24000	27000	W
Overall System Degradation Loss for 25 yr	0.1777	0.1785	0.1764	0.1777	0.1764	0.1777	0
System Degradation Loss per year	0.0071	0.0071	0.0071	0.0071	0.0071	0.0071	0
Change in Energy Requirement Between the Two Methods	-2%	-4%	-13%	-2%	-1%	0%	

Using the rated and installed 315 Wp module, the 11.3 kW solar PV generator with 17 lithium-ion batteries is designed for a 1.1 kW Mmasemouse BS for 2.5 days of autonomy. The number of modules to be connected in series for the solar PV array to generate the maximum power possible was found to be seven (7) using 270 V as the optimal nominal input voltage to the solar PV charge controller described in Figure 21. Using 290 V as the input voltage increases the number of modules in series from 7 to 8 and the total number of solar PV-array increases from 35 to 42. As a result, for non-hub BSs with no dependencies or standalone BS, 270 V was found to be the optimal and economical design value while not compromising system reliability and improved PR.



The results of Table 11 further show a 15% derating factor at EoL for all six solar plants regardless of the selected solar modules for 25 years, hence a 0.6% derating factor per year. Therefore, for illustration, under proper maintenance, the 315 Wp solar PV module for Mmasemouse BS will derate to 268 Wp as well as current for maximum power  $I_{mp}$  from 8.51 A to 7.22 A after 25 years.

#### 4.5 Base Station Audits Results and Redesign

This section discusses the BSs audit results such as electrical wirings, components sizing and solar PV charge controller configurations from the solar PV-battery system configurations compared to the optimally designed solar PV-battery system using the design steps in the methodology. Table 12 summarizes the major components sizing as per the traditional way of designing using the DEBM without derating factors and other system losses compensations. The results obtained from the audited BSs are discussed, compared and assessed against the optimally sized solar PV-battery summarized in Table 9 and Table 11. Both results show the current number of solar PV modules, solar PV array capacities, number of batteries, total battery storage capacity, number of solar PV chargers and total solar PV charge controller capacity. Only the Makebe BS is to be discussed in this subsection as it was found to have some abnormalities. Other results are to be found in Appendix D.

*Table 12: The traditional BS system sizing using DEBM without derating factors and losses*

Base Stations Current Sizing							
Site Name	No PV Modules	PV Rated Capacity(W)	Batteries	B_Capacity AH	No: PV Charger	PV Charger mod (W)	Controller Capacity(V)
Makebe_ 0.45 kW	14	4640	24	400	3	2200	6600
Malimong_ 0.95 kW	36	10750	24	1500	6	2200	13200
Mmasemouse_ 1.2 kW	30	9450	24	1500	5	2200	11000
Thloro 1.6kW_	39	11340	12	1200	7	2200	15400
Kolo Sys 2 1.1 kW	48	14760	48	3000	7	2200	15400
Scout 2.1kW	0	0	8	800	0	2200	0

The Makebe BS solar PV array was made up of 14 solar PV modules, composed of five different specifications or types, divided into three strings making a 4.640 kWp solar power plant facing north (magnetic or true north) at the tilt angle of  $5^\circ$  as opposed to the  $30^\circ$  recommended in the literature for South Africa [57]. String 1 and string 2 each have four solar PV panels connected in series, resulting in a 151 Vmp input voltage to the solar PV charger that requires at least 290V for maximum power as shown in Appendix A. String 3 also has six solar PV panels connected in series, resulting in a 222 Vmp input voltage to the solar PV charger that is also less than the normal input voltage required for the maximum power as per Figure 21. The Makebe BS solar PV-battery was dimensioned with a 400 Ah



battery storage capacity and 6.6 kW solar PV chargers made up of a 2.2 kW solar PV charge controller per string. The optimized sizing as per Table 9 and Table 11 recommends a 700 Ah storage, two strings connected to a 6 kW solar charger, and a 4.620 kWp solar array.

#### 4.6 Base Station Solar PV- Battery: Key Performance Indicators Analysis

Using the three months' (Nov-Jan) historical BS power database, some key indicators or parameters such as the load current ( $I_{load}$ ), battery current ( $I_{battery}$ ), solar PV generator output current ( $I_{pvc}$ ), solar PV power ( $P_{pvc}$ ), state of charge (SOC), System Voltages ( $U_{sys}$ ), and the actual system power ( $P_{sys}$ ) against the actual BS traffic are analyzed and discussed in this section. The three months' (Nov-Jan) historical data gives the before-optimization results while February to May represents the after-optimization results. For demonstration purposes, only Mmasemouse BS's KPIs are discussed in the next sub-sections. Other results are referenced from Appendices E to M. Mmasemouse was found to be meeting both the regulator and MNO KPIs; it was used as a template or reference for other solar-power BS hence the need to audit how this BS was optimally designed for further optimization. The findings from the key indicators assessment influenced the main objective of the case study to optimally redesign the solar PV hybrid system based on the location radiation data.

##### 4.6.1 Base Station Power Consumption Against Traffic

As it may be recalled, during sunshine hours, the solar generator supplies the actual BS load and charges batteries for night traffic in order to attain 100% network reliability. Figure 26 outlines the BS's actual power consumption against the data traffic measured in Gigabyte (GB) while Figure 27 shows the power consumption against the voice traffic measured in Erlang (Erl) for Mmasemouse BS. Results for other BSs are provided in Appendix E. The obtained results show that the BS power consumption does follow the actual BS traffic pattern but does not go below the typical power consumption during low traffic. This may result in a very high energy intensity defined as the energy used per unit of traffic. Based on the results, the BS's energy-saving features are strongly encouraged for energy conservation as well the BS's reliability improvement to meet the KPIs by reserving energy during less traffic time, mostly between 23H00 and 05H00.

It is vital to note that voice traffic goes to zero between the same time interval (23H00 - 05H00) while data is at its minimal usage, making it difficult to completely shut off the radios. Equally fundamental to highlight is that the actual traffic peaks from around 18H00 to about 22H00 for all of the assessed solar PV-powered BSs and compares well with the power

consumption peaks except the grid-powered and urban BS (Scout) due to its unique load profile as already discussed, thus emphasizing the importance of backup batteries during high revenue-generating time that occurs after sunset.

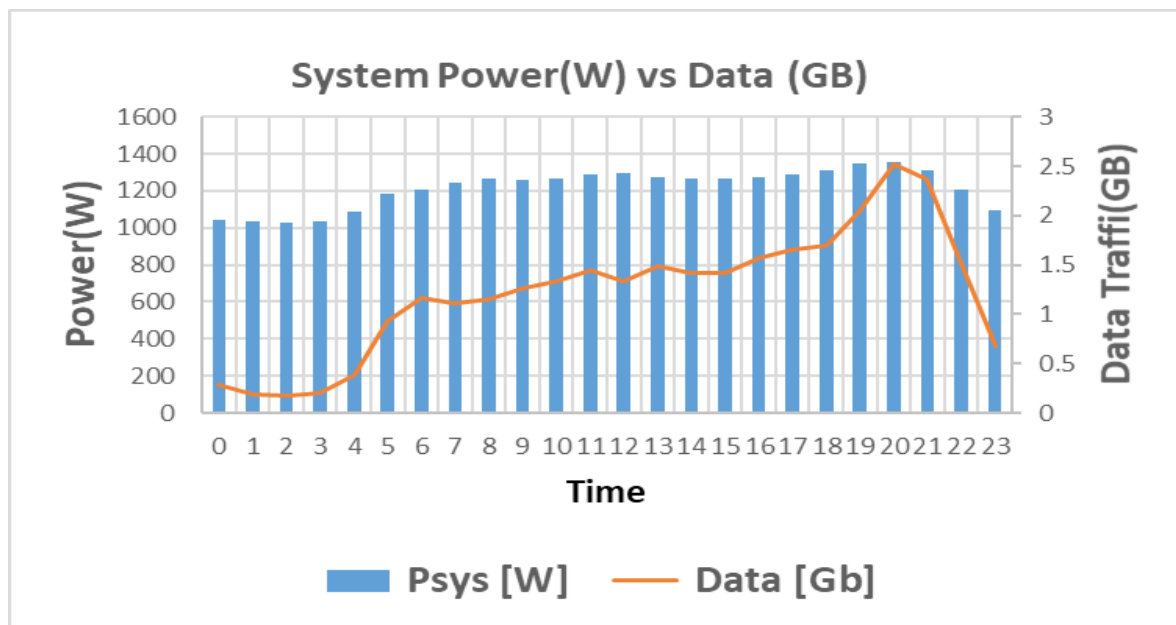


Figure 26: Power consumption against data traffic for Mmasemouse BS

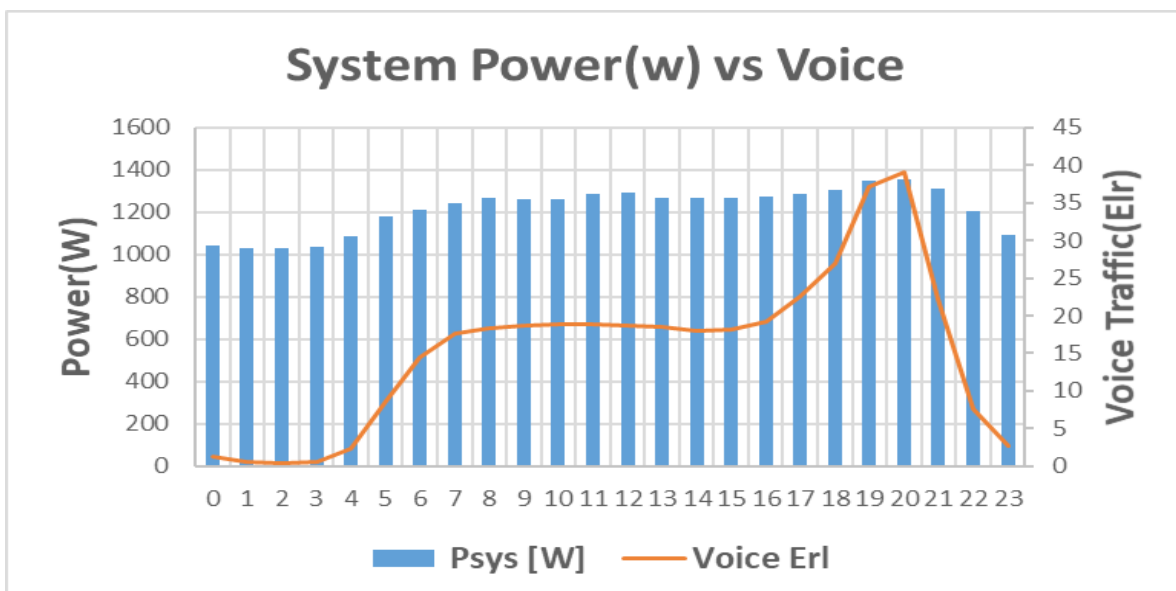


Figure 27: Power consumption against voice traffic for Mmasemouse BS

#### 4.6.2 Base Station Solar PV Currents, Voltages and State of Charge

It is essential to point out that although three months' data from Nov-2022 to Jan-2023 was used for the analyses; the results for the months of January and May are to be compared and discussed following retrofitting or system adjustments implemented from February to April for Mmasemouse BS. One of the major findings from this research is that the existing battery charging current follows a lead acid battery charging characteristics for all the BSs with lead acid batteries as shown in Figure 28 and Appendix F. Figure 28 shows that the batteries are charged from 65.44% SOC to 75.27%, showing an increase of 9.84% within the first four hours (06H00 to 10H00) due to the set float charge voltage at 55.0V. Once the batteries have reached the maximum float charge voltage, the solar PV charge controller starts to limit the charging current and continues to charge the batteries at a very small charging current or declining current till they reach the maximum 86.37% SOC at 16H00 less than the expected SOC of 100% hence showing an increase of only 20.92% from (06H00 to 16H00). It should be noted that in all the audited BSs with lead acid batteries, the solar PV generator failed to fully charge the batteries and start to discharge the batteries before sunset between 15H00-16H00 as shown in Figure 28 and Appendix E.

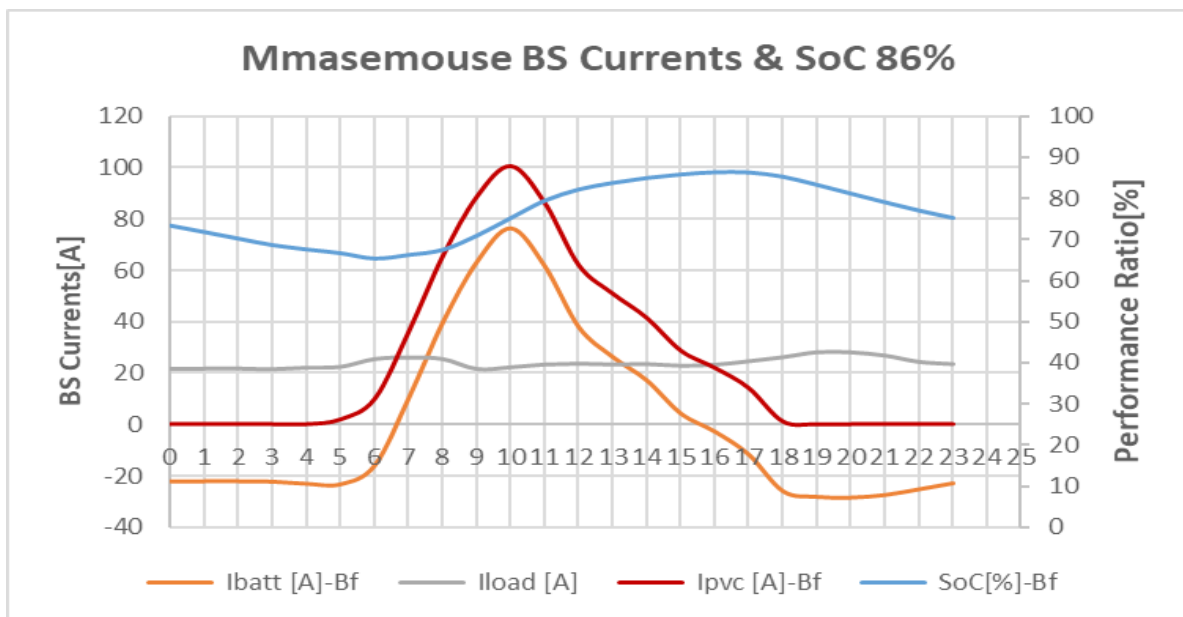


Figure 28: Mmasemouse BS currents against SOC for before optimization

The peak current from the Mmasemouse solar PV generator ( $I_{pvc}$ ) before any optimization was found to be 100.35 A shared between the batteries charging at 76.60 A and the actual load DC load as 22.10 A. Another observation is that; this peak was obtained before the

expected solar radiation peak at 12H00 for the southern hemisphere solar PV power plants. The total energy generated from the PV generator was found to be 606.97 Ah which compares well with the determined daily load requirement in Table 11 for Mmasemouse BS. One observation from this audit was that once the batteries have reached the configured float charge voltage limit, the batteries start to draw less charging current and maintain the float charge state until the solar PV generator ( $I_{pvc}$ ) is not able to meet the demand and the deficit is supplied from the battery storage before sunset. Another observation is that the solar PV current equates to the charging current ( $I_{battery}$ ) and load current ( $I_{load}$ ).

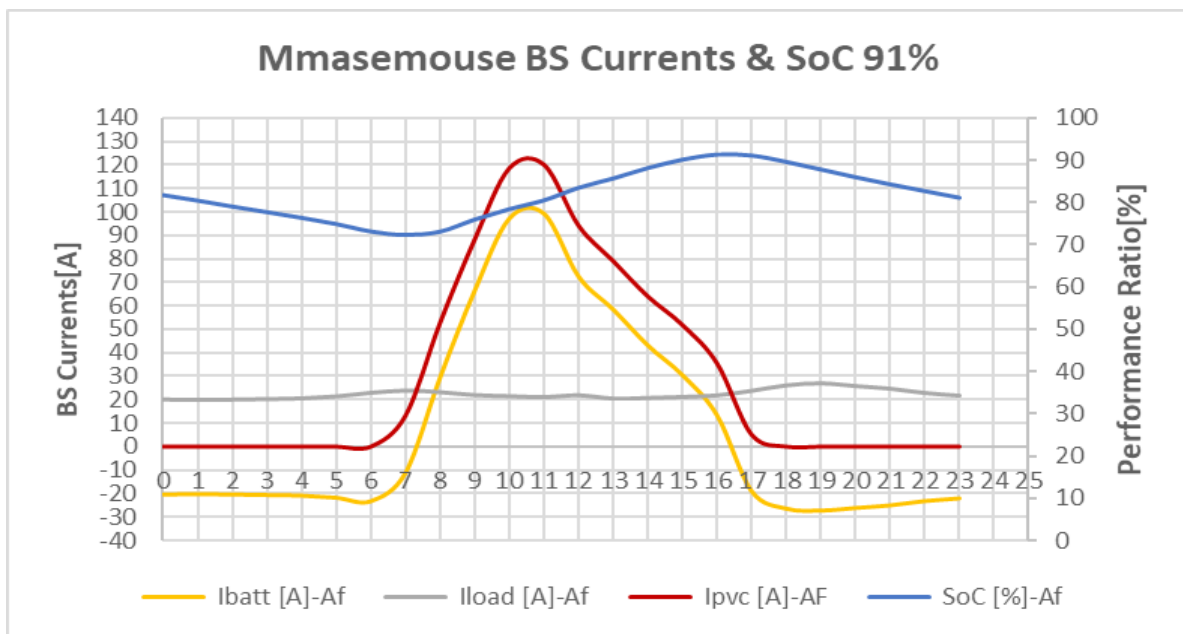


Figure 29: Mmasemouse BS currents against SOC for after optimization

Figure 29 and Appendix G show the results obtained after the solar PV array rewiring and system configuration optimizations. The boost charge voltage was enabled and set to 56.4V for 12hrs to cover the maximum charging duration. The correct float voltage was also set at 56.4 V being the upper limit threshold as opposed to the recommended float of 53.4 V as per the battery specifications. The float charge was set for 12 hrs as it was initially configured. The reconfigured float charge voltage allows the batteries to charge at the maximum rate, whereas the extended boost allows charging at the maximum current for a longer duration while managing the temperature increase through the temperature compensation feature set at 55°C maximum. The optimized parameters and the rewiring from 6 panels per string to 7 increased the input voltage from 270 V to 317 V for the solar PV charger to operate at the maximum output described in Figure 21, hence increasing the solar PV generator current and

charging current for the relatively constant telecom BS load. Figure 30 and Appendix I compare the before and after battery charging currents with an increase of 34% and now discharging at sunset. It can be confirmed that indeed the telecom BS load is constant by comparing discharging currents in January and May in Figure 30 and Appendix I.

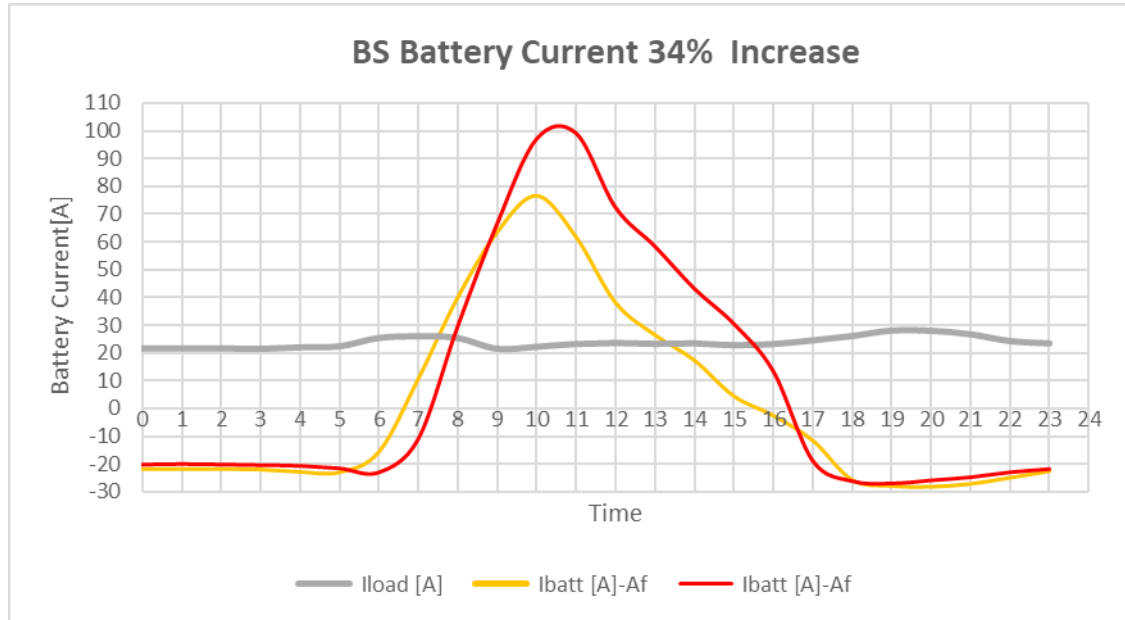


Figure 30: Mmasemouse BS solar PV generator charging currents

The SoC reached 91% at 16H00 showing an increase of 5% compared to the 86.37% SoC obtained before optimization regardless of the increased discharge time in winter, consequently improving the state of health for the batteries by minimizing the number of cycles. It is worth noting that the maximum solar PV generator current improved from 100.35 A to 120.22 A showing an increase of 20% and the harvested energy increased from 606.97 Ah to 723.10 Ah equating to a 19% improvement as shown in Figure 31 and Appendix J. It can be noticed from Figure 30 and Figure 31 that the solar PV generator is currently able to supply the BS load during generation time until sunset at 17H00 while also charging the backup batteries as opposed to January where it discharges at 15H30 before 18H00 at sunset. It should be emphasized that the compared results for January and May have different radiation and PSH as summarized in Table 6 and Figure 31, with January having higher levels of radiation and longer generation time but less solar PV generator energy yield due to optimizations parameter results observed in May. It is also critical to underscore that the earlier the system discharges, the higher the storage requirement, resulting in a high levelised

cost of energy (LCOE), low-performance ratio and negatively impacting the battery EoL cycle.

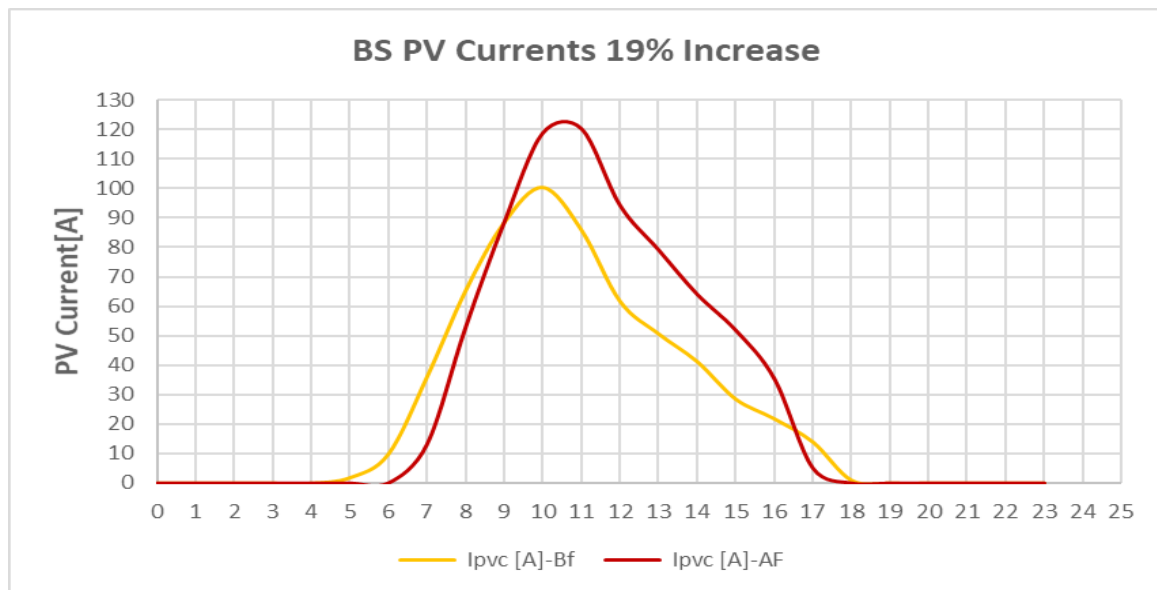


Figure 31: Mmasemouse BS solar PV array currents before and after optimization

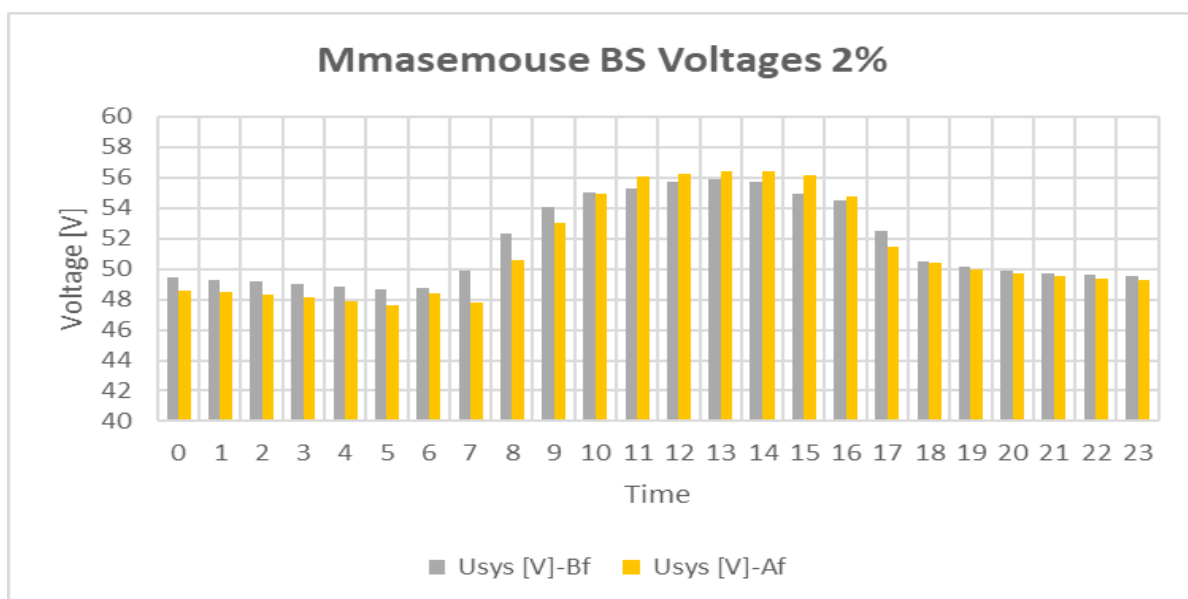


Figure 32: Mmasemouse BS solar PV-battery system voltage before and after optimization

Figure 32 shows the solar PV system voltage ( $U_{sys}$ ) before and after configurations optimization. The solar PV chargers were initially configured to fast-charge the batteries for the first four hours depending on the location's radiation until it reaches the configured float

voltage limit of 55.0 V as opposed to the recommended 53.2 V as per supplier 2V/1500 Ah Shoto lead acid specifications. It can be noted from Figure 32 and Appendix H that the system voltage is slightly higher than before with a peak voltage increase of 2% at 55.9 V after enabling both float charge and boost charge voltage. The obtained results from reconfiguration show improvements in the battery's state of charge as well as the overall energy regenerated. The system voltages dropped to a minimum voltage of 48.8 V which is above the 48 V needed to power the BS. The voltage increases as the radiations increase and maintain the peak value as a result of the extended boost charge voltage to twelve hours.

#### 4.6.3 Base Station Solar PV Power

This section compares and discusses the Mmasemouse BS solar PV generator output power before and after the solar-PV Battery optimization as shown in Figure 33 and other BSs in Appendix J. The solar PV generator gives a maximum power of 5.54 kW at 10H00 compared to 6.69 kW at 11H00 after optimization, showing an energy yield increase of 21%. It should be put forth that the optimized solar PV battery maintains the maximum power for an extended duration, resulting in a 39.484 kWh/day generated energy compared to 32.907 kWh showing an increase of 17%. As it has already been discussed, the rewired and optimized solar PV-Battery system follows the lead acid charging curve characteristics not the radiation pattern as in other standalone solar plants without backup batteries.

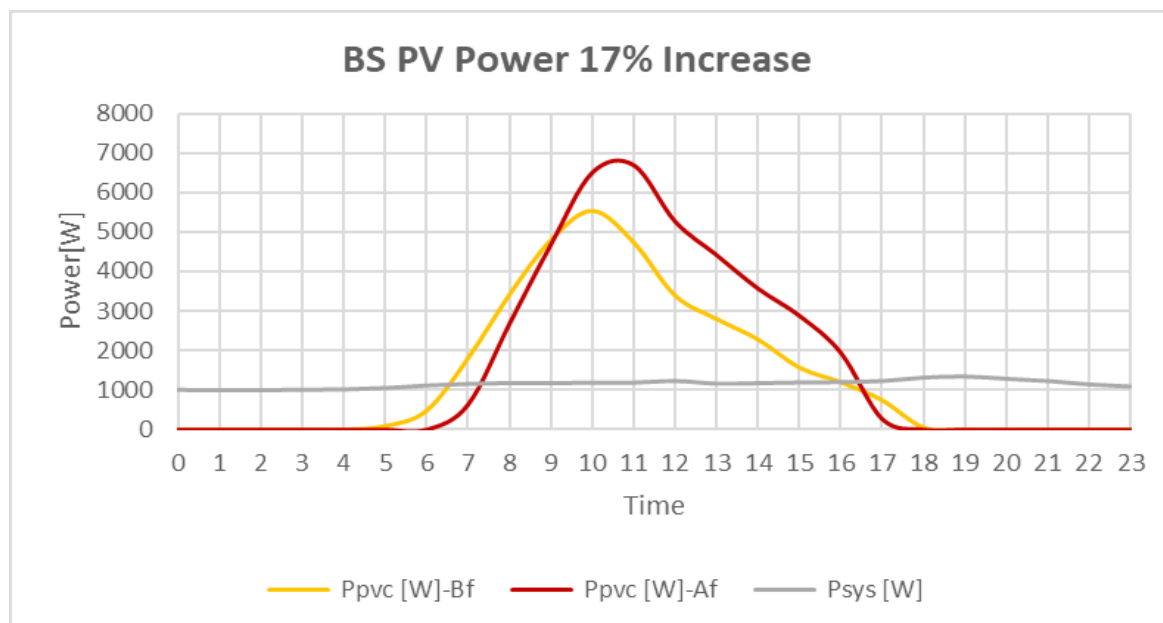


Figure 33: Mmasemouse BS solar PV power before and after optimization

These noticeable improvements in KPIs were not only obtained in May with fewer radiation levels but also at a reduced cost since there were no additional resources added to increase capacity, rather some solar PV chargers and modules were recovered after solar rewiring and faulty components replacement. It should also be recalled that before this research experiment, only two BSs (Mmasemouse and Malimong) were meeting the targets of 100% overall system reliability without DG except for Ha Tlhorho as it has a standby DG. The Makebe BS failed due to poor design and solar panels mismatch while the Kolo BS failed due to poor design.

#### 4.7 Base Stations Performance Ratio

This subsection discusses and compares the before-optimization and after-optimization performance ratios (PRs) of five selected solar-powered BS. The four selected BSs namely; Makebe, Malimong, Kolo, and Mmasemouse have lead-acid backup batteries while Tlhorho has Lithium-ion batteries as shown in Table 5. The performance ratio was calculated using the actual solar PV power (Ppvc) from the historical data and the calculated PV power on the tilted angle using ..... (2 from the literature based on the BS location meteorological data. The month of January before changes and May after optimizations are used for comparison. The hourly averages are used with the average PR calculated from 08H00 to 16H00 for both months.

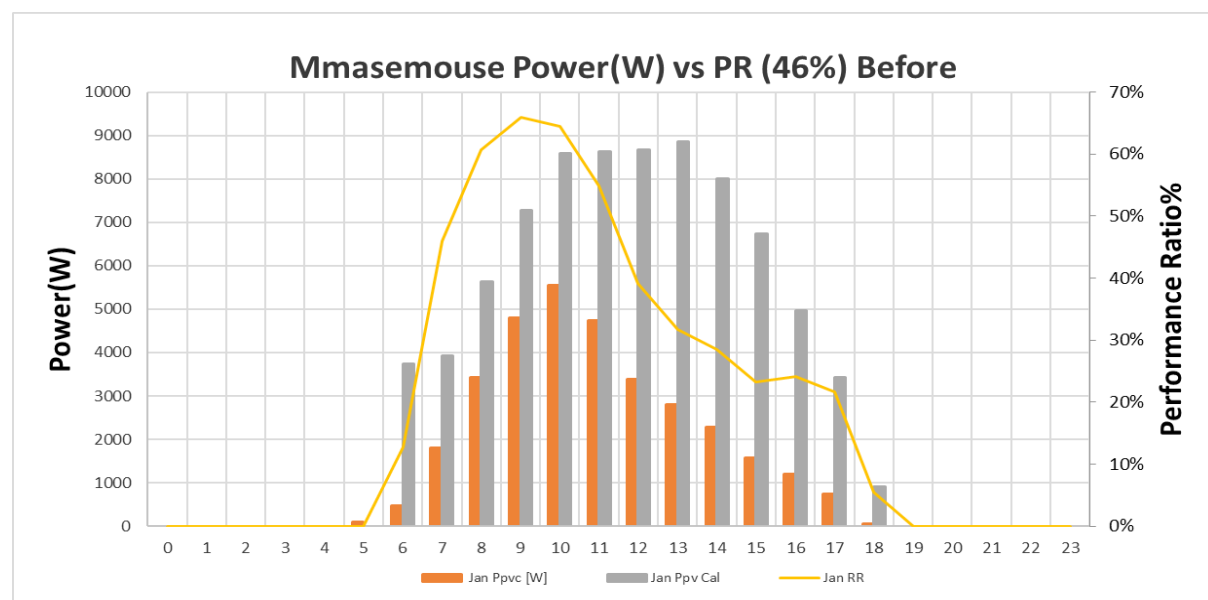


Figure 34: Mmasemouse BS performance ratio before optimization



Figure 34 shows the PR for the Mmasemouse BS before solar array rewiring and parameter optimizations and other BS's PRs are summarised in Appendix L. The planned and installed solar array capacity for the Mmasemouse BS solar plant was 11.3 kW. The solar array was composed of 36 solar PV modules, each rated at 315 Wp and covering a 1.9 m<sup>2</sup> cross-sectional area. The solar array was made up of 6 strings connected in parallel and each string was made up of 6 solar panels connected in series. Mmasemouse BS solar PV-battery plant shows a PR of 46.07% on average using

.....  
 ..... (12 and a peak of 65.89% around 10H00 which is less than the 75% recommended value. It should be noted that this peak does not correlate with radiation peaks which normally occur at 12H00. It can safely be concluded that the actual power consumption does not follow the radiation pattern leading to poor PR or overall system efficiency.

Figure 35 shows the PR for the Mmasemouse BS after rewiring and parameter optimization. The optimised solar PV-battery plant now shows an average PR of 53.46%, showing an increase of 7.39% compared to 46.07% obtained before improvement initiatives as shown in Figure 34. The obtained PR peaks at 77.03% at 11H00 slightly above the recommended value of 75%. It should be noted that this peak does not correlate with the radiation that peaks at 12H00 for May as per ..... (2 described in Figure 35 using radiation data from Meteornorm, indicating that further optimization can be considered. It is also significant to emphasize that the improved PR is due to the increased charging time and charging currents as well as the improved output power from the PV chargers as a result of optimum solar array rewiring.

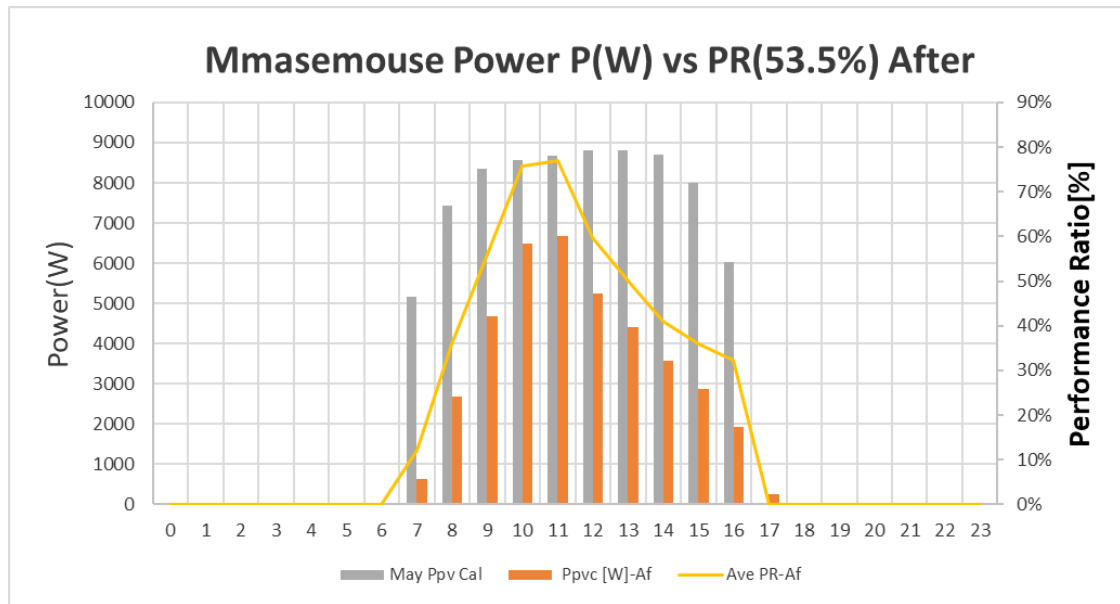


Figure 35: Mmasemouse BS performance ratio after optimization

#### 4.8 The Base Station Solar PV-Battery System Reliability

Having designed and optimized the selected solar hybrid systems, the last step is to compare their simulated annual performance before doing any optimization, and their annual performance after optimization. Figure 36 shows the annual performance for Mmasemouse BS before doing any optimization and indicates that the BS was stable and had an excess of 0.11 kW in June for a 1.1 kW load. On average, for over 12 months, the solar-PV battery system had a 2.1 kW hourly solar contribution leading to a 0.95 kW surplus before any optimization.

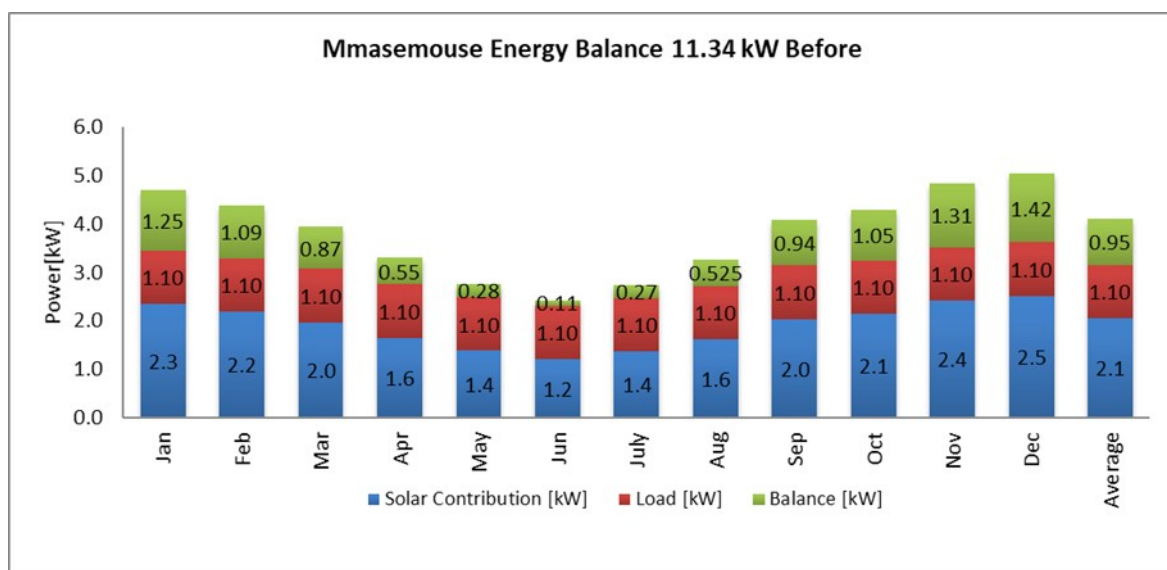


Figure 36: 11.34 kW Mmasemouse BS's simulated annual performance before optimization

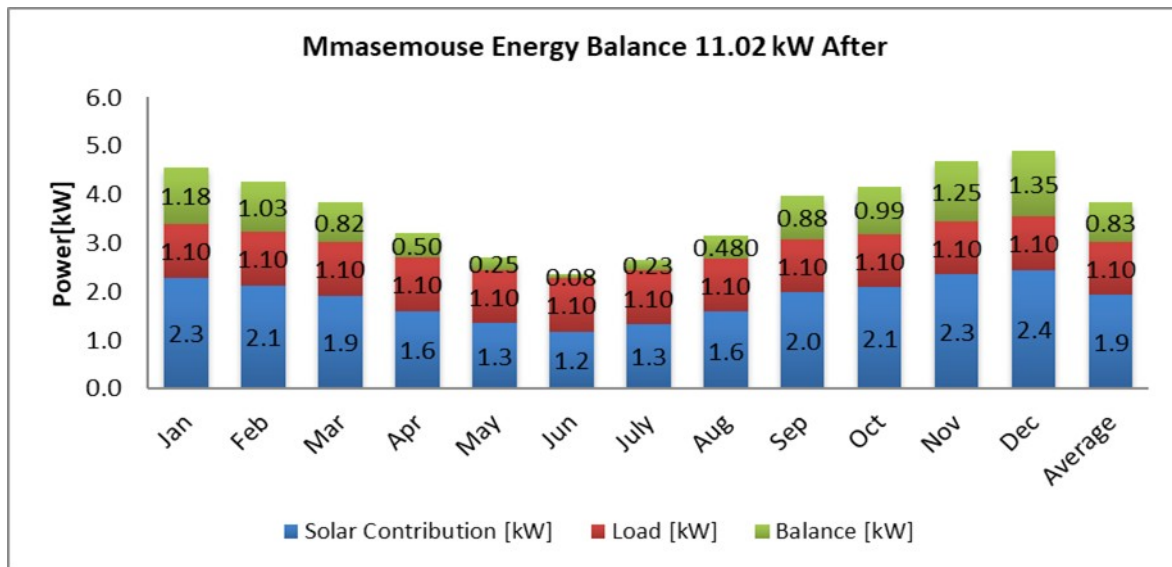


Figure 37: 11.02 kW Mmasemouse BS's simulated annual performance after optimization

Figure 37 shows the current performance of the Mmasemouse BS after it was optimally sized with an 11.02 kW solar PV array and an installed 1500 Ah backup battery capacity. Using the lowest PSH from Table 6 which can also be defined as the average daily energy production from the given system measured in kWh/d, the results show that the planned solar plant will meet the demand for the whole year. The month of June with the lowest PSH is used as the design month, and the plant will only dump 0.08 kW in June compared to the 0.11 kW dumped before optimization. It is worth noting that the maximum solar contributions are to be expected in November with 2.34 kW, December with 2.44 kW, and January with 2.28 kW, resulting in excesses of 1.24 kW, 1.34 kW and 1.18 kW respectively for a 1.1 kW load BS. On average, the currently designed solar-PV battery system has a 1.99 kW hourly solar contribution leading to a 0.89 kW surplus after optimization compared to 0.95 kW before optimization.

Although most of the results showed positive results. There were some challenges meet, to mention but few: Allocation of budget to implement the recommendations that need capital investment for better results, lack of long duration historical data at least for twelve months for detailed analysis as opposed to four months' data and lastly no standard solar controller configurations resulting is different results for sites with similar power and radio configurations.



## 5 CONCLUSION AND RECOMMENDATIONS

The solar PV resource and high altitudes in Lesotho are among the best and highest in the world. Recently, MNOs in Lesotho have seen an increase in the deployment of solar PV-powered base stations in rural areas to improve network coverage for the mostly compromised communities. This justifies the need to model and design an optimal solar PV-battery system to power telecom base stations operating in high-speed technologies that meet both the MNO and regulator targets. Historical data from five solar-powered and one grid-connected BS was used to assess the BS's performance and calculate their solar array performance ratios.

The meteorological assessment results for the Mmasemouse BS showed the maximum global horizontal radiation of 249 kWh/m<sup>2</sup> in December and averages at 182 kWh/m<sup>2</sup> with 21.7°C ambient temperature in January and the lowest PSH being 2.57 hrs in June which is used as the design month. It was observed that all the selected BSs have favourable ambient temperatures and high radiation levels as well as the highest PSHs in summer starting in November to March, but very low clearness indices due to the highest levels of precipitation compared to winter starting in April to July having high clearness indices but low radiation levels and smallest PSHs. Based on these results, the maximum PR is expected between August and October due to favourable radiation levels, clearness index, fewer levels of precipitation and average PSH compared to other months.

The daily energy balance method and time step method were used for load determination using the equipment's technical specifications as well the historical data. The time step method is highly recommended as it relies on the historical data for load profiles; it was used to determine the normalized load coefficients that can be extrapolated to new BS deployments with similar radio configurations integrated with DEBM. The TSM resulted in a 0.4 kW load requirement for Makebe BS, 0.9 kW for Malimong BS, 1.1 kW for Mmasemouse BS, 1.5 kW for Tlhoru BS, 1.9 kW for Kolo BS, and 2.2 kW load for Scout BS respectively.

Based on the determined load requirements, the solar PV-battery system components were audited and optimally resized to meet the highest reliability which will not only assist in protecting the MNO's revenue and meeting the MNO and regulator targets, but also in maintaining a good customer experience. The optimized system sizing results and solar PV-

battery's major KPIs were analysed and compared with the results prior to optimization. The results show that the power consumption follows the actual traffic and is not as constant as other researchers revealed, it however does not go below the typical power consumption, hence a recommendation for power-saving features activation to conserve more energy.

The optimized results show an increase of 6% in SoC from 86% to 91% in January and May for the Mmasemouse BS while other BSs were found not configured to measure the SoC. The rewiring and solar PV charger/MPPT controller optimization resulted in a 20% increase in the solar PV generator current for Mmasemouse BS, an improvement of 34% in charging current, and a 17% increase in solar PV power resulting in a 7.4% performance ratio increase from 46% to 53.5% with only 0.08 kW surplus in June. The only recommendation for the Mmasemouse BS is to increase the backup capacity from a 1500 Ah lead acid battery to a 1700 Ah battery to meet 2.5 days of autonomy time.

There is no noticeable improvement from the Makebe BS; a recommendation is therefore made to replace the existing mismatching solar PV panels, increase the tilt angle from 5° to 30°, and backup storage from 400 Ah to 700 Ah so as to improve the PR from 35%. The solar PV output current for Malimong increased by 12%, the battery charging current by 23%, solar PV power by 11%, and the PR by 3.5% from 31% to 34.5%. To further improve the Malimong BS's PR, it is highly recommended to downgrade the solar plant from a 10.8 kW capacity to 8.4 kW or introduce new technologies, thus increasing the BS load and generating more revenue with the current surplus that is being dumped.

After replacing faulty backup batteries at Ha Tlhoru BS, the following improvements were noticed: a solar PV generator current increased by 90%, charging current by 60%, solar PV power by 46%, and PR by 27% from 20% to 47%. The recommendation for Ha Tlhoru BS is to replace the existing solar panels that have reached EoL with a 15.8 kW solar array and a 2300 Ah battery without the backup DG. After integrating the two standalone solar arrays into one, rewiring the solar panels, increasing the charging current limitation and replacing faulty batteries for a high-capacity solar-powered BS in Kolo, the following results were obtained: solar PV generator current increased by 7%, battery charging current by 19% while solar PV power improved by 40%, and PR by 59% from 34% to 53.2% peaking at 90%. It is worth mentioning that, the installed lithium batteries were then managed directly from the battery management system (BMS) leading to 100% SoC at 15H00. To achieve close to 100% reliability for the Kolo BS, it is recommended to increase the current 14.7 kW solar

array to 17.6 kW and storage from 1200 Ah to 2900 Ah for 2.5 days of autonomy. It can be deduced from this research that the backup battery health status, BS load, and solar PV charge controller configuration, solar PV array wiring have a direct impact on the overall solar PV array performance ratio.

As a result of the optimal redesign, there was a significant improvement in the BSs' performance ratios as well as the system reliability, implying MNO revenue protection and good customer experience. The same procedure can be used by other local MNOs, solar PV-battery systems, and mini-grid developers to improve their system efficiencies. The determined BS's normalized load profile coefficients summarized in Appendix N can be extrapolated to new BS deployments using the supplier's technical specifications.

Although there are visible improvements, some challenges were encountered while conducting this research. These challenges and limitations include access to prolonged historical data (as most of the Delta Orion charge controllers can only keep data for a maximum of four months), inconsistent configurations throughout the network, limited time, and restrictive budget to optimize the solar PV collector's tilt angles to improve PR. It is therefore recommended that old charge controllers should be replaced with new versions, standardized configurations be implemented and the BS's plants information or data collection be connected to the cloud for end-to-end monitoring and data processing. A proposition is therefore made for further studies in the telecom industry with a direct focus on the techno-economic analysis between solar-powered and grid-powered BS, determination of the optimal backup batteries autonomy time as well as energy management principles to control operational costs while reducing carbon emissions as well.

## REFERENCES

- [1] C.-N. Wang, T.-T. Dang, N.-A.-T. Nguyen, and J.-W. Wang, "A combined Data Envelopment Analysis (DEA) and Grey Based Multiple Criteria Decision Making (G-MCDM) for solar PV power plants site selection: A case study in Vietnam," *Energy Reports*, vol. 8, pp. 1124–1142, Nov. 2022, doi: 10.1016/j.egyr.2021.12.045.
- [2] K. R. Santhi and G. Senthil Kumaran, "Solar Powered Wi-Fi with Wimax Enables Third World Phones," in *Proceedings from the International Conference on Advances in Engineering and Technology*, Elsevier, 2006, pp. 635–646. doi: 10.1016/B978-008045312-5/50069-8.
- [3] Shorai Kavu (PhD Student), Professor Maria Tsvere, Professor Wilbert Mtangi, and Tawanda Hove, "Establishing the most cost effective reliability for off-grid solar systems in Zimbabwe: Trade-off, between energy supply reliability and levelised cost of energy.," vol. 1, no. 1, 2022.
- [4] D. F. Birol, "World Energy Outlook 2022", [Online]. Available: <https://iea.blob.core.windows.net/assets/830fe099-5530-48f2-a7c1-11f35d510983/WorldEnergyOutlook2022.pdf>
- [5] A. Ayough, S. Boshruai, and B. Khorshidvand, "A new interactive method based on multi-criteria preference degree functions for solar power plant site selection," *Renewable Energy*, vol. 195, pp. 1165–1173, Aug. 2022, doi: 10.1016/j.renene.2022.06.087.
- [6] B. M. Taele, L. Mokhutsoane, I. Hapazari, S. B. Tlali, and M. Senatla, "Grid electrification challenges, photovoltaic electrification progress and energy sustainability in Lesotho," *Renewable and Sustainable Energy Reviews*, vol. 16, no. 1, pp. 973–980, Jan. 2012, doi: 10.1016/j.rser.2011.09.019.
- [7] S. Paudel, J. N. Shrestha, F. J. Neto, J. A. F. Ferreira, and M. Adhikari, "Optimization of hybrid PV/wind power system for remote telecom station," in *2011 International Conference on Power and Energy Systems*, Chennai, India: IEEE, Dec. 2011, pp. 1–6. doi: 10.1109/ICPES.2011.6156618.
- [8] A. El Hammoumi, S. Chtita, S. Motahhir, and A. El Ghzizal, "Solar PV energy: From material to use, and the most commonly used techniques to maximize the power output of PV systems: A focus on solar trackers and floating solar panels," *Energy Reports*, vol. 8, pp. 11992–12010, Nov. 2022, doi: 10.1016/j.egyr.2022.09.054.
- [9] M. S. Dahal, J. N. Shrestha, and S. R. Shakya, "Energy saving technique and measurement in green wireless communication," *Energy*, vol. 159, pp. 21–31, Sep. 2018, doi: 10.1016/j.energy.2018.06.066.
- [10] Dulip Tillekeratne, "Renewable Energy for Mobile Towers: Opportunities for low- and middle-income countries.," Sep. 2020. [Online]. Available: <https://www.gsma.com/mobilefordevelopment/resources/renewable-energy-for-mobile-towers-opportunities-for-low-and-middle-income-countries/>
- [11] J. Guo, L. Wang, W. Zhou, and C. Wei, "Powering green digitalization: Evidence from 5G network infrastructure in China," *Resources, Conservation and Recycling*, vol. 182, p. 106286, Jul. 2022, doi: 10.1016/j.resconrec.2022.106286.
- [12] L. Z. Thamae, "Simulation and Optimization of Renewable Energy Hybrid Power System for Semonkong, Lesotho," in *Africa-EU Renewable Energy Research and Innovation Symposium 2018 (RERIS 2018)*, M. Mpholo, D. Steuerwald, and T. Kukeera, Eds., in Springer Proceedings in Energy. Cham: Springer International Publishing, 2018, pp. 105–115. doi: 10.1007/978-3-319-93438-9\_9.



- [13] A. Israr, Q. Yang, W. Li, and A. Y. Zomaya, "Renewable energy powered sustainable 5G network infrastructure: Opportunities, challenges and perspectives," *Journal of Network and Computer Applications*, vol. 175, p. 102910, Feb. 2021, doi: 10.1016/j.jnca.2020.102910.
- [14] O. Shurdi, L. Ruci, A. Biberaj, and G. Mesi, "5G Energy Efficiency Overview," *ESJ*, vol. 17, no. 03, Jan. 2021, doi: 10.19044/esj.2021.v17n3p315.
- [15] G. J. May, "Standby battery requirements for telecommunications power," *Journal of Power Sources*, vol. 158, no. 2, pp. 1117–1123, Aug. 2006, doi: 10.1016/j.jpowsour.2006.02.083.
- [16] J. Simo-Reigadas *et al.*, "Sharing low-cost wireless infrastructures with telecommunications operators to bring 3G services to rural communities," *Computer Networks*, vol. 93, pp. 245–259, Dec. 2015, doi: 10.1016/j.comnet.2015.09.006.
- [17] I. P. Chochliouros *et al.*, "Energy Efficiency Concerns and Trends in Future 5G Network Infrastructures," *Energies*, vol. 14, no. 17, p. 5392, Aug. 2021, doi: 10.3390/en14175392.
- [18] M. S. Hossain Lipu *et al.*, "A review of controllers and optimizations based scheduling operation for battery energy storage system towards decarbonization in microgrid: Challenges and future directions," *Journal of Cleaner Production*, vol. 360, p. 132188, Aug. 2022, doi: 10.1016/j.jclepro.2022.132188.
- [19] "Connecting for a better future – digital, sustainable and inclusive." Apr. 2021. [Online]. Available: [https://www.vodafone.com/sites/default/files/2021-06/Vodafone\\_Green\\_credentials\\_report\\_PUBLIC.pdf](https://www.vodafone.com/sites/default/files/2021-06/Vodafone_Green_credentials_report_PUBLIC.pdf)
- [20] Vodacom Internal Report, "LS\_PRWL007\_Weekly\_NED\_Report\_20220731.xlsx," Vodacom Lesotho, Network Performance Weekly Reports, Jun. 2022.
- [21] M. Mpholo, T. Nchaba, and M. Monese, "Yield and performance analysis of the first grid-connected solar farm at Moshoeshoe I International Airport, Lesotho," *Renewable Energy*, vol. 81, pp. 845–852, Sep. 2015, doi: 10.1016/j.renene.2015.04.001.
- [22] A. Srivastava, M. S. Gupta, and G. Kaur, "Energy efficient transmission trends towards future green cognitive radio networks (5G): Progress, taxonomy and open challenges," *Journal of Network and Computer Applications*, vol. 168, p. 102760, Oct. 2020, doi: 10.1016/j.jnca.2020.102760.
- [23] G. Jansen, Z. Dehouche, and H. Corrigan, "Cost-effective sizing of a hybrid Regenerative Hydrogen Fuel Cell energy storage system for remote & off-grid telecom towers," *International Journal of Hydrogen Energy*, vol. 46, no. 35, pp. 18153–18166, May 2021, doi: 10.1016/j.ijhydene.2021.02.205.
- [24] Y. Noorollahi, A. Ghenaatpisheh Senani, A. Fadaei, M. Simaee, and R. Moltames, "A framework for GIS-based site selection and technical potential evaluation of PV solar farm using Fuzzy-Boolean logic and AHP multi-criteria decision-making approach," *Renewable Energy*, vol. 186, pp. 89–104, Mar. 2022, doi: 10.1016/j.renene.2021.12.124.
- [25] H. Z. Al Garni and A. Awasthi, "Solar PV power plant site selection using a GIS-AHP based approach with application in Saudi Arabia," *Applied Energy*, vol. 206, pp. 1225–1240, Nov. 2017, doi: 10.1016/j.apenergy.2017.10.024.
- [26] H. Z. Al Garni and A. Awasthi, "Solar PV Power Plants Site Selection," in *Advances in Renewable Energies and Power Technologies*, Elsevier, 2018, pp. 57–75. doi: 10.1016/B978-0-12-812959-3.00002-2.
- [27] A. Srivastava, M. S. Gupta, and G. Kaur, "Energy efficient transmission trends towards future green cognitive radio networks (5G): Progress, taxonomy and open challenges," *Journal of Network and Computer Applications*, vol. 168, p. 102760, Oct. 2020, doi: 10.1016/j.jnca.2020.102760.

- [28] E. Jedou *et al.*, “A cartographic approach coupled with optimized sizing and management of an on-grid hybrid PV-solar-battery-group based on the state of the sky: An african case study,” *Solar Energy*, vol. 227, pp. 101–115, Oct. 2021, doi: 10.1016/j.solener.2021.08.079.
- [29] “India Energy Security Scenarios, 2047 User guide for telecom Sector.” [Online]. Available: <https://smartnet.niua.org/sites/default/files/resources/telecom.pdf>
- [30] Č. Zeljković, P. Mršić, B. Erceg, Đ. Lekić, N. Kitić, and P. Matić, “Optimal sizing of photovoltaic-wind-diesel-battery power supply for mobile telephony base stations,” *Energy*, vol. 242, p. 122545, Mar. 2022, doi: 10.1016/j.energy.2021.122545.
- [31] I. A. Ibrahim, S. Sabah, R. Abbas, M. J. Hossain, and H. Fahed, “A novel sizing method of a standalone photovoltaic system for powering a mobile network base station using a multi-objective wind driven optimization algorithm,” *Energy Conversion and Management*, vol. 238, p. 114179, Jun. 2021, doi: 10.1016/j.enconman.2021.114179.
- [32] K. Anoune, M. Bouya, A. Astito, and A. B. Abdellah, “Sizing methods and optimization techniques for PV-wind based hybrid renewable energy system: A review,” *Renewable and Sustainable Energy Reviews*, vol. 93, pp. 652–673, Oct. 2018, doi: 10.1016/j.rser.2018.05.032.
- [33] R. Satpathy and V. Pamuru, “Off-grid solar photovoltaic systems,” in *Solar PV Power*, Elsevier, 2021, pp. 267–315. doi: 10.1016/B978-0-12-817626-9.00007-1.
- [34] H. Abid, J. Thakur, D. Khatiwada, and D. Bauner, “Energy storage integration with solar PV for increased electricity access: A case study of Burkina Faso,” *Energy*, vol. 230, p. 120656, Sep. 2021, doi: 10.1016/j.energy.2021.120656.
- [35] L. Ren, S. Zhang, L. Li, X. Xu, Y. Zhang, and F. Wang, “Efficiency diagnosis and optimization in distributed solar plants,” *Energy for Sustainable Development*, vol. 63, pp. 24–32, Aug. 2021, doi: 10.1016/j.esd.2021.05.001.
- [36] W. Bingbing, Y. Zhongdong, and X. Xiangning, “Design of Simulation Model of PV Cells Based on VSR PWM Rectifier Circuit,” in *2009 International Conference on Energy and Environment Technology*, Guilin, China: IEEE, 2009, pp. 127–130. doi: 10.1109/ICEET.2009.268.
- [37] B. Patra, P. Nema, M. Z. Khan, and O. Khan, “Optimization of solar energy using MPPT techniques and industry 4.0 modelling,” *Sustainable Operations and Computers*, vol. 4, pp. 22–28, 2023, doi: 10.1016/j.susoc.2022.10.001.
- [38] D. Scamman, M. Newborough, and H. Bustamante, “Hybrid hydrogen-battery systems for renewable off-grid telecom power,” *International Journal of Hydrogen Energy*, vol. 40, no. 40, pp. 13876–13887, Oct. 2015, doi: 10.1016/j.ijhydene.2015.08.071.
- [39] E. Gul *et al.*, “A techno-economic analysis of a solar PV and DC battery storage system for a community energy sharing,” *Energy*, vol. 244, p. 123191, Apr. 2022, doi: 10.1016/j.energy.2022.123191.
- [40] W. Margaret Amutha and V. Rajini, “Techno-economic evaluation of various hybrid power systems for rural telecom,” *Renewable and Sustainable Energy Reviews*, vol. 43, pp. 553–561, Mar. 2015, doi: 10.1016/j.rser.2014.10.103.
- [41] B. A. Bhayo, H. H. Al-Kayiem, and S. I. Gilani, “Assessment of standalone solar PV-Battery system for electricity generation and utilization of excess power for water pumping,” *Solar Energy*, vol. 194, pp. 766–776, Dec. 2019, doi: 10.1016/j.solener.2019.11.026.
- [42] S. Roy, M. S. Baruah, S. Sahu, and B. B. Nayak, “Computational analysis on the thermal and mechanical properties of thin film solar cells,” *Materials Today: Proceedings*, vol. 44, pp. 1207–1213, 2021, doi: 10.1016/j.matpr.2020.11.241.

- [43] “IS/IEC 61724 (1998): Photovoltaic System Performance Monitoring - Guidelines for Measurement, Data exchange and Analysis”.
- [44] “How to calculate PV performance ratio and performance index,” Hukseflux Thermal Sensors, Version 1806. [Online]. Available: [https://www.hukseflux.com/uploads/inline/note-how\\_to\\_calculate\\_pv\\_power\\_plant\\_performance\\_ratio\\_and\\_performance\\_index\\_v2007.pdf](https://www.hukseflux.com/uploads/inline/note-how_to_calculate_pv_power_plant_performance_ratio_and_performance_index_v2007.pdf)
- [45] T. Salamah *et al.*, “Effect of dust and methods of cleaning on the performance of solar PV module for different climate regions: Comprehensive review,” *Science of The Total Environment*, vol. 827, p. 154050, Jun. 2022, doi: 10.1016/j.scitotenv.2022.154050.
- [46] A. H. Alami *et al.*, “Management of potential challenges of PV technology proliferation,” *Sustainable Energy Technologies and Assessments*, vol. 51, p. 101942, Jun. 2022, doi: 10.1016/j.seta.2021.101942.
- [47] S. Şevik and A. Aktaş, “Performance enhancing and improvement studies in a 600 kW solar photovoltaic (PV) power plant; manual and natural cleaning, rainwater harvesting and the snow load removal on the PV arrays,” *Renewable Energy*, vol. 181, pp. 490–503, Jan. 2022, doi: 10.1016/j.renene.2021.09.064.
- [48] Z. Song, J. Liu, and H. Yang, “Air pollution and soiling implications for solar photovoltaic power generation: A comprehensive review,” *Applied Energy*, vol. 298, p. 117247, Sep. 2021, doi: 10.1016/j.apenergy.2021.117247.
- [49] M. Alian Fini, D. Gharapetian, and M. Asgari, “Efficiency improvement of hybrid PV-TEG system based on an energy, exergy, energy-economic and environmental analysis; experimental, mathematical and numerical approaches,” *Energy Conversion and Management*, vol. 265, p. 115767, Aug. 2022, doi: 10.1016/j.enconman.2022.115767.
- [50] A. K. Hamzat, A. Z. Sahin, M. I. Omisanya, and L. M. Alhems, “Advances in PV and PVT cooling technologies: A review,” *Sustainable Energy Technologies and Assessments*, vol. 47, p. 101360, Oct. 2021, doi: 10.1016/j.seta.2021.101360.
- [51] A. O. M. Maka, S. Salem, and M. Mehmood, “Solar photovoltaic (PV) applications in Libya: Challenges, potential, opportunities and future perspectives,” *Cleaner Engineering and Technology*, vol. 5, p. 100267, Dec. 2021, doi: 10.1016/j.clet.2021.100267.
- [52] Y. Wu *et al.*, “A review of self-cleaning technology to reduce dust and ice accumulation in photovoltaic power generation using superhydrophobic coating,” *Renewable Energy*, vol. 185, pp. 1034–1061, Feb. 2022, doi: 10.1016/j.renene.2021.12.123.
- [53] A. F. Sagonda and K. A. Folly, “A comparative study between deterministic and two meta-heuristic algorithms for solar PV MPPT control under partial shading conditions,” *Systems and Soft Computing*, vol. 4, p. 200040, Dec. 2022, doi: 10.1016/j.sasc.2022.200040.
- [54] I. Shams, S. Mekhilef, and K. S. Tey, “Advancement of voltage equalizer topologies for serially connected solar modules as partial shading mitigation technique: A comprehensive review,” *Journal of Cleaner Production*, vol. 285, p. 124824, Feb. 2021, doi: 10.1016/j.jclepro.2020.124824.
- [55] D. Adak, R. Bhattacharyya, and H. C. Barshilia, “A state-of-the-art review on the multifunctional self-cleaning nanostructured coatings for PV panels, CSP mirrors and related solar devices,” *Renewable and Sustainable Energy Reviews*, vol. 159, p. 112145, May 2022, doi: 10.1016/j.rser.2022.112145.
- [56] A. A. Ashetehe, B. B. Gessesse, and F. Shewarega, “A generalized approach for the determination of optimum tilt angle for solar photovoltaic modules with selected locations in Ethiopia as illustration examples,” *Scientific African*, vol. 18, p. e01433, Nov. 2022, doi: 10.1016/j.sciaf.2022.e01433.

- [57] W. G. Le Roux, "Optimum tilt and azimuth angles for fixed solar collectors in South Africa using measured data," *Renewable Energy*, vol. 96, pp. 603–612, Oct. 2016, doi: 10.1016/j.renene.2016.05.003.
- [58] "ZTE Renewable Energy Solutions." [Online]. Available: [https://www.smartcitiescouncil.com/sites/default/files/main/public\\_resources/ZTE%20Renewable%20Energy%20Solutions\\_0.pdf](https://www.smartcitiescouncil.com/sites/default/files/main/public_resources/ZTE%20Renewable%20Energy%20Solutions_0.pdf)
- [59] "RRU3908 Description." HUAWEI TECHNOLOGIES CO., LTD., 02052012. [Online]. Available: [https://cosconor.fr/GSM/Divers/Equipment/Huawei/-%20Huawei%20RRU%20\(2019\)/RRU%203908/Description.pdf](https://cosconor.fr/GSM/Divers/Equipment/Huawei/-%20Huawei%20RRU%20(2019)/RRU%203908/Description.pdf)
- [60] "OptiX RTN 905 2F." Huawei Technologies Co., Ltd. Huawei Industrial Base Bantian, Longgang Shenzhen 518129 People's Republic of China. [Online]. Available: <https://cosconor.fr/GSM/Divers/Equipment/Huawei/-%20RTN%20Microwave/RTN%20905%20Brochure.pdf>
- [61] M. Deruyck, E. Tanghe, W. Joseph, and L. Martens, "Modelling and optimization of power consumption in wireless access networks," *Computer Communications*, vol. 34, no. 17, pp. 2036–2046, Nov. 2011, doi: 10.1016/j.comcom.2011.03.008.
- [62] H. T. Co, "Product Description," no. 03.
- [63] Huawei Technologies Co., Ltd. Huawei Industrial Base, "RRU5909 Description." Huawei Industrial Base Bantian, Longgang Shenzhen 518129 People's Republic of China. [Online]. Available: <https://www.huawei.com>
- [64] A. O. Amole, Olakunle E. Olabode, D. O. Akinyele, and Bayode S. Olarotimi, "Comparative Analysis of Techno-Environmental Design of Wind and Solar Energy for Sustainable Telecommunications Systems in Different Regions of Nigeria," *IJRER*, Dec. 2021, doi: 10.20508/ijrer.v11i4.12524.g8329.
- [65] Delta Electronics Inc., "PVC 2500B RenE." 3 Tungyuan Road, Chungli Industrial Zone, Taoyuan City 32063, Taiwan. T +886 3 452 6107 / F +886 3 452 7314. [Online]. Available: [https://deltaelectronicsindia.com/wp-content/uploads/2019/07/Fact-sheet\\_PVC-2500B-48\\_IDA1-1.pdf](https://deltaelectronicsindia.com/wp-content/uploads/2019/07/Fact-sheet_PVC-2500B-48_IDA1-1.pdf)
- [66] "48V100Ah Lithium-ion Battery module for telecommunication." [Online]. Available: [https://storage.ua.prom.st/1614805\\_shoto\\_sda10\\_48100\\_manual.pdf](https://storage.ua.prom.st/1614805_shoto_sda10_48100_manual.pdf)
- [67] "Renosola virtus II(5bb)330W." [Online]. Available: <https://si-datastore.s3.us-west-2.amazonaws.com/documents/aAvLVtnL7Ry7C8UzZDcZSxp8J8LOAPun0wYQ2ygE.pdf>
- [68] Delta Electronics Inc., "PVC 2200B RenE." 3 Tungyuan Road, Chungli Industrial Zone, Taoyuan City 32063, Taiwan. T +886 3 452 6107 / F +886 3 452 7314. [Online]. Available: [https://filecenter.deltaww.com/products/Download/09/0908/Catalogue/Fact-sheet\\_TPS\\_PV-Converter\\_PVC-2200B-48\(W\)\\_for-India.pdf](https://filecenter.deltaww.com/products/Download/09/0908/Catalogue/Fact-sheet_TPS_PV-Converter_PVC-2200B-48(W)_for-India.pdf)
- [69] M. Issahaku and F. Kemausuor, "Techno-economic comparison of standalone solar PV and hybrid power systems for remote outdoor telecommunication sites in northern Ghana," *GJSTD*, vol. 8, no. 2, pp. 1–23, Dec. 2022, doi: 10.47881/371.967x.

## Appendix A: 2.2 kW and 3.0 kW Solar PV Charger Controllers

### PVC 2200B RenE



G00CAQ-11-ZL

#### INPUT

Voltage (nominal)	292V <sub>oc</sub>
Voltage (range)	50 - 440V <sub>oc</sub>
Lightening Protection	EN 61000-4-5

#### OUTPUT

Voltage (default)	-54.5V <sub>oc</sub>
Voltage (adjustable range)	-42 to -58V <sub>oc</sub>
Output Current	40.37A @ default voltage
Maximum Power @ nominal Input	2200W
Power Density	27.7W/in <sup>3</sup>
Static MPPT Efficiency	≥ 99% (CEC Efficiency)
	≥ 99% (European Efficiency)
Load Regulation	≤ ± 400mV (0.2A - 40.37A)
Ripple	≤ 150mV
Protection	EN 61000-4-5

#### USER INTERFACE

Alarm and Signaling	CANbus to System Controller		
Indications	OK	Green	Normal Operation
	LD	Yellow	Output current < 5%
	COM	Green	Communication Status

#### MECHANICAL

Dimensions (W x H x D)	125.5 x 41.0 x 273.0mm (4.94 x 1.61 x 10.74in)
Weight	1.8kg (3.96lb)

#### ENVIRONMENTAL

Operating Temperature	-40 to +75 °C (40 to +167 °F) ; De-rating above 65°C (149 °F)
Storage Temperature	-40 to +80 °C (40 to +176 °F)
Altitude	0 to +4000m
Related Humidity	0 - 95 % RH non-condensing
Acoustic Noise	≤ 55dBA

#### STANDARDS

CEC	2200B
-----	-------

(a)

### PVC 3000B RenE



ECAGAG-05-TC

#### INPUT

Voltage (operation range)	70 - 440V <sub>oc</sub>
Voltage (full power range)	200 - 440V <sub>oc</sub>
Max input current	16.7 A
Lightening Protection	EN 61000-4-5, 4kV Line-to-Ground / 2kV Line-to-Line

#### OUTPUT

Voltage (default)	-54.5V <sub>oc</sub>
Voltage (adjustable range)	-42 to -58V <sub>oc</sub>
Output Current	55.05A @ default voltage
Maximum Power @ nominal Input	3000W
Power Density	56.6W/in <sup>3</sup>
Static MPPT Efficiency	≥ 99% (CEC Efficiency)
	≥ 99% (European Efficiency)
Static Voltage Regulation	≤ ± 300mV
Ripple	≤ 200mV
Protection	EN 61000-4-5, 2kV Line-to-Line

#### USER INTERFACE

Alarm and Signaling	CANbus to System Controller		
Indications	OK	Green	Normal Operation
	LD	Yellow	Output current < 5%
	COM	Green	Communication Status

#### MECHANICAL

Dimensions (W x H x D)	84 x 41 x 265mm (3.30 x 1.61 x 10.43in)
Weight	1.3kg (3.0lb)

#### ENVIRONMENTAL

Operating Temperature	-40 to +80 °C (40 to +176 °F); De-rating above +55°C (131 °F)
Storage Temperature	-40 to +80 °C (40 to +176 °F)
Altitude	0 to +4000m
Related Humidity	0 - 95 % RH non-condensing
Acoustic Noise	≤ 58dBA

#### STANDARDS

CEC	3000B
-----	-------

(b)

## Appendix B: 330W Solar PV Module and 48V/100AH Lithium-ion Battery

Electrical Parameters (Standard Test Condition)							
	6M-330	6M-335	6M-340	6M-345	6M-350	6M-355	6M-360
Rated Maximum Power(Mp)	330W	335W	340W	345W	350W	355W	360W
Power Tolerance	0- +5W						
Module Efficiency	17.01%	17.26%	17.52%	17.78%	18.04%	18.30%	18.55%
Open Circuit Voltage(Voc)	47.3V	47.6V	47.8	48.0V	48.1V	48.3V	48.6V
Maximum Power Voltage(Vmp)	38.4V	38.6V	38.8V	38.9V	39.0V	39.2V	39.3V
Short Circuit Current(Isc)	9.11A	9.20A	9.29A	9.40A	9.51A	9.60A	9.70A
Maximum Power Current(Imp)	8.59A	8.68A	8.76A	8.87A	8.97A	9.06A	9.16A
Temperature Coefficient of Isc	+0.06%						
Temperature Coefficient of Voc	-0.32%						
Temperature Coefficient of Pmp	-0.45%						
Standard Test Condition	Irradiance:1000W/M2,Cell Temperature:25℃,Spectrum AM:1.5						
The Electrical Parameters of the module are the average theory figure under the standard test condition, each one exists difference. Can not be treated as the basis of module delivery.							
A- 330W Solar PV Module							

### Application Scenarios


- Backup Power Supply For FTTB, FTTH, ONU, EPON
- applicable to stable grid, half-grid and other scenes

### Key advantages

- High energy density: more energy with less weight and footprint
- High charge and discharge currents (short charge period)
- Long battery life (up to 3 times the battery life of a conventional battery)
- High efficiency between charging and discharging
- Higher continual power available
- Wide operating temperature
- Predictable end of life due BMS controller
- Multiple anti-theft solutions (optional): software, gyroscope, material, etc.
- Other functions (optional): Heating/LCD/Dry Contact

### Product Certificates

- ISO9001
- ISO14001
- CE
- UN38.3
- UL
- IEC62619



### Technical Parameters

Item	Parameters	
1. Performance parameters		
Model	15S	16S
Nominal voltage	48V	51.2V
Rated capacity	100Ah(C <sub>g</sub> 0.2C to 40V at 25℃ )	
Operating voltage range	40V-56.4V	42V-57.6V
Boost charge/Float charge voltage	54.5V/52.5V	57.6V/54V
Charging current (current-limiting )	10A	10A
Charging current (Maximum)	100A	100A
Discharge current (Maximum)	100A	100A
Discharge cut-off voltage	40V	40V
Dimensions	Width	442±1mm
	Height	177±1mm
	Depth	400±1mm
Weight	About 44.7±1kg	About 46.5±1kg

B- 48V/100AH Lithium-ion battery system for telecom

## Appendix C: Selected Base Station's Meteorological Data

0.45 kW Makebe Base Station						
BS Latitude	-29.180665	BS Longitude:	27.58968	Altitude [m a.s.l.]	1537m	
Units	H_Gh	H_Dh	Clearance Index	Ta	RR	PSH
Month	[kWh/m2]	[kWh/m <sup>2</sup> ]	[K]	[°C]	[mm]	[kWh/d]
January	247.00	74	0.6	21.7	92	5.21
February	204.00	54	0.58	21	74	4.85
March	196.00	55	0.586	19.2	59	4.31
April	158.00	35	0.62	15.3	37	3.6
May	135.00	30	0.666	11.6	18	3.14
June	117.00	25	0.681	8.3	15	2.87
July	127.00	26	0.691	8.1	4	3.13
August	154.00	28	0.688	11.2	11	3.71
September	181.00	43	0.649	15.2	11	4.57
October	226.00	41	0.596	18.3	44	4.93
November	241.00	60	0.596	19.7	69	5.49
December	253.00	64	0.606	21.2	85	5.51
<b>Totals</b>	<b>2239.00</b>	<b>535.00</b>			<b>519.00</b>	<b>51.32</b>
<b>Averages</b>	<b>186.58</b>	<b>44.58</b>	<b>0.63</b>	<b>15.90</b>	<b>43.25</b>	<b>4.28</b>
<b>Maximum</b>	<b>253.00</b>	<b>74.00</b>	<b>0.69</b>	<b>21.70</b>	<b>92.00</b>	<b>5.51</b>
<b>Mininum</b>	<b>117.00</b>	<b>25.00</b>	<b>0.58</b>	<b>8.10</b>	<b>4.00</b>	<b>2.87</b>

0.9 kW Malimong Base Station						
BS Latitude	-29.233	BS Longitude:	27.932	Altitude [m a.s.l.]	2056	
Units	H_Gh	H_Dh	Clearance Index	Ta	RR	PSH
Month	[kWh/m2]	[kWh/m <sup>2</sup> ]	[K]	[°C]	[mm]	[kWh/d]
January	246.00	74	0.6	17.8	110	5.14
February	205.00	62	0.58	17.3	82	4.87
March	196.00	48	0.586	15.7	64	4.32
April	159.00	40	0.62	12.3	38	3.56
May	137.00	29	0.667	8.8	16	3.14
June	119.00	25	0.682	5.7	15	2.85
July	129.00	27	0.692	5.4	4	3.11
August	157.00	31	0.689	8.5	11	3.66
September	186.00	42	0.649	12.2	12	4.5
October	230.00	48	0.596	14.7	57	4.84
November	243.00	69	0.596	16	71	5.35
December	254.00	79	0.606	17.3	98	5.44
<b>Totals</b>	<b>2261.00</b>	<b>574.00</b>	<b>7.56</b>	<b>151.70</b>	<b>578.00</b>	<b>50.78</b>
<b>Averages</b>	<b>188.42</b>	<b>47.83</b>	<b>0.63</b>	<b>12.64</b>	<b>48.17</b>	<b>4.23</b>
<b>Maximum</b>	<b>254.00</b>	<b>79.00</b>	<b>0.69</b>	<b>17.80</b>	<b>21.7</b>	<b>5.44</b>
<b>Mininum</b>	<b>119.00</b>	<b>25.00</b>	<b>0.58</b>	<b>5.40</b>	<b>4.00</b>	<b>2.85</b>

1.1 kW Mmasemouse						
BS Latitude	-29.233	BS Longitude:	27.932	Altitude [m a.s.l.]	1606	
Units	H_Gh	H_Dh	Clearance Index	Ta	RR	PSH
Month	[kWh/m2]	[kWh/m <sup>2</sup> ]	[K]	[°C]	[mm]	[kWh/d]
January	244.00	77.00	0.599	21.70	80.00	4.97
February	199.00	58.00	0.581	21.00	84.00	4.64
March	192.00	57.00	0.590	19.10	68.00	4.17
April	153.00	37.00	0.628	15.20	40.00	3.49
May	132.00	24.00	0.678	11.40	18.00	2.93
June	113.00	24.00	0.696	8.00	21.00	2.57
July	124.00	26.00	0.706	7.80	8.00	2.89
August	149.00	32.00	0.699	11.00	9.00	3.44
September	175.00	41.00	0.654	15.00	9.00	4.32
October	221.00	51.00	0.598	18.20	38.00	4.54
November	237.00	57.00	0.595	19.70	61.00	5.11
December	249.00	66.00	0.604	21.30	83.00	5.33
<b>Totals</b>	<b>2188.00</b>	<b>550.00</b>			<b>519.00</b>	<b>48.40</b>
<b>Averages</b>	<b>182.33</b>	<b>45.83</b>	<b>0.64</b>	<b>15.78</b>	<b>43.25</b>	<b>4.03</b>
<b>Maximum</b>	<b>249.00</b>	<b>77.00</b>	<b>0.71</b>	<b>21.70</b>	<b>84.00</b>	<b>5.33</b>
<b>Mininum</b>	<b>113.00</b>	<b>24.00</b>	<b>0.58</b>	<b>7.80</b>	<b>8.00</b>	<b>2.57</b>

Kolo						
BS Latitude	-29.558	BS Longitude:	27.353	Altitude [m a.s.l.]	1641	
Units	H_Gh	H_Dh	Clearance Index	Ta	RR	PSH
Month	[kWh/m2]	[kWh/m <sup>2</sup> ]	[K]	[°C]	[mm]	[kWh/d]
January	247.00	77.00	0.60	15.30	81.00	5.31
February	202.00	59.00	0.58	11.60	75.00	4.90
March	195.00	50.00	0.59	8.30	61.00	4.39
April	155.00	38.00	0.63	8.10	39.00	3.61
May	133.00	30.00	0.68	11.20	20.00	3.12
June	114.00	22.00	0.70	15.20	18.00	2.80
July	126.00	27.00	0.71	18.30	5.00	3.08
August	151.00	30.00	0.70	19.70	11.00	3.66
September	178.00	43.00	0.65	21.20	10.00	4.53
October	225.00	53.00	0.60	15.90	36.00	4.99
November	240.00	57.00	0.60	0.00	66.00	5.55
December	253.00	63.00	0.60	17.80	78.00	5.62
<b>Totals</b>	<b>2219.00</b>	<b>549.00</b>			<b>500.00</b>	<b>51.56</b>
<b>Averages</b>	<b>184.92</b>	<b>45.75</b>	<b>0.64</b>	<b>13.55</b>	<b>41.67</b>	<b>4.30</b>
<b>Maximum</b>	<b>253.00</b>	<b>77.00</b>	<b>0.71</b>	<b>21.20</b>	<b>81.00</b>	<b>5.62</b>
<b>Mininum</b>	<b>114.00</b>	<b>22.00</b>	<b>0.58</b>	<b>0.00</b>	<b>5.00</b>	<b>2.80</b>



Thloro Base Station						
BS Latitude	-30.062	BS Longitude:	28.318	Altitude [m a.s.l.]	2237	
Units	H_Gh	H_Dh	Clearance Index	Ta	RR	PSH
Month	[kWh/m2]	[kWh/m <sup>2</sup> ]	[K]	[°C]	[mm]	[kWh/d]
January	227.00	85.00	0.57	16.70	95.00	5.16
February	189.00	59.00	0.56	16.20	88.00	4.95
March	184.00	60.00	0.57	14.60	70.00	4.34
April	149.00	40.00	0.60	11.40	41.00	3.71
May	129.00	30.00	0.65	8.00	16.00	3.33
June	112.00	25.00	0.66	4.90	20.00	3.03
July	124.00	30.00	0.66	4.60	8.00	3.31
August	149.00	29.00	0.66	7.60	10.00	3.91
September	174.00	52.00	0.62	11.20	11.00	4.70
October	213.00	62.00	0.57	13.60	48.00	4.98
November	227.00	69.00	0.57	14.80	66.00	5.36
December	234.00	75.00	0.57	16.20	94.00	5.32
<b>Totals</b>	<b>2111.00</b>	<b>616.00</b>		<b>139.80</b>	<b>567.00</b>	<b>52.10</b>
<b>Averages</b>	<b>175.92</b>	<b>51.33</b>	<b>0.60</b>	<b>11.65</b>	<b>47.25</b>	<b>4.34</b>
<b>Maximum</b>	<b>234.00</b>	<b>85.00</b>	<b>0.66</b>	<b>16.70</b>	<b>95.00</b>	<b>5.36</b>
<b>Mininum</b>	<b>112.00</b>	<b>25.00</b>	<b>0.56</b>	<b>4.60</b>	<b>8.00</b>	<b>3.03</b>

Scout						
BS Latitude	-29.442	BS Longitude:	27.715	Altitude [m a.s.l.]	1664	
Units	H_Gh	H_Dh	Clearance Index	Ta	RR	PSH
Month	[kWh/m2]	[kWh/m <sup>2</sup> ]	[K]	[°C]	[mm]	[kWh/d]
January	246.00	77.00	0.60	20.90	94.00	5.19
February	204.00	56.00	0.58	20.30	78.00	4.86
March	195.00	59.00	0.59	18.50	62.00	4.35
April	157.00	43.00	0.62	14.90	39.00	3.58
May	135.00	30.00	0.67	11.30	18.00	3.11
June	117.00	24.00	0.69	8.00	16.00	2.81
July	126.00	26.00	0.70	7.80	5.00	3.08
August	154.00	30.00	0.69	10.90	11.00	3.64
September	181.00	42.00	0.65	14.70	11.00	4.49
October	227.00	52.00	0.60	17.60	45.00	4.91
November	241.00	63.00	0.60	19.00	68.00	5.39
December	252.00	63.00	0.61	20.40	86.00	5.50
<b>Totals</b>	<b>2235.00</b>	<b>565.00</b>			<b>533.00</b>	<b>50.91</b>
<b>Averages</b>	<b>186.25</b>	<b>47.08</b>	<b>0.63</b>	<b>15.36</b>	<b>44.42</b>	<b>4.24</b>
<b>Maximum</b>	<b>252.00</b>	<b>77.00</b>	<b>0.70</b>	<b>20.90</b>	<b>94.00</b>	<b>5.50</b>
<b>Mininum</b>	<b>117.00</b>	<b>24.00</b>	<b>0.58</b>	<b>7.80</b>	<b>5.00</b>	<b>2.81</b>



## Appendix D: Base Stations Audit Assessment Results

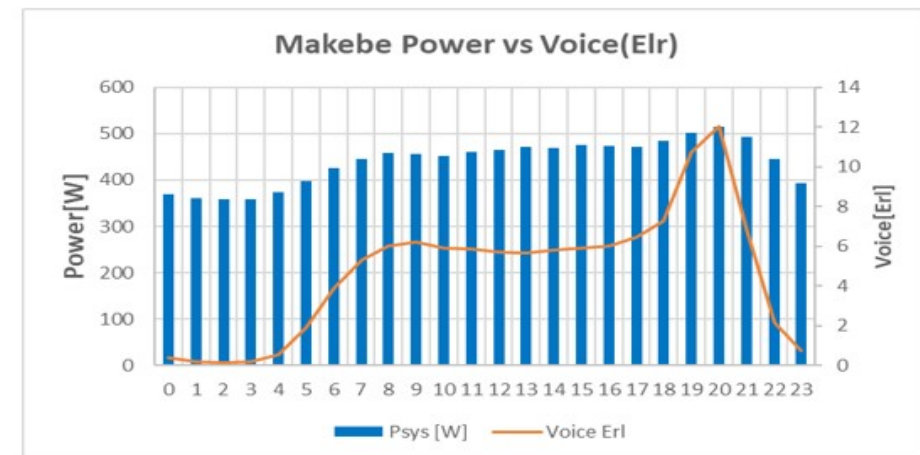
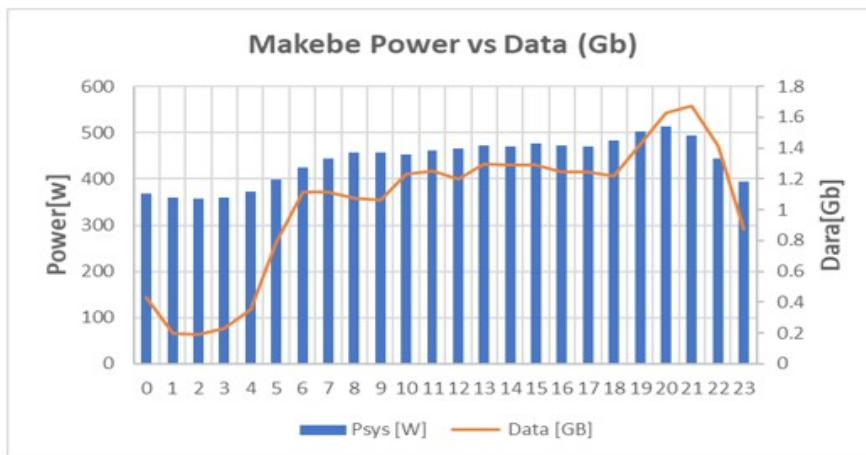
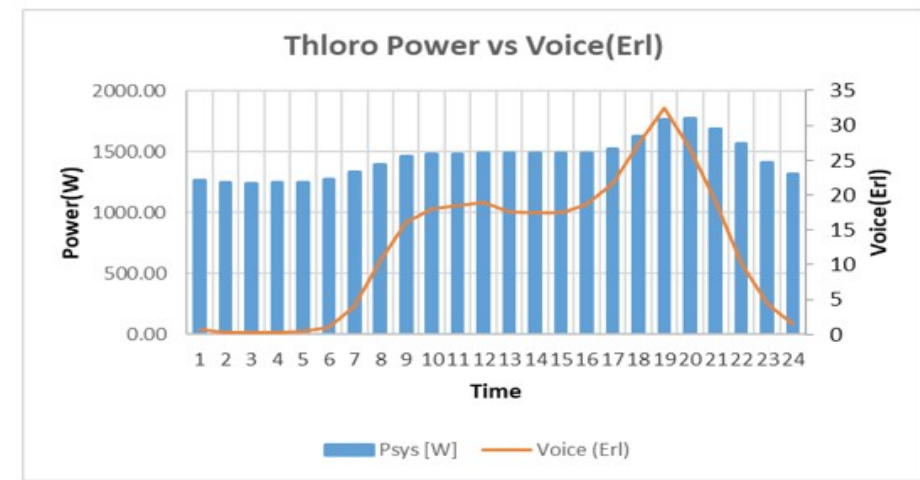
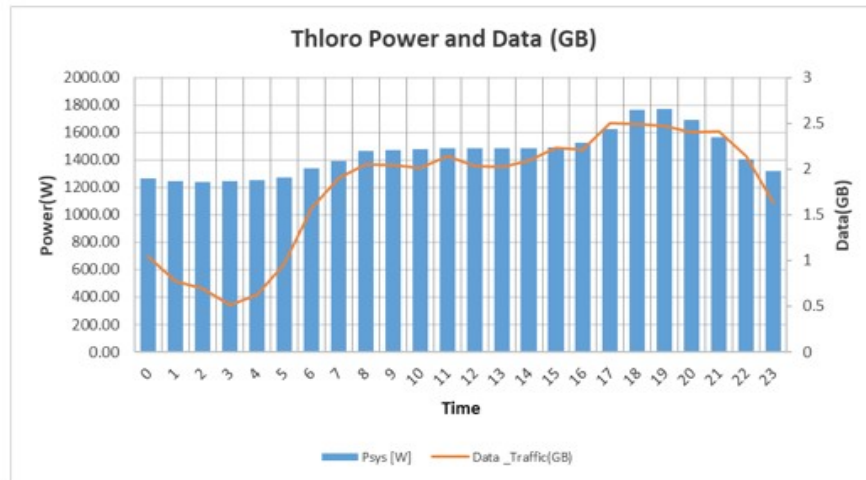
Base Stations Current Sizing							
Site Name	No PV Modules	PV Rated Capacity(W)	Batteries	B_Capacity AH	No: PV Charger	PV Charger mod (W)	Controller Capacity(V)
Makebe_0.45 kW	14	4640	4	400	3	2200	6600
Malimong_0.95 kW	36	10750	12	1200	6	2200	13200
Mmasemouse_1.2 kW	30	9450	12	1200	5	2200	11000
Thloro 1.6kW_	39	11340	12	1200	7	2200	15400
Kolo Sys 2 1.1 kW	48	14760	12	1200	4	2200	8800
Scout 2.1kW	0	0	8	800	0	2200	0

Base Stations System Sizing: Daily Energy Balance Method							
Site Name	No PV Modules	PV Rated Capacity(W)	Batteries	B_Capacity AH	No: PV Charger	PV Charger mod(W)	PV Controller W
Makebe_0.45 kW	14	4620	5	503	2	3000	6000
Malimong_0.95 kW	28	8820	11	1144	4	2200	8800
Mmasemouse_1.2 kW	42	13230.00	15	1521	6	2200	13200
Thloro 1.6kW_	48	15840.00	18	1829	6	300	1800
Kolo Sys2 1.1 kW	56	17640.00	22	2236	8	2200	17600
Scout 2.1kW	63	20790.00	26	2565	9	3000	27000

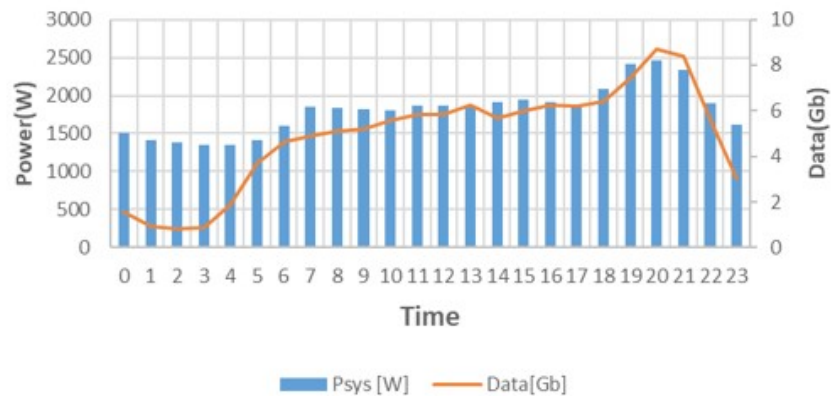
Base Stations System Sizing :Time Step Method							
Site Name	No PV Modules	PV Rated Capacity(W)	Batteries	B_Capacity AH	No: PV Charger	PV Charger mod(W)	PV Controller W
Makebe_0.45 kW	14	4620	5	517	2	3000	6000
Malimong_0.95 kW	28	8820	11	1096	4	2200	8800
Mmasemouse_1.2 kW	35	11025.00	14	1350	5	2200	11000
Thloro 1.6kW_	48	15840.00	18	1789	6	300	1800
Kolo Sys2 1.1 kW	56	17640.00	22	2232	8	2200	17600
Scout 2.1kW	63	20790.00	26	2553	9	3000	27000

Research Findings							
Site Name	No PV Modules	Capacity Gap (W)	Batteries	B_Capacity AH	No: PV Charger	PV Charger mod (W)	PV Controller W
Makebe_0.45 kW	0	-20	1	117	-1	800	-600
Malimong_0.95 kW	-8	-1930	-1	-104	-2	0	-4400
Mmasemouse_1.2 kW	5	1575	2	150	0	0	0
Thloro 1.6kW_	9	4500	6	589	-1	-1900	-13600
Kolo Sys2 1.1 kW	8	2880	10	1032	4	0	8800
Scout 2.1kW	63	20790	18	1753	9	800	27000

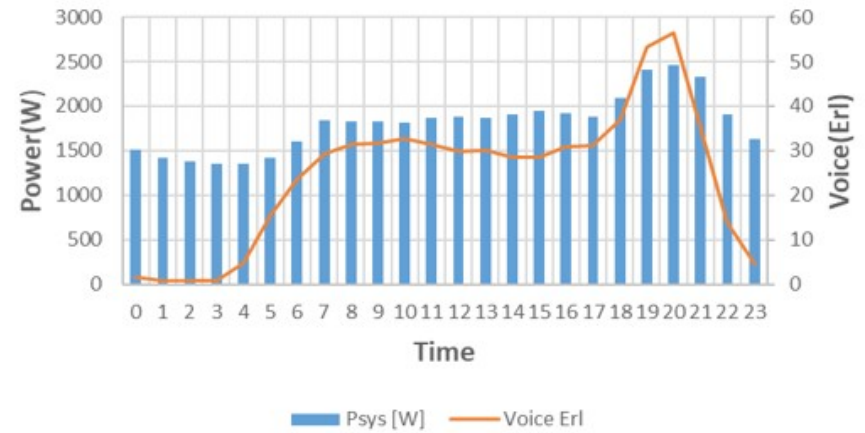
## Appendix E: Base Stations Power vs Actual Traffic



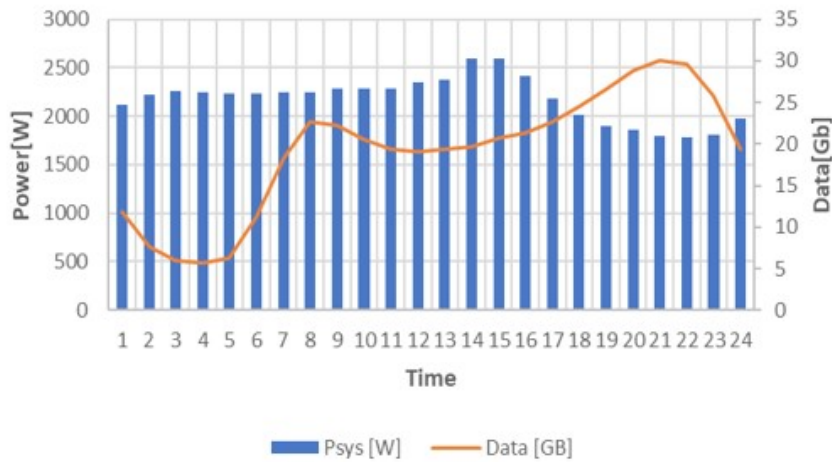
### Kolo Power vs Data(Gb)



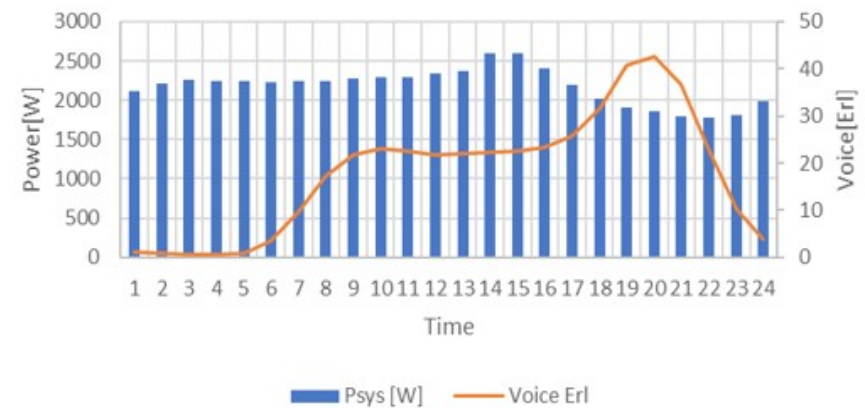
### Kolo Power vs Voice(Erl)



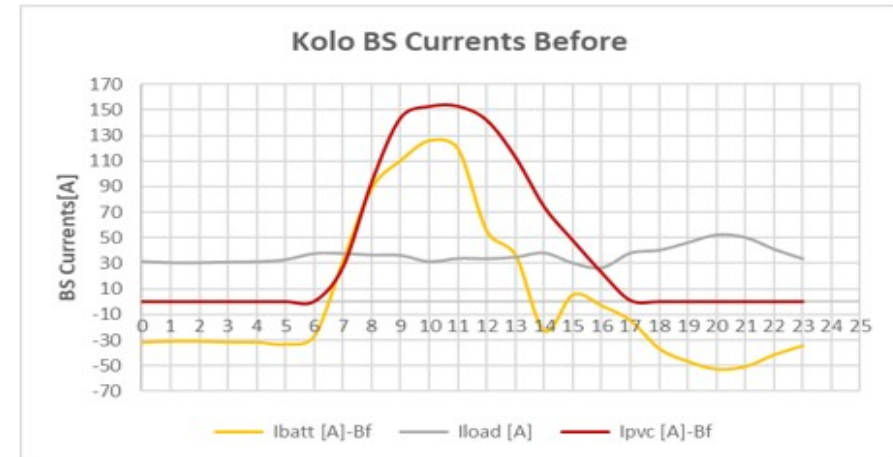
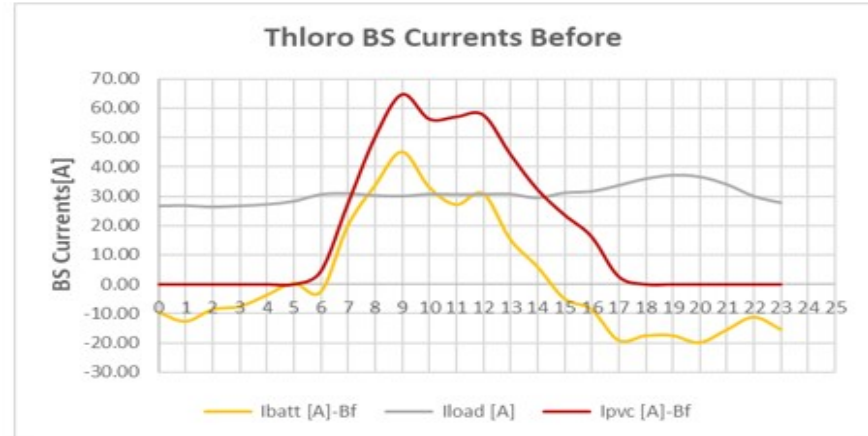
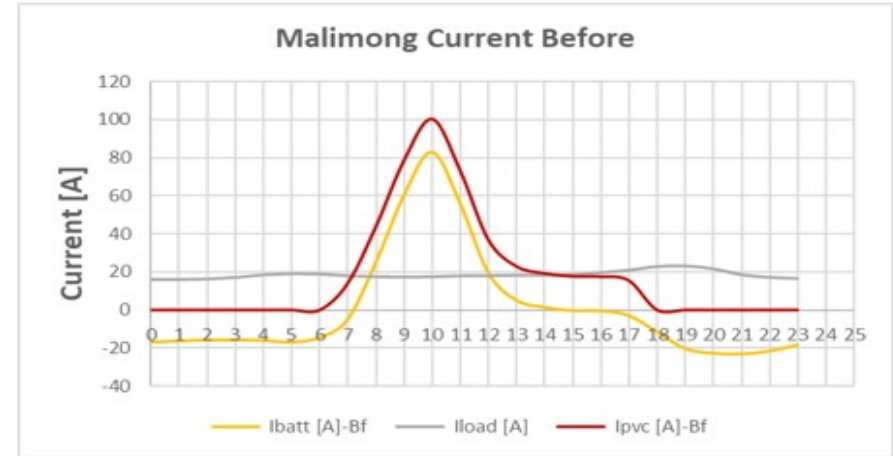
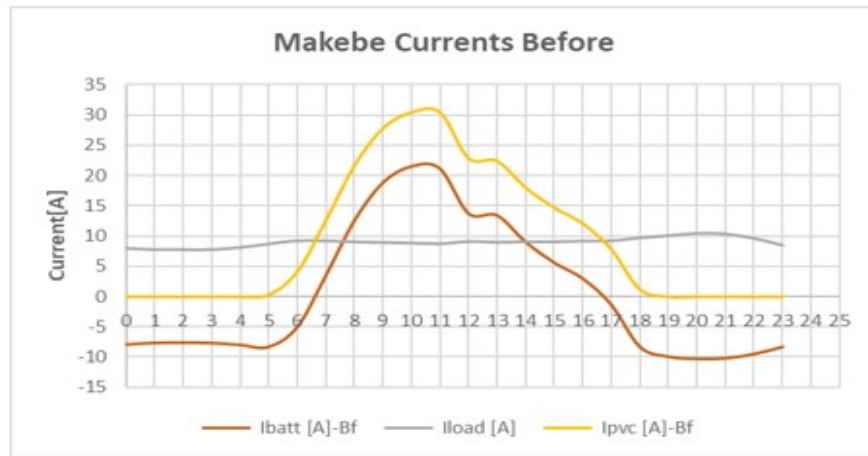
### Scout Power vs Data(Gb)



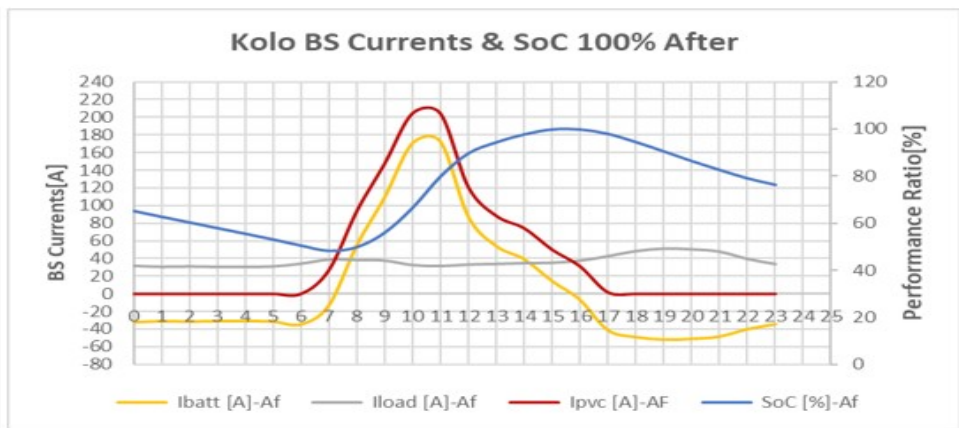
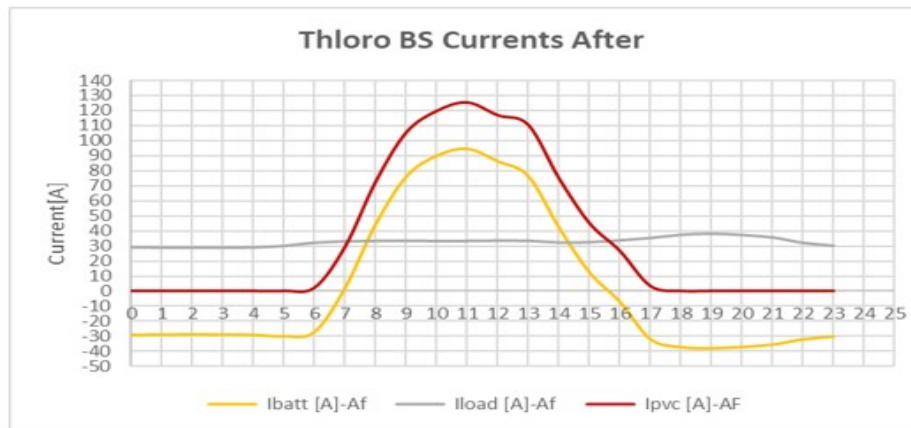
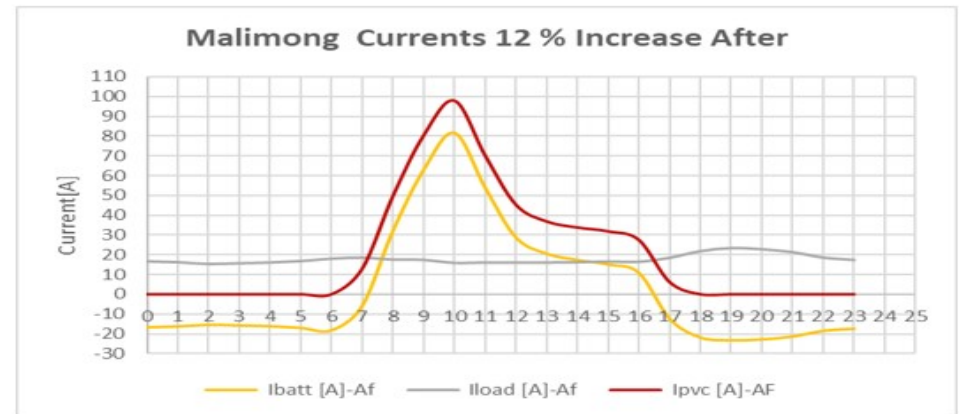
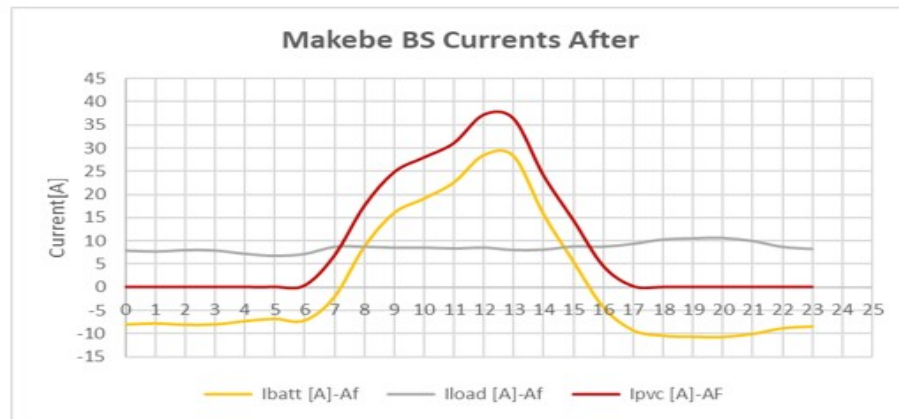
### Scout Power vs Voice(Erl)



## Appendix F: The Base Stations Current Before Rewiring and Parameter Optimizations

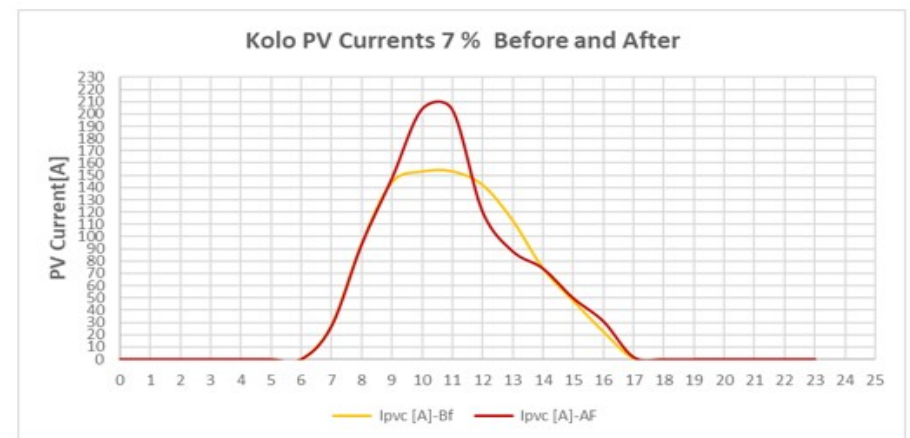
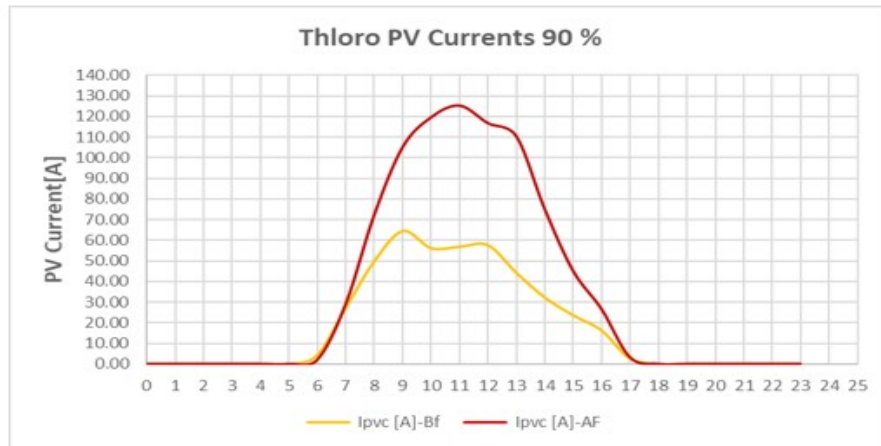
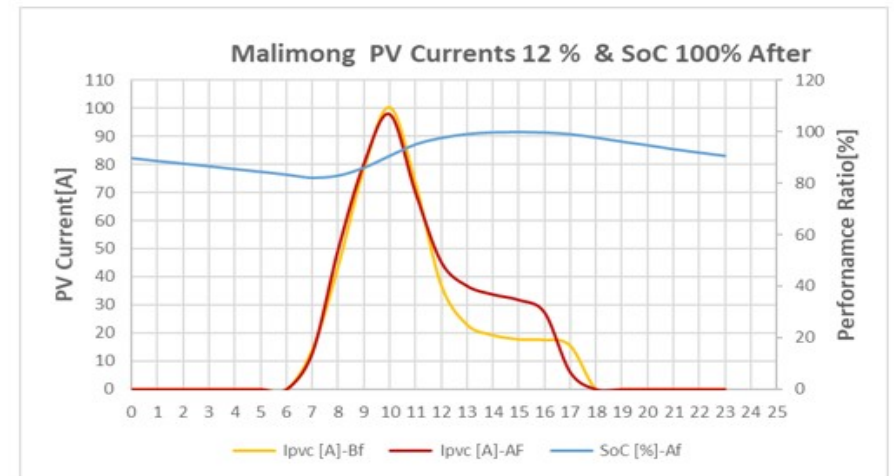
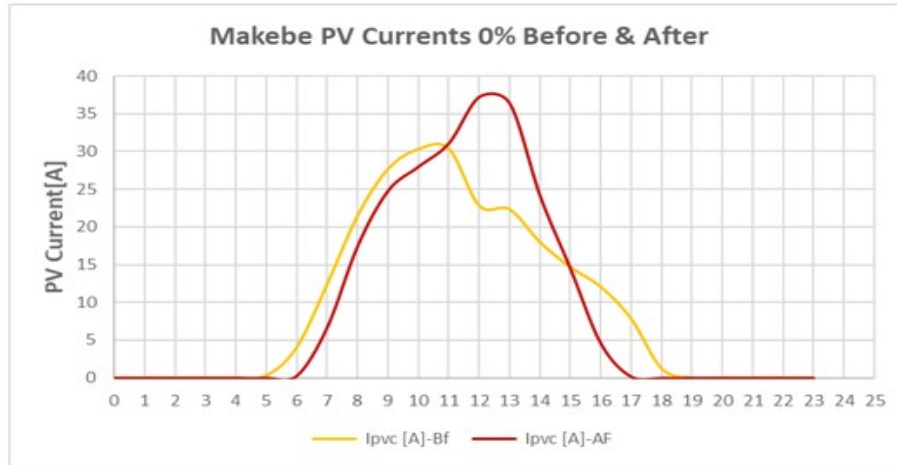


## Appendix G: The Base Stations Current After Rewiring and Parameter Optimizations

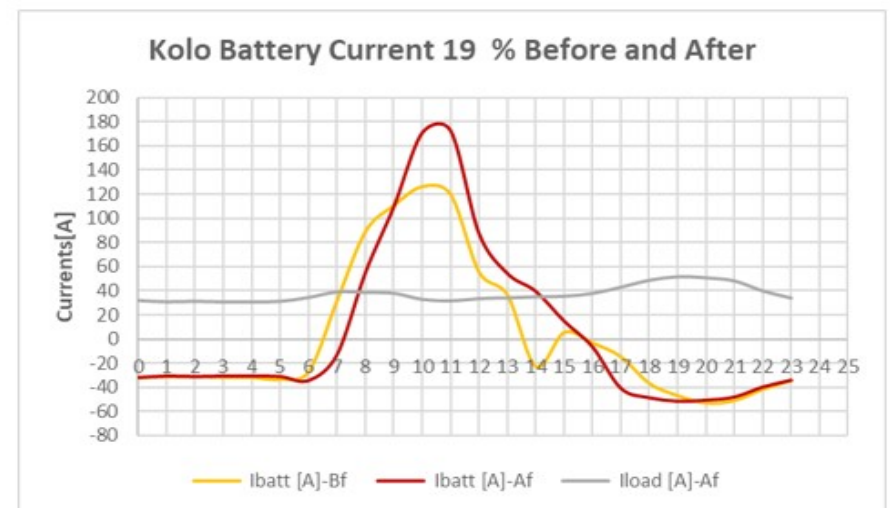
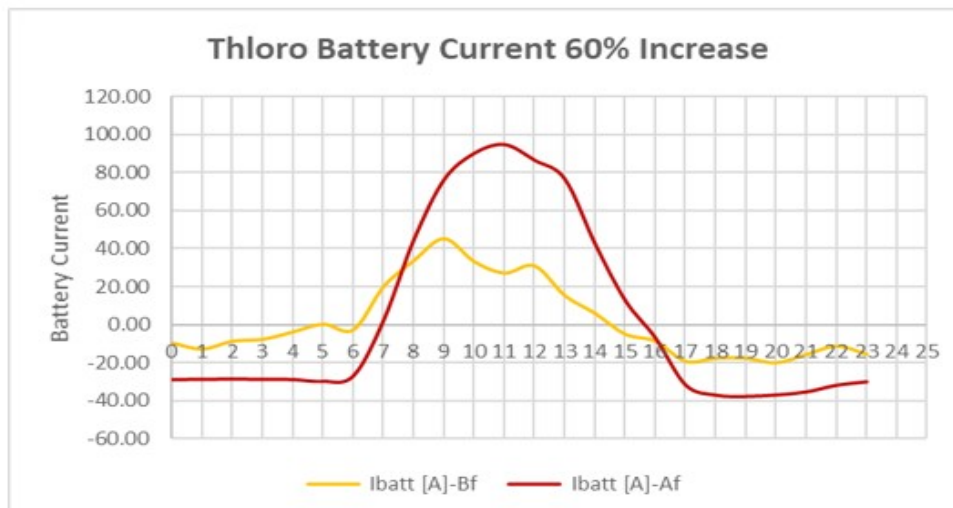
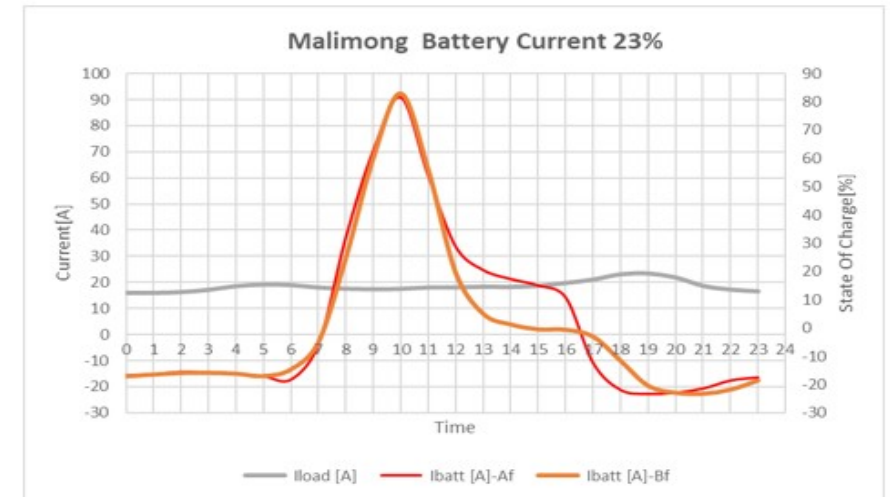
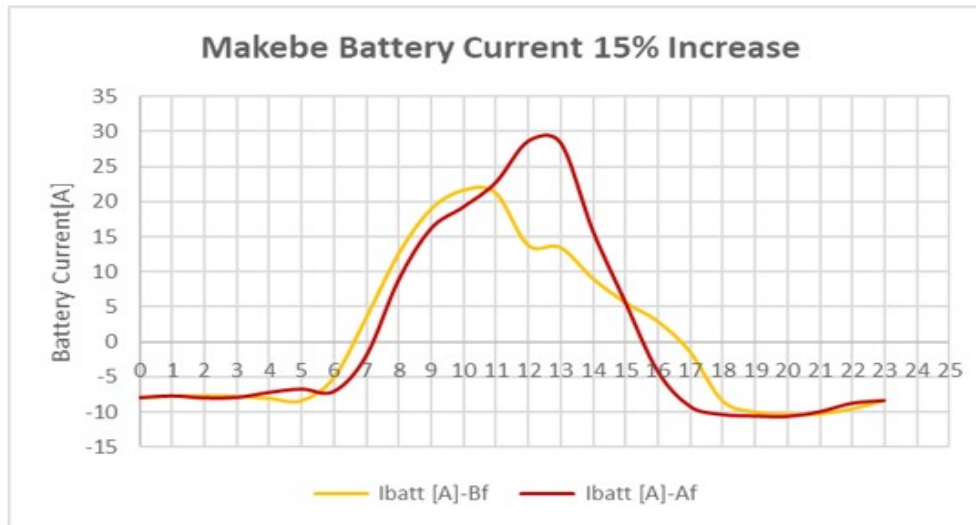




## Appendix H: The Base Stations Solar PV Currents Before and After Optimization

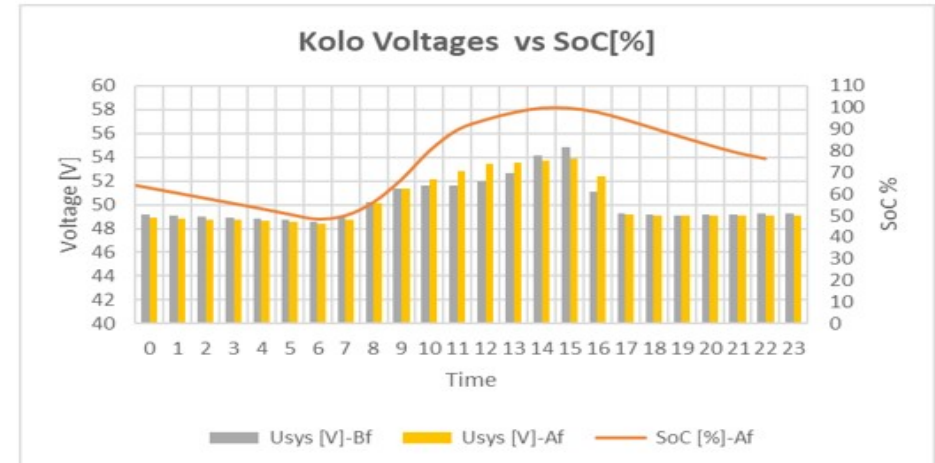
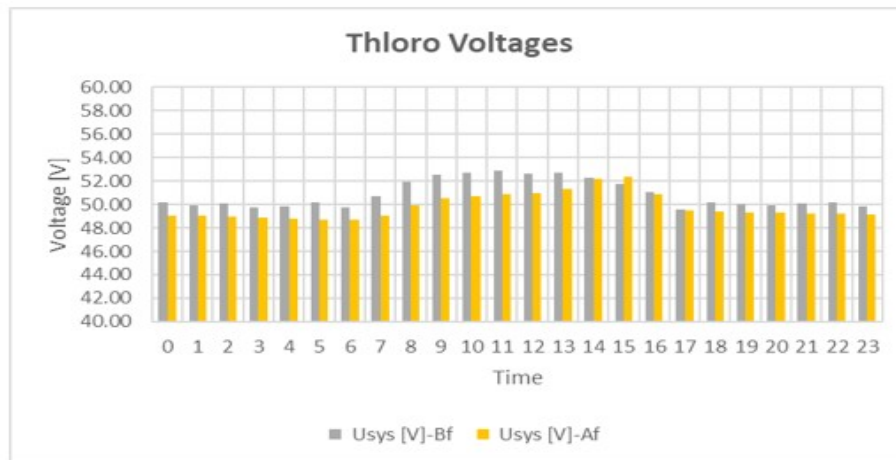
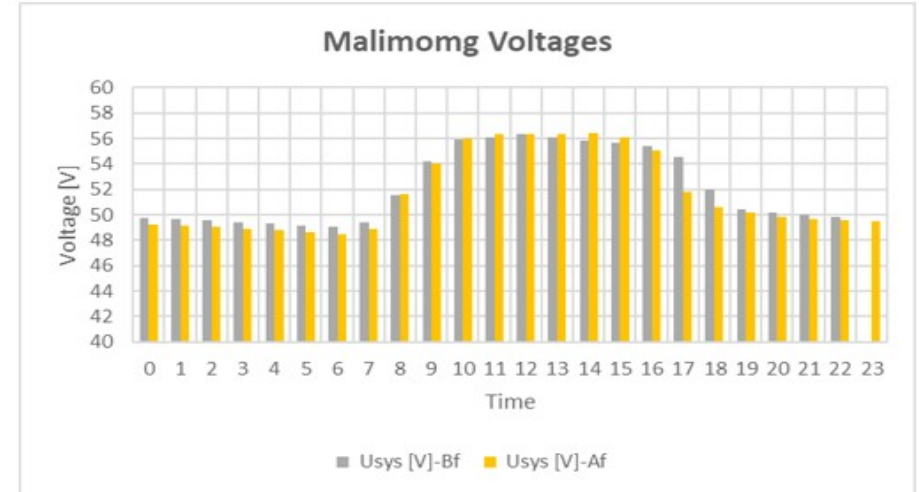
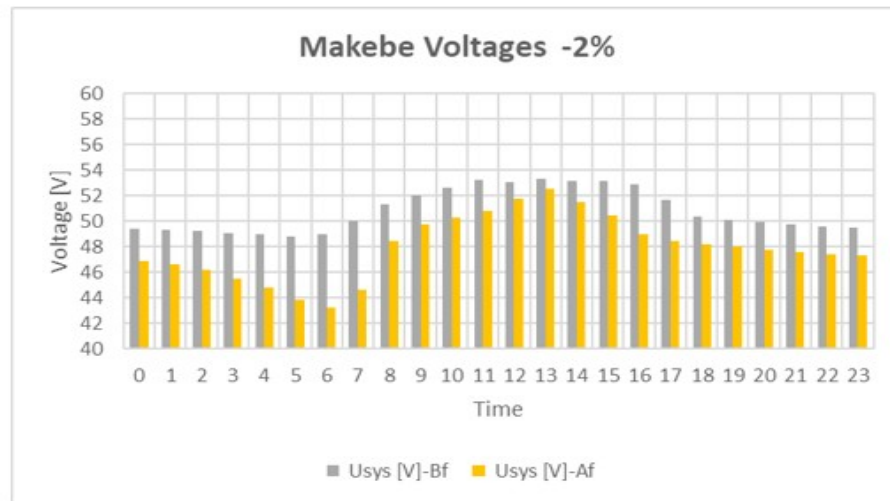


## Appendix I: The Base Stations Battery Currents Before and After Optimization

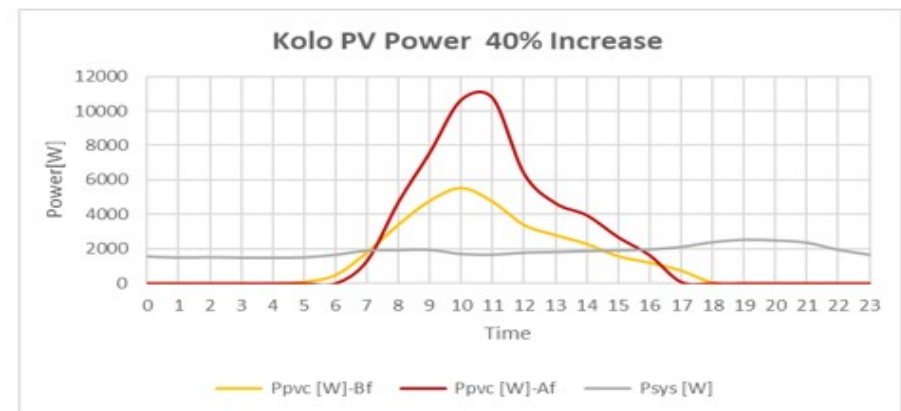
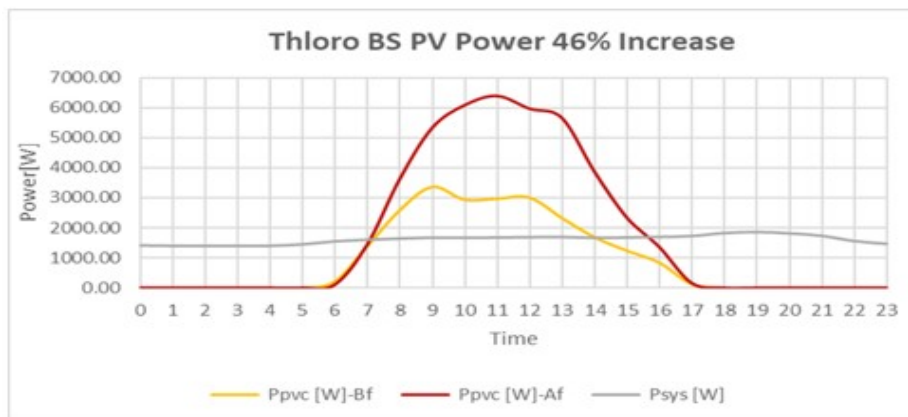
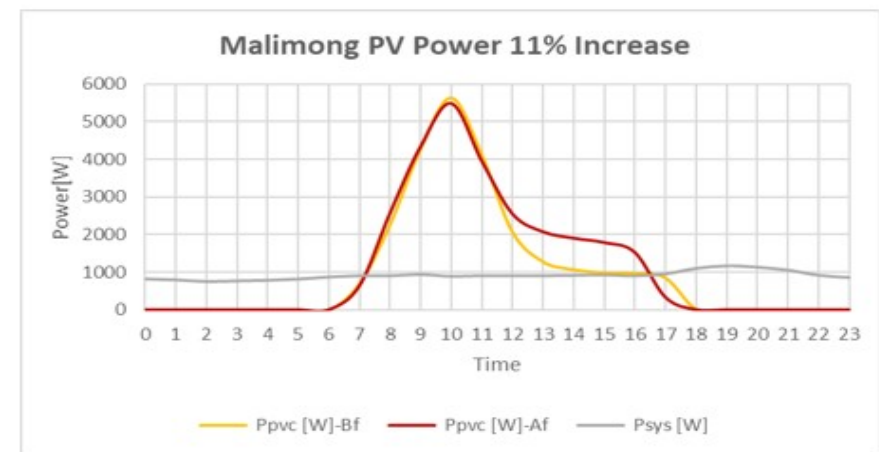
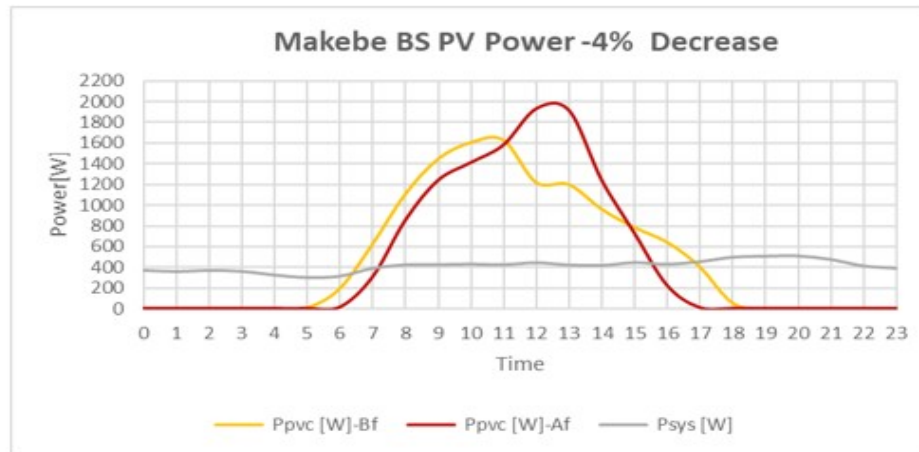




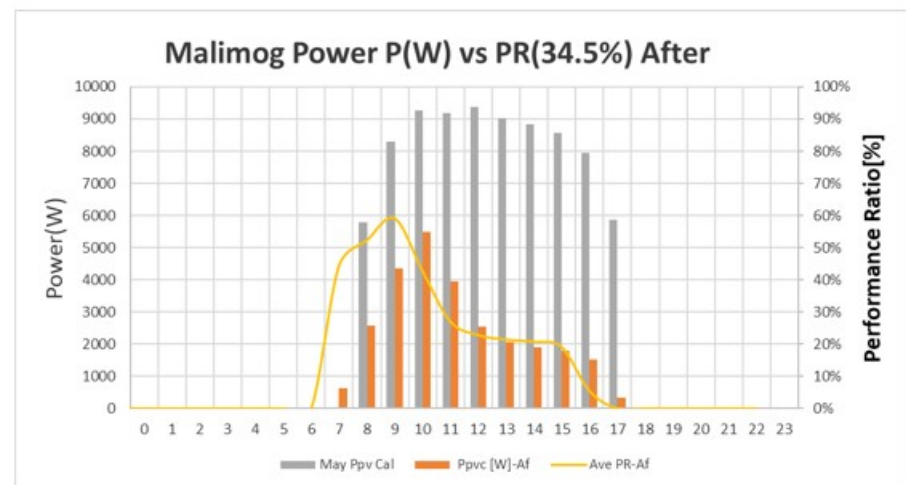
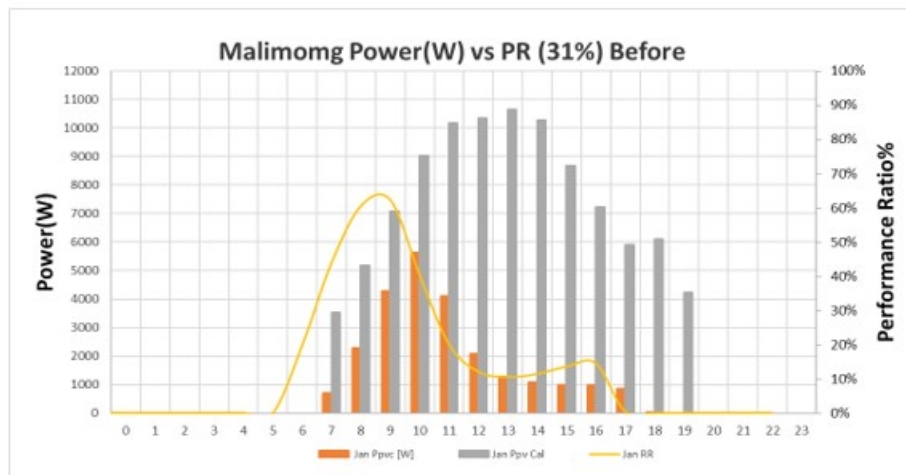
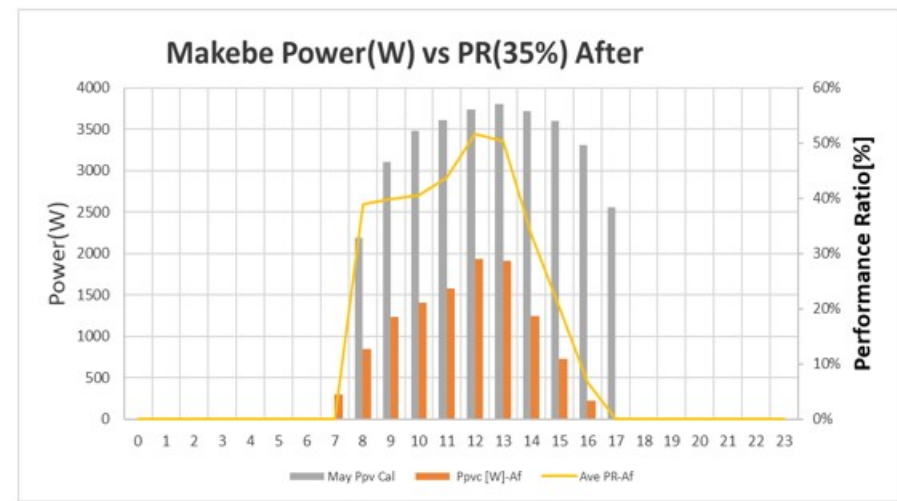
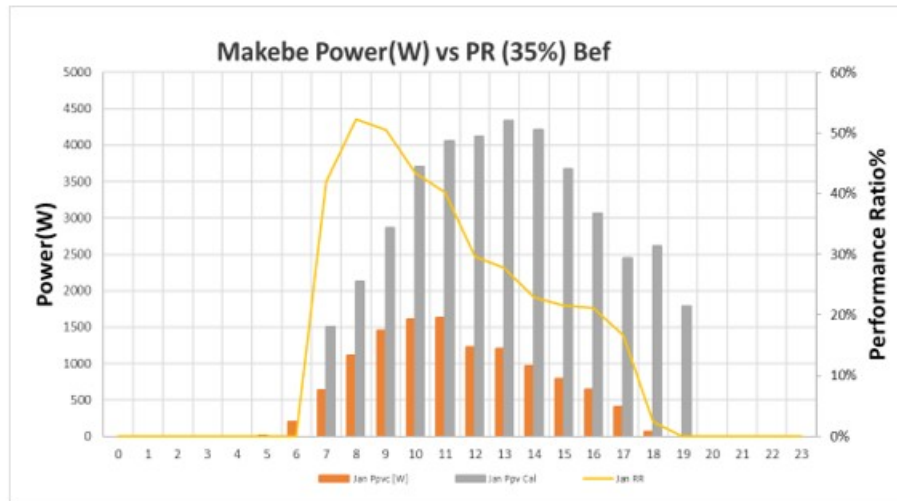
## Appendix J: The Base Stations Systems Voltages Before and After Optimization

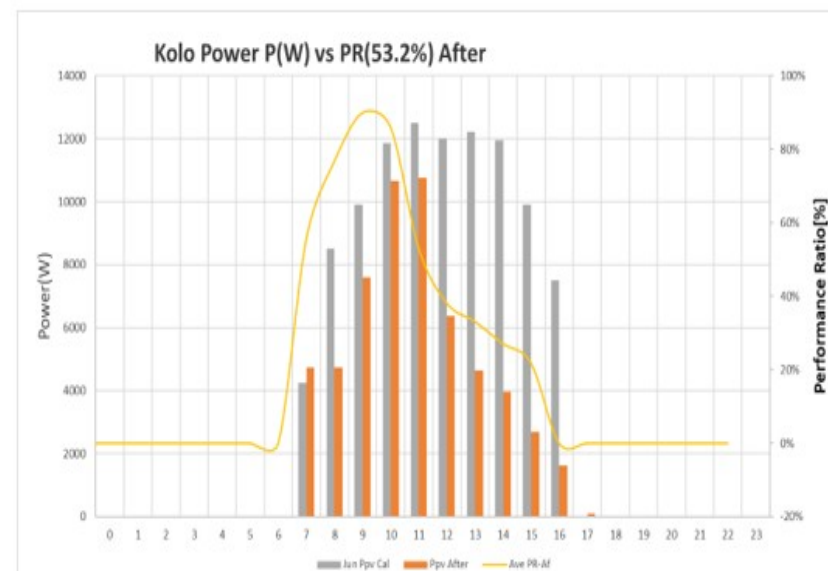
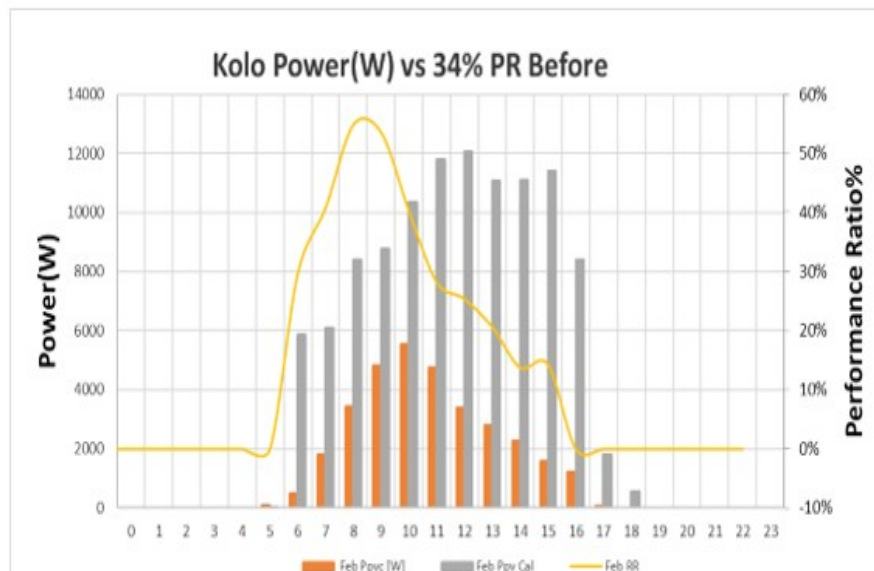
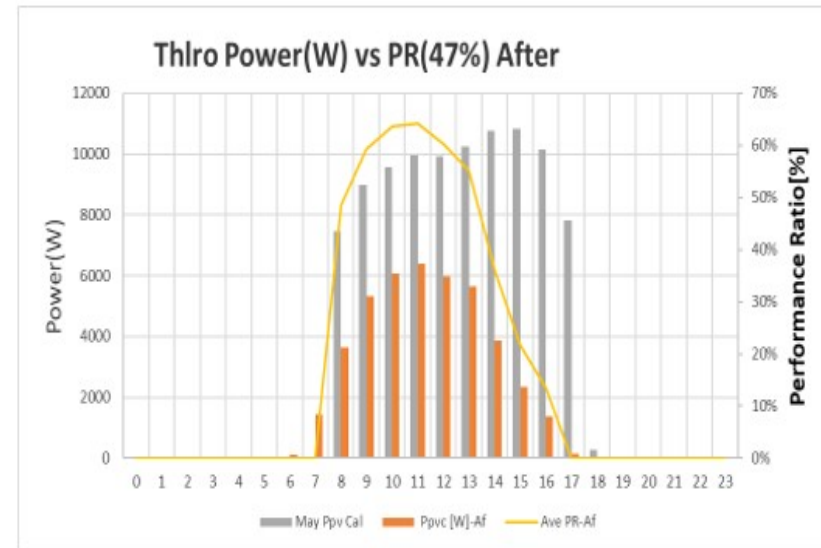
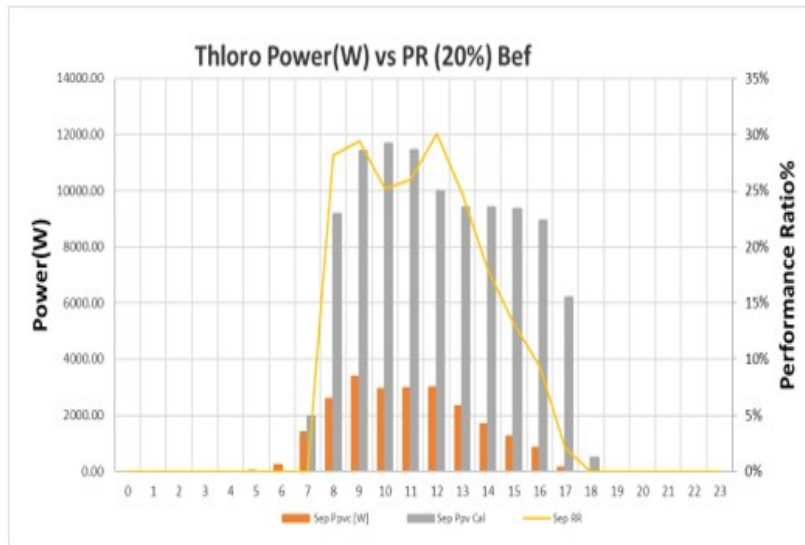


## Appendix K: The Base Stations Solar PV Power Before and After Optimization

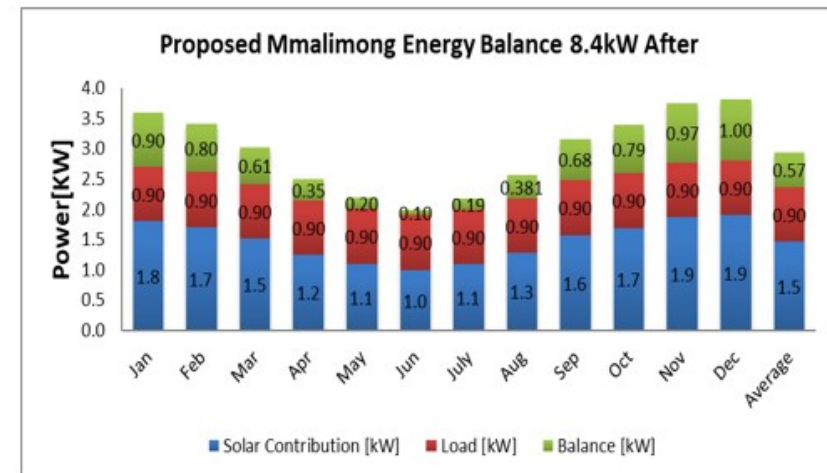
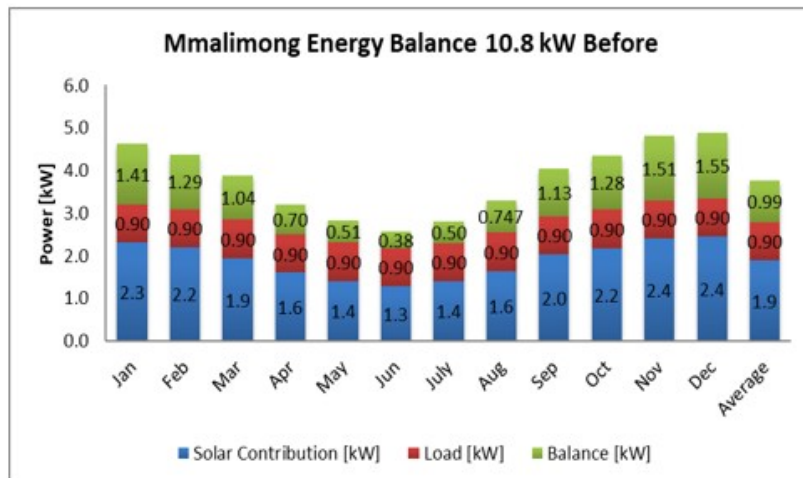
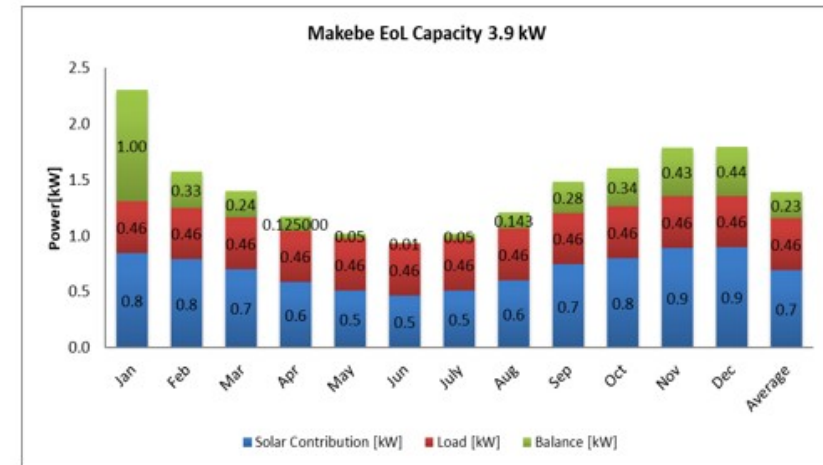
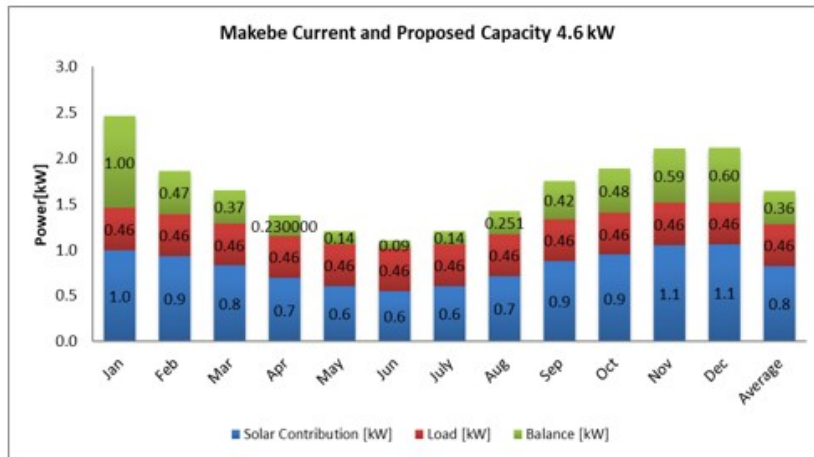


## Appendix L: The Base Stations Performance Ratios Before and After Optimization

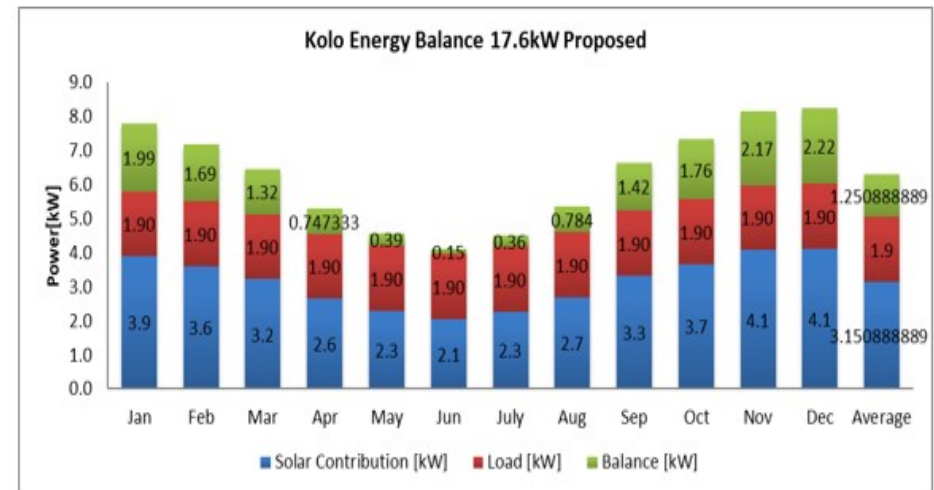
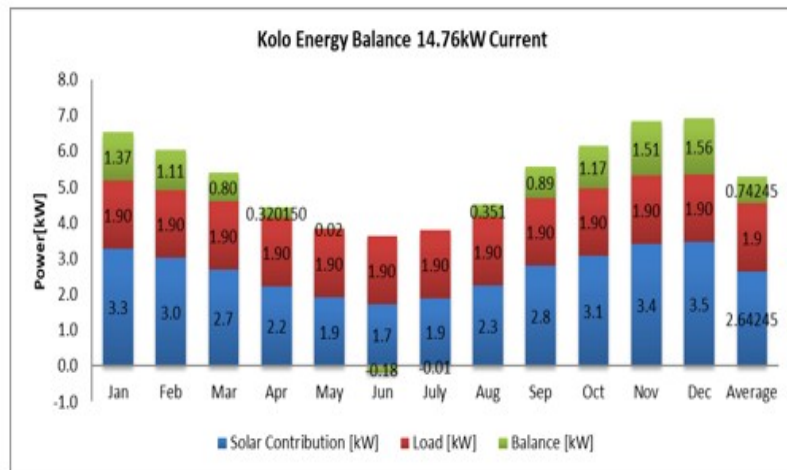
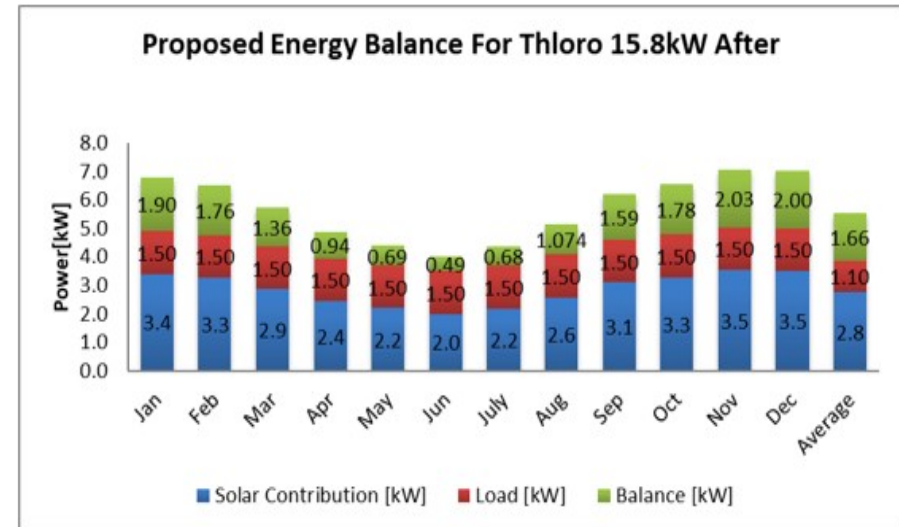
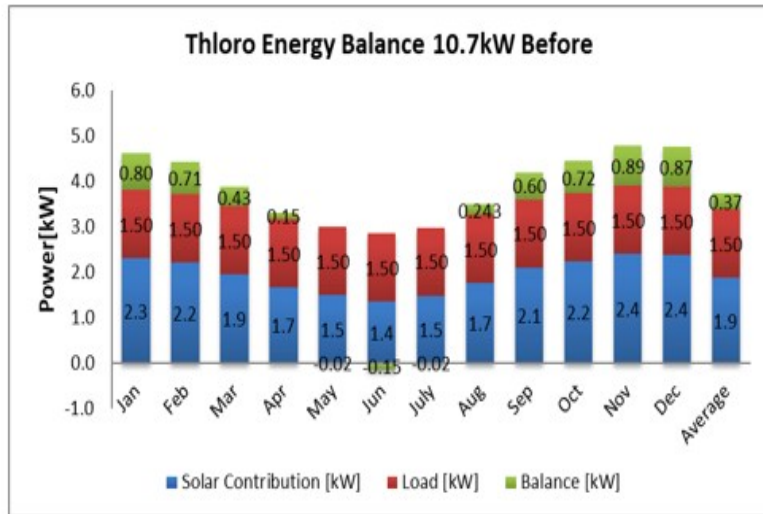




## Appendix M: The Base Stations Annual Performance Assessment Before and After Optimization







## Appendix N: The Base Stations Load Profile Coefficients (Solar and Grid)

Time	0.5 kW Makebe	0.9 kW Malimong Ave	1.2 kW Masemouse	1.5 kW Thloro	1.9 kW Kolo-Solar	3.7 kW Mabote-Grid	2.4 Mapetla -Grid	3.4 TY-Grid	2.1 kW Scout-Grid	0.57 kW Ha Thaba-Grid
0	0.0348	0.0348	0.0358	0.0353	0.0332	0.0376	0.0358	0.0369	0.0391	0.0418
1	0.0340	0.0347	0.0354	0.0356	0.0332	0.0374	0.0368	0.0366	0.0414	0.0423
2	0.0338	0.0352	0.0354	0.0359	0.0334	0.0373	0.0366	0.0366	0.0423	0.0422
3	0.0340	0.0373	0.0356	0.0359	0.0332	0.0378	0.0367	0.0368	0.0421	0.0413
4	0.0353	0.0398	0.0379	0.0362	0.0339	0.0396	0.0366	0.0365	0.0421	0.0421
5	0.0377	0.0410	0.0409	0.0376	0.0357	0.0415	0.0391	0.0372	0.0427	0.0414
6	0.0402	0.0423	0.0416	0.0396	0.0396	0.0423	0.0421	0.0404	0.0432	0.0412
7	0.0421	0.0421	0.0427	0.0407	0.0424	0.0423	0.0427	0.0416	0.0435	0.0412
8	0.0433	0.0415	0.0431	0.0430	0.0424	0.0416	0.0418	0.0428	0.0431	0.0411
9	0.0432	0.0424	0.0432	0.0434	0.0446	0.0420	0.0422	0.0424	0.0431	0.0410
10	0.0428	0.0426	0.0431	0.0437	0.0396	0.0420	0.0426	0.0430	0.0434	0.0422
11	0.0437	0.0429	0.0432	0.0436	0.0395	0.0427	0.0438	0.0419	0.0439	0.0417
12	0.0440	0.0430	0.0437	0.0430	0.0421	0.0420	0.0429	0.0429	0.0456	0.0414
13	0.0447	0.0431	0.0433	0.0432	0.0453	0.0431	0.0431	0.0434	0.0481	0.0413
14	0.0444	0.0430	0.0435	0.0430	0.0422	0.0430	0.0440	0.0432	0.0485	0.0421
15	0.0451	0.0433	0.0431	0.0434	0.0415	0.0433	0.0435	0.0435	0.0463	0.0416
16	0.0446	0.0445	0.0433	0.0440	0.0415	0.0434	0.0438	0.0443	0.0433	0.0414
17	0.0446	0.0473	0.0441	0.0456	0.0464	0.0448	0.0444	0.0448	0.0403	0.0417
18	0.0459	0.0505	0.0454	0.0486	0.0542	0.0464	0.0454	0.0468	0.0377	0.0419
19	0.0476	0.0498	0.0466	0.0495	0.0569	0.0462	0.0462	0.0483	0.0366	0.0420
20	0.0487	0.0455	0.0465	0.0483	0.0549	0.0448	0.0460	0.0472	0.0357	0.0418
21	0.0466	0.0398	0.0448	0.0442	0.0485	0.0417	0.0436	0.0445	0.0355	0.0417
22	0.0418	0.0375	0.0408	0.0396	0.0399	0.0394	0.0407	0.0407	0.0356	0.0420
23	0.0370	0.0360	0.0371	0.0370	0.0359	0.0380	0.0395	0.0378	0.0370	0.0415
	1	1	1	1	1	1	1	1	1	1